UNIVERSITÀ DEGLI STUDI DI PARMA
DIPARTIMENTO DI FISICA

Spin dynamics in magnetic molecules

Studio delle dinamiche di spin in sistemi molecolari magnetici

Alberto Bianchi

Thesis submitted for the award of the degree of Ph.D. in Physics

Dottorato di Ricerca in Fisica

Supervisor: Prof. Paolo Santini

XXI ciclo - Gennaio 2009

This document was typeset in Adobe® Utopia and Computer Modern Roman
by the author using the LaTeX2ε software.
The file in Portable Document Format was generated with pdfTeX version 13c.

Author's address

Alberto Bianchi
Dipartimento di Fisica
Università degli Studi di Parma
Viale G. P. Usberti 7/A, I-43100 Parma, Italy
E-mail: mailto:alberto.bianchi@fis.unipr.it

to my mother and my brother, my endless present
to my father and my grandparents, my sweet memories
to Irida, my sunny future

Contents

List of Figures

Summary

In questo lavoro sono stati sviluppati modelli teorici nell'ambito dell'approccio spin Hamiltoniana al fine di studiare le dinamiche di spin coerente e incoerente in varie classi di molecole magnetiche. Questi sistemi sono formati da un core di ioni magnetici, tipicamente ioni di metalli di transizione, circondato da ligandi organici. I ligandi organici impediscono un'interazione effettiva tra i cores, mentre all'interno di un core i diversi spin sono fortemente accoppiati tra loro da interazioni di superscambio. In particolare, nella classe dei cosiddetti nanomagneti molecolari l'interazione tra gli ioni è così forte, che a bassa temperatura ciascuna molecola si comporta come una particella magnetica a spin totale fissato in presenza di un potenziale effettivo. In questi sistemi, la dinamica coerente, caratterizzata da scale di tempo brevi, è coinvolta in vari fenomeni quantistici di interesse fondamentale (come il tunneling della magnetizzazione). La dinamica incoerente, che implica scale di tempo più lunghe, ricopre un ruolo fondamentale dal momento che rappresenta l'ostacolo principale per le potenziali applicazioni tecnologiche delle molecole magnetiche come memorie ad alta densità o come bit quantistici. Nel presente lavoro, la dinamica coerente è stata studiata direttamente mediante l'analisi e l'interpretazione di misure di scattering anelastico di neutroni, e, indirettamente, attraverso l'analisi di misure di bulk (come magnetizzazione e calore specifico ad alti campi). In questo modo è stato inoltre possibile studiare le interazioni microscopiche alla base delle dinamiche di spin descritte all'interno di Hamiltoniane di spin microscopiche. I relativi parametri sono stati determinati dal confronto tra teoria ed esperimenti quali scattering anelastico di neutroni, suscettività magnetica, calore specifico e magnetizzazione. In particolare, sono stati determinati i parametri microscopici (dello scambio, dei campi cristallini, dell'interazione dipolare) dell'Hamiltoniana microscopica della molecola denominata Cr_8Zn. Trattandosi di un anello aperto il Cr_8Zn rappresenta un sistema modello per lo studio delle conseguenze della rottura della simmetria ad anello. Conseguenze di tale rottura si trovano non solo nel diagramma dei livelli energetici, ma anche nella struttura degli autostati e si riflettono in particolare nelle misure di scattering anelastico di neutroni in funzione del momento trasferito. Inoltre, mediante l'analisi di misure macroscopiche sono state determinate le Hamiltoniane microscopiche di anelli antiferromagnetici come il Cr_7Ni, il Cr_8Cd e il Cr_8Ni. Quest'ultimo in particolare, essendo un sistema magneticamente

frustrato, ha permesso di investigare a fondo le conseguenze della frustrazione magnetica nella dinamica quantistica. Per quanto riguarda la dinamica di rilassamento, vari tipi di molecole magnetiche sono stati presi in considerazione: i ben noti nanomagneti Mn_{12} e Fe_8, la molecola icosidodecaedrica Fe_{30}, il sistema antiferromagnetico V_{12} e il noto anello antiferromagnetico Cr_7Ni. Nel caso dei nanomagneti si è mostrato come raffreddando il campione e applicando un campo magnetico sufficientemente grande si può velocizzare la dinamica di rilassamento della magnetizzazione, facendo così venire meno la nota legge di Arrhenius. Per il Fe_{30}, il V_{12} e il Cr_7Ni l'analisi della dinamica di rilassamento è supportata da misure NMR. Si è provato come nei primi due casi le misure NMR restituiscono direttamente informazioni sulla dinamica di rilassamento della magnetizzazione. Per l'anello eterometallico Cr_7Ni, invece, misure di NMR di $1/T_1$ restituiscono informazioni sulla dinamica di osservabili molecolari non direttamente riconducibili alla magnetizzazione. In tutti e tre i casi l'analisi delle dinamiche di spin conduce a un ottimo accordo tra le misure NMR e le relative predizioni teoriche. Il modello sviluppato per lo studio delle dinamiche di spin, dunque, coglie gli aspetti fondamentali alla base dei fenomeni di rilassamento.

Chapter 1

Introduction

Molecular Magnetism is an interdisciplinary area in Condensed Matter Research which brings together Chemists and Physicists to the major challenge of investigating the magnetic properties of matter. Magnetic molecules have been intensively studied so far because of their potential technological applications and for the possibility they offer to investigate fundamental properties of matter at the nanoscopic scale. These systems contain a core of magnetic ions (typically 3d transition metal ions) surrounded by organic ligands. Molecules are embedded in a crystal structure with the organic ligands preventing interaction among the cores. On the other hand, the magnetic ions within a core are usually strongly coupled through superexchange interactions. Since the interaction between clusters is negligible, effects related to a single molecule can be probed by means of bulk techniques. An intensively studied class of magnetic molecules is constituted by the so called *single molecule magnets* (shortly, SMMs) or molecular nanomagnets [1, 2, 3]. These systems are characterized by a slow relaxation of magnetization at low T and give rise to magnetic hysteresis. This is one condition for storing information in a molecule. Therefore, since a SMM represents an isolated magnetic entity, it might be considered as the smallest practical unit for magnetic memories. This would increadibly increase the amount of information storable with respect to current devices. There are other classes of molecules (antiferromagnetic rings, grids, mesoscopic molecules ...) for which the envisaged technological applications cover the fields of quantum computation and magnetorefrigeration. In order to have a deeper understanding of fundamental features and a major control on technological aspects, the spin dynamics constitutes the key point. Both from a theoretical and an experimental point of view, the spin dynamics is characterized by two distinct regimes: coherent and incoherent. At short times it is the coherent spin dynamics which gives rise to

quantum effects in magnetic molecules, such as the quantum tunneling of magnetization. Furthermore, the ability to control this dynamics turns out to be crucial to carry out logic gates for quantum computing. On the other hand, the incoherent part of spin dynamics involves longer times, tipically of the order of 10^{-6} s ore more at low temperature. The understanding of relaxation mechanisms is fundamental since relaxation and more generally decoherence constitute a major obstacle to the technological applications of magnetic molecules in the fields of high density memory storage and quantum computation.

This thesis is organized as follows. In the next sections, a brief introduction on molecular nanomagnets will be given, with particular attention to the relaxation mechanisms which characterize the dynamics of magnetization in the prototype of these systems, the so called Mn_{12} [1]. Chapter 2 will focus on the spin Hamiltonian approach here followed to theoretically describe magnetic molecules. The typical microscopic interactions in magnetic molecules will be taken into account, and a general expression of the molecular spin Hamiltonian will be given in terms of tensor operators [4, 5, 6, 2]. Chapter 3 will be devoted to the experimental techniques most of the theoretical results refer to, i.e. inelastic neutron scattering (INS) and nuclear magnetic resonance (NMR). Chapters 4, 5, 6 will summarize the main results of this thesis on the static and dynamic magnetic properties of these materials [7, 8, 9, 10, 11]. The coherent part of spin dynamics has been directly investigated through analysis of inelastic neutron scattering (INS) data, and indirectly through analysis of macroscopic measurements such as magnetization and specific heat. In Chapter 4, the microscopic spin hamiltonian of Cr_8Zn compound has been determined by comparing the experimental cross sections with theoretical predictions. The nature of elementary excitations in open spin segments has been thus clarified and is apparent in experimental data. Macroscopic magnetization measurements at high fields carried out for the parent Cr_8Cd compound corroborate the results obtained from neutron spectroscopy. This proves that the spin hamiltonian approach gives a good description of incoherent spin dynamics even for spin multiplets not accessible to the INS technique. The same holds for the case of Cr_7Ni, a cluster which has been shown to be a good candidate for quantum computing. In Chapter 5 magnetization measurements on Cr_7Ni confirm the picture derived in existing interpretation of INS data. Besides, in this chapter macroscopic measurements on another heterometallic ring named Cr_8Ni have been analyzed. This compound is magnetically frustrated and has offered the unique opportunity of investigating the effects of frustration on quantum dynamics. As regards relaxation phenomena, several

molecules have been taken into account in Chapter 6: the Mn_{12} and Fe_8 nanomagnets, the Fe_{30} icosidodecaedron, the V_{12} antiferromagnetic cluster containing ions with spin 1/2 and the already mentioned Cr_7Ni heterometallic ring. The incoherent dynamics on nanomagnets has been intensively studied in recent years, but non completely understood. Fe_{30} represents a mesoscopic molecule of great fundamental interest. V_{12} shows an anomalous behaviour in NMR data. At last, the study of the relaxation dynamics in Cr_7Ni is crucial for the envisaged application of the molecule as a qubit. In all studied clusters, there is a good agreement between available data and calculations and thus the theory captures the main features of relaxation phenomena.
Finally, in Chapter 7 general conclusions will be given with particular consideration on future perspectives and developments of the here presented research activity.

1.1 Magnetic Molecules

A magnetic molecule is a system containing a finite number of magnetic centers (transition metal ions, rare-earth ions, organic radicals) which are ferro- or antiferro- magnetically coupled through superexchange pathways [2,6]. Shells of organic ligands sorround each cluster preventing effective inter-cluster interactions. Thus, each molecule can be considered as an isolated magnetic entity. A nanomagnet can be defined as a system that shows slow relaxation of the magnetization of purely molecular origin. Under the so called *blocking temperature* [2, 12] a magnetic cluster behaves as a nanomagnet giving rise to magnetic hysteresis of purely molecular origin. This is the reason for which these systems have also been named single molecule magnets. A SMM has dimensions small enough to show fascinating quantum effects such as the quantum tunneling of magnetization (or QTM). This phenomenon is the magnetic analogue of the tunneling of an α particle in a radioactive nucleus. The magnetic moment is aligned along the easy-axis, and changes its orientation by tunneling through the energy barrier. In recent years there has been an enormous progress in chemical techniques to synthetize new compounds with all envisaged properties: number of interacting spins, type of metallic centers, amount and kind of anisotropy, and so on.
Beyond information storage, magnetic molecules have been thought as building blocks for quantum computing. For instance, a system with an $S = 1/2$ ground state can be regarded as a qubit, or quantum bit, the quantum analogue of the classic bit, and used to implement algorithms of quantum computation. One of the best candidates for this purpose has been proved to be the heterometallic ring known as Cr_7Ni [13],

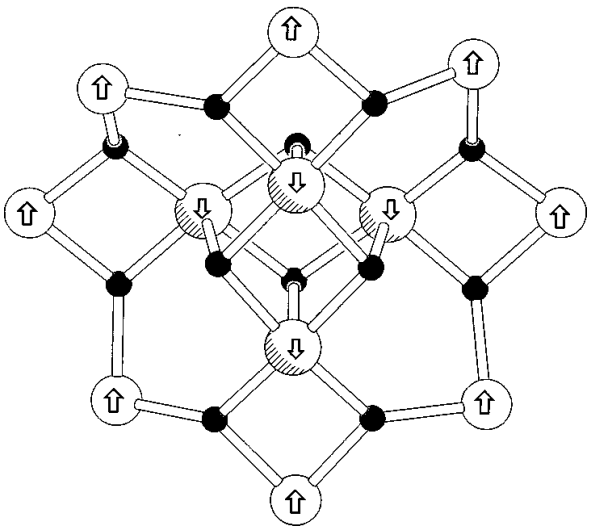

Figure 1: Structure of the Mn_{12} cluster. The outer ring is formed by eight ions Mn(III) with four unpaired electrons and spin 2, whilst the inner four ions Mn(IV) have three unpaired electrons and thus spin 3/2. Arrows indicate the configuration of the ground state of the molecule, a multiplet $S = 10$.

which shows an effective $S = 1/2$ ground state well separated by excited levels. It has also been demonstrated how magnetic molecules can be used as magnetocaloric refrigerants at low temperature. It is the case of another Chromium-based magnetic ring named Cr_7Cd [14]. Both Cr_7Ni and Cr_7Cd were derived by the well known Cr_8 compound, a fact which demonstrates the possibility of tuning the properties of magnetic molecules by a chemical substitution of magnetic centers. We will see in the next chapters how this possibility will turn out to be extremely useful in order to evaluate the consequences of the various types of breaking of ring symmetry.

1.2 The archetipal nanomagnet: Mn_{12}

In the early nineties, it was discovered that the dodecanuclear compound $[Mn_{12}O_{12}(CH_3COO)_{16}(H_2O)_4]$, shortly Mn_{12} [15], shows a slow relaxation behaviour of magnetization at low temperature. It has been theoretically and experimentally demonstrated that the time characterizing the thermally activated relaxation process in the interval 2-15 K follows an Arrhenius law:

$$\tau = \tau_0 exp(\frac{\Delta}{k_B T}) \tag{1}$$

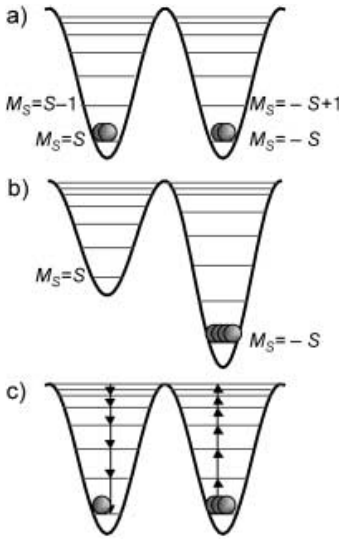

Figure 2: Level diagram within the ground multiplet $S = 10$ of Mn_{12} as inferred from Eq. (2). Levels with $M > 0$ and with $M < 0$ are localized in the left and in the right potential hole respectively. (a): At zero magnetic field the two groups of levels are equally populated. (b): The application of a magnetic field selectively populates the right hand hole. (c): After the removal of the magnetic field the system returns back to equilibrium through multi-step Orbach processes.

with τ_0=2.1×10^{-7} and $\frac{\Delta}{k_B}$=61 K [16, 17, 18]. It can be argued that at 2 K it takes several months for the magnetization to relax back to equilibrium. This behaviour results from thermally activated multi-step Orbach processes as shown in Fig. 2. At low temperature, i.e. $T < 2$ K, measurements of the relaxation time τ shows that the Arrhenius law is not satisfied and τ tends to a finite value when $T \to 0$. This has been interpreted as a QTM involving the two lowest levels. This phenomenology can be well understood by analyzing the interactions which govern the low T behaviour of the spin dynamics of the Mn_{12} molecule. In order to give a complete theoretical description of Mn_{12} one should explore the complete Hilbert spin space spanned by the twelve spins: the eight outer Mn(III) ions with spin s_a=2, and the four inner Mn(IV) ions with spin s_b=3/2. The computation of the number of spin levels would give $(2s_a + 1)^8 \times (2s_b + 1)^4 = 10^8$. As a result, an exact spin Hamiltonian approach is unfeasible even though modern computing machines are exploited. For many purposes, it is sufficient to describe the spin dynamics of the molecule at low T, by observing that the antiferromagnetic (AFM) exchange interactions among the eight Mn(III) and the four Mn(IV) ions lead to a $S = 10$ ground multiplet. Fig. 1 represents the arragement of the twelve ions in the ground state of the molecule: the Mn(III) ions have their spins pointing in the upward direction, while the other Mn(IV) ions point downward [1, 19].

At low T the Mn_{12} cluster can be well described within the ground $S = 10$ multiplet by an unperturbed Hamiltonian which includes the effects of the crystal field up to second order:

$$H_0 = D[S_z^2 - S(S+1)/3] + g\mu_B H_z S_z, \tag{2}$$

where the second term represents the coupling with a magnetic field H_z, taken along the z direction, which is the easy axis of magnetic anisotropy, $g \approx 2$ and μ_B is the Bohr magneton. The level diagram can be easily obtained from the above hamiltonian, and the levels

$$E(M_S) = D(M_S^2 - 110/3) + g\mu_B H_z M_S \tag{3}$$

with $H_z = 0$ are shown in Fig. 2(a). In absence of an applied magnetic field, levels with $M_S = \pm S$ constitute the degenerate ground doublet. Besides, levels with $M_S > 0$ and $M_S <$ are supposed to be in the left and in the right side of the double well potential respectively. Though the above hamiltonian contains only the axial part of 2nd order crystalline anisotropy, some aspects of the thermally activated relaxation mechanisms in the temperature range 2-15 K can be well understood. Let us suppose to prepare the system in a magnetized state [see Fig. 2(b)] by the application of a magnetic field along the z-axis. If T is low and H_z applied on the z-axis strong enough, only the $M_S = -10$ state is populated. Thus the cluster magnetization reaches the saturation value. At the removal of the field, the molecule will be out of thermodynamic equilibrium: in fact, at zero field the two ground $M_S = \pm S$ states are degenerate and as a consequence should be equally populated. The system returns back to equilibrium thanks to the coupling of the spins with other degrees of freedom. At $T > 1$ K the most important source which causes relaxation processes is constituted by phonons [20, 21]. The spin phonon interaction has its main origin in a perturbation of the crystal fields induced by lattice vibrations. The effects of such a perturbation are experienced by each magnetic ion and can be taken into account in terms of a spin-phonon hamiltonian, whose leading terms are second order spin operators. Therefore, transitions between $|M_S >$ and $|M_S \pm 1 >$, $|M_S \pm 2 >$ are allowed. For the sake of simplicity, at this level only transitions with selection rule $|\Delta M| = |M_S - M_S'| = 1$ will be considered. As a consequence, a spin flip may occure from, say, $M_S = -10$ to $M_S = -9$, if the molecule absorbs a quantum of energy corresponding to the energy difference $E(M_S = -9) - E(M_S = -10)$. In order to relax back to equilibrium, i.e. a spin-flip between $|M_S >= -10$ and $|M_S >= 10$, consecutive transitions from adiacent levels have to be performed [see Fig. 2(c)]. This is

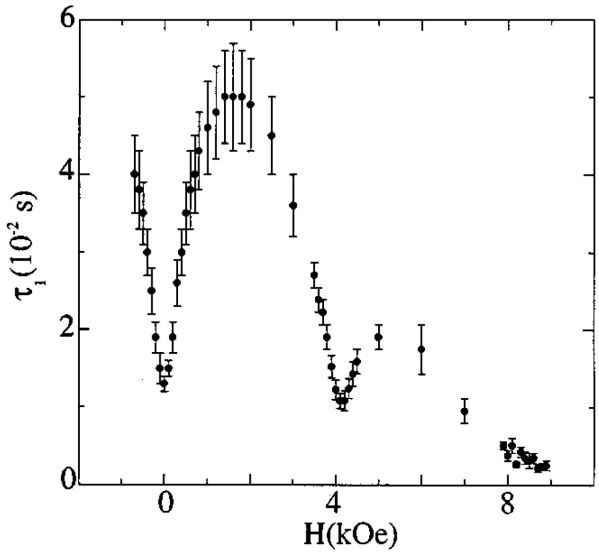

Figure 3: Relaxation time τ of magnetization in the Mn_{12} cluster as a function of magnetic field applied along the easy axis. At given fields τ shows sharp minima and the system undergoes a faster relaxation mechanism: the quantum tunneling of magnetization. Measurements were made at $T = 5$ K [17].

the phonon-induced mechanism which takes place through multi-step Orbach processes. Another relaxation mechanism has been found in Mn_{12} which is a clear manifestation of the quantum mechanical nature of this spin system and, in general, of SMMs: the so called quantum tunneling of magnetization (QTM). Fig. 3 shows the relaxation time τ as a function of magnetic field applied along z, the easy axis of magnetization. It can be observed that τ increaseas up to $H = 1.5$ KOe, where it reaches a maximum, then it decreases again showing minima at $H = 4.5$ KOe and $H = 8.5$ KOe. This behaviour was completely unexpected: in fact, in traditional superparamagnets the relaxation time diminishes in a monotonic way when H increases since the magnetic anisotropy barrier progressively reduces. The QTM novel phenomenon can be understood if in the Hamiltonian (2) further crystal field terms allowed by the tetragonal symmetry of the cluster [1] are taken into account:

$$H_{S=10} = \frac{D}{3}O_2^0 + B_4^0 O_4^0 + B_4^4 O_4^4. \tag{4}$$

The above hamiltonian contains CF contributions up to fourth order. In particular, the last term represents a weak transverse anisotropy and removes the degeneracy between

[1] The here reported microscopic parameters were determined by means of inelastic neutron scattering experiments: D=-0.457 cm^{-1}, B_4^0=-2.33×10^{-5} cm^{-1}, $B_4^4 = \pm 3 \times 10^{-5}$ cm^{-1} [22].

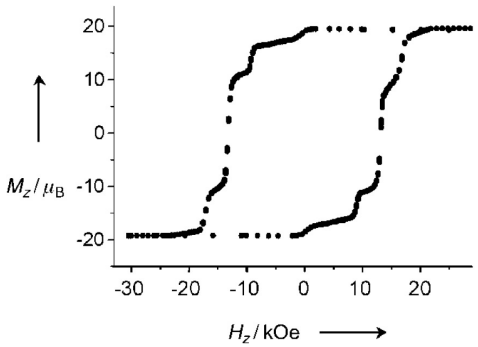

Figure 4: Hysteresis loop measured on a Mn_{12} monocrystal at T=2.1 K. At anticrossing fields the hysteresis shows sharp steps due to the QTM between the couples of quasi-degenerate levels. In correspondence of each anticrossing the relaxation of magnetization becomes faster and a steps occurs.

levels $M_S = \pm 10$, $M_S = \pm 6$ and $M_S = \pm 2$ thus allowing the tunneling of magnetization to manifest. The occurrence of clear minima in τ at particular magnetic fields in Fig. 3 can be explained if the Zeeman term $H_{Zeeman} = g\mu_B H_z$ is added in Eq. (4). At given magnetic fields, a couple of levels becomes quasi-degenerate and a so called *anti-crossing* takes place. In correspondence with these anticrossing fields the system is subjected to a faster relaxation since the involved levels allow a thermally assisted quantum tunneling. This explaines the behaviour shown in Fig. 3. Consequences of the thermal assisted QTM phenomenon are directly seen in magnetization measurements. In Fig. 4 an hysteresis loop measured at T =2.1 K on a Mn_{12} monocrystal is shown. In correspondence of an anticrossing field a thermally assisted QTM occurs between the quasi degenerate pair of levels. The magnetization has not to overcome the overall double-well potential to relax back to equilibrium, indeed tunnels it and the relaxation process becomes faster. This is the origin of the steps in the hysteresis loop, which it is worth to rembember is an effect of purely molecular origin.

1.3 Beyond the Mn_{12} nanomagnet

There are several reasons behind the great efforts researchers devote to the synthesis of new types of magnetic molecules and to the investigation of their magnetic properties. Some of these reasons are the potential technological applications envisaged in the fields of information storage, quantum computation and magnetorefrigeration [2, 16, 23]. In order to have molecules which are suitable to be used as high-density memories, a high blocking temperature T_B is needed [2,12], at least higher than the helium melting point.

In fact, the height of the barrier potential stabilizes the sample magnetization against thermal disorder. Therefore, a large U is required to have a high T_B: for this purpose a molecule with a high spin ground state is needed together with a large Ising-type anisotropy. The magnetic molecule with the highest energy barrier observed so far is the Mn_6 cluster, with $U \approx 86.4$ K. Nonetheless, it is insufficient for technological applications. In fact, since the τ_0 in the prefactor of Eq. (1) is very small, magnetization blocking only occurs below about 4.5 K [24]. Since in conventional SMMs the energy barrier seems difficult to be significantly increased, other compounds have been taken into account. In particular, the new family of lanthanide single molecule magnets has gained great attention [25, 26, 27, 28, 29].

As regards the field of quantum computation, one of the best candidates to be used as a qubit has been proved to be the Cr_7Ni compound [13]. This is a Chromium-based heterometallic ring, in which magnetic centers are antiferromagnetically coupled [30]. This molecule was obtained from the well-know homometallic ring Cr_8 by substitution of a Cr^{3+} ion (s=3/2) with a Ni^{2+} ion (s=1). While in Cr_8 the compensation of antiferromagnetic interactions leads to a singlet $S = 0$ ground state, in Cr_7Ni the ground Kramers doublet $S = 1/2$ accounts for the presence of a Ni^{2+} ion. In Ref. [13] it has been demonstrated that at low T Cr_7Ni well behaves as an effective two level system. In fact, the S-mixing between the ground state doublet $|S = 1/2>$ and higher levels $|S > 1/2>$ (<1%) is low enough that transitions between $|S = 1/2>$ and $|S > 1/2>$ induced by transverse field required in qubit manipulation are negligible.

The last of the above mentioned technological applications of magnetic molecules lies in the field of magnetorefrigeration [31]. Recent results demonstrate that the magnetocaloric effect can be exploited in a Chromium based cluster named Cr_7Cd at temperatures $T < 2$ K [14].

Chapter 2

Theoretical description of molecular magnets

In order to give a theoretical description of magnetic clusters we exploit the irreducible tensor operator (ITO) technique.

2.1 The spin Hamiltonian

A magnetic molecule formed by a number N of magnetic ions can be described in terms of the following spin Hamiltonian:

$$H = H_0 + H_{CF} + H_{DIP}, \tag{5}$$

where H_0 is the isotropic Heisenbgerg-Dirac interaction, H_{CF} represents the local crystal fields while H_{DIP} contains both the dipolar intracluster interaction and the anisotropic exchange. In general, other terms may compare in Eq. (5), such as the antisymmetric, biquadratic and anisotropic exchange as we will see in the next section. Here Eq. (5) gathers the usually leading interactions in the spin Hamiltonian of a magnetic molecule. The three contributions of Eq. (5) can be written as:

$$H_0 = \sum_{i>j} J_{i,j} \mathbf{s}_i \cdot \mathbf{s}_j \tag{6}$$

$$H_{CF} = \sum_{i} \sum_{k,q} b_k^q(i) O_k^q(\mathbf{s}_i) \tag{7}$$

$$H_{DIP} = \sum_{i>j} \mathbf{s}_i \cdot \mathbf{D}_{ij} \cdot \mathbf{s}_j, \tag{8}$$

where $\mathbf{s}_i$ is the spin operator of the ion on i-th site, J_{ij} are the isotropic exchange integrals, and $\mathbf{D}_{ij}$ is the second order dipolar tensor, usually evaluated within the

point dipole approximation [32]. The second term represents the local crystal fields (CFs), with $O_k^q(\mathbf{s}_i)$ Stevens operator equivalents for the i-th ion [6, 33, 34], and $b_k^q(i)$ CF parameters. Here $k = 2, 4$ for d electrons and $k = 2, 4, 6$ for f electrons [6], while $q = -k, \ldots, k$. The total dimensions of the Hamiltonian matrix is:

$$D = \prod_{i=1}^{N}(2s_i + 1). \tag{9}$$

Depending on the values of N and s_i D can be very large. For instance, $D = 2^4 = 16$ for V_{12}, but this value is enormous for Fe_{30} for which $D = 6^{30}$, of the order of the Avogadro's number. In order to represent the interactions of Eq. (5), it is natural the choice of the product states

$$|s_1 m_1\rangle\,|s_2 m_2\rangle \cdots |s_N m_N\rangle$$

as basis functions. Nonetheless, H_0 is often the dominant term in Eq. (5). Thus a better choice of the basis states is constituted by the eigenstates of the total spin $\mathbf{S} = \sum_i \mathbf{s}_i$. Besides, an appropriate coupling schemes is to be chosen. For a cluster with N magnetic ions with spins $S_1, S_2, \ldots, S_N$ a successive coupling scheme leads to the following basis vectors:

$$\left|s_1 s_2(\tilde{S}_2) s_3(\tilde{S}_3) \ldots s_{N-1}(\tilde{S}_{N-1}) s_N SM\right\rangle = \left|(\tilde{S})SM\right\rangle \tag{10}$$

where $(\tilde{S})$ represents the complete set of intermediate spin quantum numbers $\tilde{S}_k$, with $k = 1, \ldots, N-1$. Here the first intermediate spin $\tilde{S}_2 = S_{12}$ is given by the coupling of s_1 with s_2. Then $\tilde{S}_2$ is coupled to s_3 to have $\tilde{S}_3 = S_{123}$ and so on. For a system with N ions $N-1$ is the number of required intermediate spins to specify each possible spin state. Different choices can be made as regards the coupling scheme. Anyway, all coupling schemes are equivalent, since the corresponding representative vectors are connected to each other by a given unitary transformation. It is wise to remark that it is much more convenient to choose a coupling scheme which reflects the symmetries of the molecular system. The eigenstates $|v\rangle$ of H will be given by linear combinations of the basis states $\left|(\tilde{S})SM\right\rangle$:

$$|v\rangle = \sum_{(\tilde{S})SM} \left\langle (\tilde{S})SM \middle| v \right\rangle \left|(\tilde{S})SM\right\rangle, \tag{11}$$

where the coefficients $\left\langle (\tilde{S})SM \middle| v \right\rangle$ can be evaluated once the spin-Hamiltonian of the system has been diagonalized. The irreducible tensor operator (ITO) technique allows

to exploit the total spin symmetry of the cluster and to simplify both analytical and numerical calculations [32, 35]. Since each term of Eq. (5) can be rewritten as a combination of tensor operators $T^{(k)}$, the generalized spin-Hamiltonian of a magnetic molecule is:

$$\begin{aligned} H_c &= \sum_{k_1,k_2,\ldots,k_N} \sum_{\tilde{k}_2,\ldots,\tilde{k}_N} \sum_{kq} C_q^{(k)}(k_1,k_2,\tilde{k}_2,\ldots,k_{N-1},(\tilde{k}_2),k_N) \times \\ &\times \; T_q^{(k)}(k_1,k_2,\tilde{k}_2,\ldots,k_{N-1},(\tilde{k}_{N-1}),k_N) \end{aligned} \tag{12}$$

where $-k \leq q \leq k$, $T_q^{(k)}(k_1,k_2,\tilde{k}_2,\ldots,k_{N-1},(\tilde{k}_{N-1}),k_N)$ is the q-th component of the ITO of rank k, which can be decomposed in terms of ITO's $S_{q_i}^{k_i}(i) \equiv S_{q_i}^{k_i}$ defined in the subspace of each single spin (k_i=0,1, ..., $2s_i$):

$$\begin{aligned} &T_q^{(k)}(k_1,k_2,\tilde{k}_2,\ldots,k_{N-1},(\tilde{k}_{N-1}),k_N) = \\ &\left\{ \left\{ \left\{ \ldots \left\{ S^{k_1} \otimes S^{k_2} \right\}^{\tilde{k}_2} \otimes S^{k_3} \right\}^{\tilde{k}_3} \ldots \right\}^{\tilde{k}_{N-1}} \otimes S^{k_N} \right\}_q^k . \end{aligned} \tag{13}$$

In the above expression the symbol $\otimes$ denotes the tensor product and $\tilde{k}_2 = k_{12}, \tilde{k}_3 = k_{123}, \ldots$. Besides, by expoliting the Wigner decomposition the values the intermediate rank $\tilde{k}_2$ assumes are:

$$\tilde{k}_2 = k_1 + k_2, k_1 + k_2 - 1, \ldots, |k_1 - k_2| ,$$

and so on for the other intermediate ranks $\tilde{k}_i$. At this point, if the Hamiltonian H_c of the spin system is known, the eigenvalue problem has to be solved in order to calculate all physical observables we are interested in. Therefore, the matrix elements of operators $T_q^{(k)}$ have to be calculated within the basis states. By exploiting the Wigner-Eckart theorem [5] we have:

$$\begin{aligned} &\left\langle (\tilde{S}')S'M' \middle| T_q^{(k)}(k_1,k_2,\tilde{k}_2,\ldots,k_{N-1},(\tilde{k}_{N-1}),k_N) \middle| (\tilde{S})SM \right\rangle = \\ = \;& (-1)^{S'-M'} \left\langle (\tilde{S}')S' \middle|\middle| T^k \middle|\middle| (\tilde{S})S \right\rangle \begin{pmatrix} S' & k & S \\ -M' & q & M \end{pmatrix} \end{aligned} \tag{14}$$

where $\begin{pmatrix} S' & k & S \\ -M' & q & M \end{pmatrix}$ is a 3-j symbol and $\left\langle (\tilde{S}')S' \middle|\middle| T^k \middle|\middle| (\tilde{S})S \right\rangle$ is the reduced matrix element between the two states. Finally, by means of successive *decoupling procedures*, this reduced matrix element can be expressed in terms of single spin reduced matrix elements and 9-j coefficients:

$$\left\langle (\tilde{S}')S' \middle|\middle| T^{(k)}(k_1,k_2,\tilde{k}_2,\ldots,k_{N-1},(\tilde{k}_{N-1}),k_N) \middle|\middle| (\tilde{S})S \right\rangle =$$

$$\left\langle S_N \left|\left| S^{k_N} \right|\right| S_N \right\rangle \prod_{1}^{N-1} \sqrt{(2k_{i+1}+1)(2\tilde{S}_{i+1}+1)(2\tilde{S'}_{i+1}+1)} + \left\langle S_i||S_i^k||S_i \right\rangle \begin{Bmatrix} \tilde{k}_i & k_{i+1} & \tilde{k}_{i+1} \\ \tilde{S'}_i & S'_{i+1} & \tilde{S'}_{i+1} \\ \tilde{S}_i & S_{i+1} & \tilde{S}_{i+1} \end{Bmatrix}, \tag{15}$$

where the $\begin{Bmatrix} ::: \end{Bmatrix}$ are the 9-j symbols. For $k = 0, 1, 2$ the single spin reduced matrix elements are:

$$\left\langle S \left|\left| S^{(0)} \right|\right| S \right\rangle = \sqrt{(2S+1)}\delta_{S,S'} \tag{16}$$

$$\left\langle S \left|\left| S^{(1)} \right|\right| S \right\rangle = \sqrt{S(S+1)(2S+1)}\delta_{S,S'} \tag{17}$$

$$\left\langle S \left|\left| S^{(2)} \right|\right| S \right\rangle = \frac{1}{\sqrt{6}}\sqrt{(2S+3)(2S+1)(S+1)S(2S-1)}\delta_{S,S'} \tag{18}$$

2.2 Spin Hamiltonian: Main Contributions

After the generalized spin-Hamiltonian formalism has been introduced, it is necessary to focus on the main physical interactions which determine the spin-Hamiltonian and to rewrite them in terms of the ITO's.
First of all, the exchange part of the spin-Hamiltonian is to be introduced:

$$H_{EX} = H_0 + H_{BQ} + H_{AS} + H_{AN}. \tag{19}$$

The first term H_0 is the Heisenberg-Dirac Hamiltonian, which represents the isotropic exchange interaction, H_{BQ} is the biquadratic exchange Hamiltonian, H_{AS} is the antisymmetric exchange Hamiltonian, and, finally, H_{AN} representes the anisotropic exchange interaction. Convetionally, they can be expressed as follows [1, 6]:

$$H_0 = \sum_{i>j} J_{i,j}\mathbf{s}_i \cdot \mathbf{s}_j \tag{20}$$

$$H_{BQ} = \sum_{i>j} j_{i,j}(\mathbf{s}_i \cdot \mathbf{s}_j)^2 \tag{21}$$

$$H_{AS} = \sum_{i>j} \mathbf{G}_{i,j} \cdot [\mathbf{s}_i \times \mathbf{s}_j] \tag{22}$$

$$H_{AN} = \sum_{i>j} \sum_{\alpha=x,y,z} J^{\alpha}_{i,j} s^{\alpha}_i s^{\alpha}_j, \tag{23}$$

where $J_{i,j}$ e $J^{\alpha}_{i,j}$ are the parameters of the isotropic and anisotropic exchange interactions respectively, $j_{i,j}$ are the coefficients of the biquadratic exchange interaction, and,

finally, $\mathbf{G}_{i,j} = -\mathbf{G}_{j,i}$ is the vector of the antisymmetric exchange. For the sake of simplicity, further low symmetry terms in the anisotropic exchange and more complicated terms between three or more spin centers in the biquadratic exchange interaction have been neglected [35]. The magnetic dipole-dipole interaction can be taken into account within the above exchange contributions [1]. In fact, both terms contain the same dependence on spin operators and differ only as regards the coefficients J_{ij}^{α}.
The terms of the spin-Hamiltonian above can be written in terms of the ITO's. By exploiting the properties of the angular momentum, the following relations can be found:

$$\begin{aligned} s^x(i) &= \frac{S_{-1}^{(1)}(i) - S_1^{(1)}(i)}{\sqrt{2}} \\ s^y(i) &= i\frac{S_{-1}^{(1)}(i) + S_1^{(1)}(i)}{\sqrt{2}} \\ s^z(i) &= S_0^{(1)}, \end{aligned} \tag{24}$$

where the $S_q^{(1)}$, $q = 0, 1, 2$, are the first rank irreducible tensors acting in the spin-spaces of individual ions. By means of the above relations and of the Wigner decomposition we have [35]:

$$H_0 = -\sqrt{3}\sum_{i>j} J_{i,j} T_0^{(0)}(11|ij) \tag{25}$$

where $T_0^{(0)}(k_i k_j|i,j)$ describes the isotropic exchange interaction between a couple of spins, and can be obtained from $T^{(k)}(k_1, k_2, \tilde{k}_2, ..., k_{N-1}, (\tilde{k}_{N-1}), k_N)$ by substituting the corresponding values of k_i and k_j, and by imposing k_l=0 $\forall \neq i, j$. Furthermore, the following expressions can be obtained:

$$H_{BQ} = -\sum_{i>j} j_{i,j}[\sqrt{5}T^{(0)}(22|ij) + \frac{\sqrt{3}}{2}T^{(0)}(11|ij)] \tag{26}$$

$$H_{AS} = -i\sqrt{2}\sum_{i>j}\sum_{q}(-1)^q G_{q,ij}^{(1)} T_{-q}^{(1)}(11|ij) \tag{27}$$

where

$$G_{q,ij}^{(1)} = \begin{cases} \frac{\mp(G_{x,ij} \pm iG_{y,ij})}{\sqrt{2}} & \text{if q} = \pm 1 \\ G_{z,ij} & \text{if q} = 0 \end{cases}$$

and:

$$H_{AN} = \sum_{i>j} J_{i,j}^a T^{(0)}(11|ij) + \sum_{i,j} J_{i,j}^u [T_2^{(2)}(11|ij) + T_{-2}^{(2)}(11|ij)] + \sum_{i,j} J_{i,j}^v T_0^{(2)}(11|ij) \tag{28}$$

where the parameters of anisotropic exchange are given by

$$\begin{aligned} J^a_{i,j} &= -\frac{1}{\sqrt{3}}(J^x_{i,j}+J^y_{i,j}+J^z_{i,j}) \\ J^u_{i,j} &= \frac{1}{\sqrt{2}}(J^x_{i,j}-J^y_{i,j}) \\ J^v_{i,j} &= \frac{1}{\sqrt{6}}(2J^z_{i,j}-J^x_{i,j}-J^y_{i,j}), \end{aligned}$$

and in the biquadratic term a costant term has been neglected.
As it can be seen in Eqs. (26), (28), both the biquadratic and the anisotropic Hamiltonians contain a scalar rank-0 contribution, i.e. $T^{(0)}(11|ij)$. This two terms can be incorporated in the isotropic exchange Hamiltonian by defining the effective isotropic parameters as $\tilde{J}_{i,j} = J_{i,j} + \frac{1}{3}(J^x_{i,j}+J^y_{i,j}+J^z_{i,j})$, thus having

$$H_0 = -\sqrt{3}\sum_{i>j}\tilde{J}_{i,j}T^{(0)}_0(11|ij). \tag{29}$$

As a result, the biquadratic and anisotropic Hamiltonians become:

$$H_{BQ} = -\sqrt{5}\sum_{i>j} j_{i,j}T^{(0)}(22|ij) \tag{30}$$

$$H_{AN} = \frac{1}{\sqrt{2}}\sum_{i>j} J^u_{i,j}[T^{(2)}_2(11|ij)+T^{(2)}_{-2}(11|ij)] + \sum_{i,j} J^v_{i,j}T^{(2)}_0(11|ij). \tag{31}$$

In order to complete the description of the spin system, contributions to the spin Hamiltonian due to local crystal fields (CFs) are to be taken into account [6, 33, 34]. By exploiting the same procedure, also the local CFs can be written in terms of the ITO's. The Hamiltonian describing the interaction of the magnetic ions with their CFs can be written as:

$$H_{CF} = \sum_i \sum_{k,q} b^q_k(i)O^q_k(\mathbf{s}_i) \tag{32}$$

with $O^q_k(\mathbf{s}_i)$ Stevens operator equivalents for the i-th ions and $b^q_k(i)$ CF parameters [6]. For transition metal ions $k = 2$ or 4 (larger values are forbidden for d electrons [6]), and $q = -k, \ldots, k$. The Stevens operator equivalents acting on site j can be expressed in terms of ITO's with all k_i's equal to zero apart from k_j. As an example, the widely used second order Hamiltonian

$$H_{CF} = \sum_i d_i(s^2_z(i) - \frac{s_i(s_i+1)}{3}) + \sum_i e_i(s^2_x(i) - s^2_y(i), \tag{33}$$

in terms of single site ITO's can be rewritten as:

$$H_{CF} = \sum_i d_i \sqrt{\frac{2}{3}} T_0^{(2)}(i) + \sum_i e_i (T_2^{(2)}(i) + T_{-2}^{(2)}(i)). \tag{34}$$

The two terms of the above equation are the axial and rhombic part of crystal field anisotropy. The $T_q^{(k)}(i)$ operators describe the single ion crystalline anisotropy and can be obtained from $T^{(k)}(k_1, k_2, \tilde{k}_2, ..., k_{N-1}, (\tilde{k}_{N-1}), k_N)$ by imposing k_i=k and k_l=0 ∀l≠i. Besides, it is worth to remark that from Eq. (14) the expression for the matrix element of a generic rank-k tensor operator is:

$$\left\langle (\tilde{S}')S'M' \left| T_q^{(k)}(k_1, k_2, \tilde{k}_2, ..., k_{N-1}, (\tilde{k}_{N-1}), k_N) \right| (\tilde{S})SM \right\rangle \propto \begin{pmatrix} S' & k & S \\ -M' & q & M \end{pmatrix}.$$

Therefore, from the definition of 3-j symbols and exploiting the properties of the angular momenta addition rules through Clebsh-Gordan coefficients [5, 36, 37], we have:
$\left\langle (\tilde{S}')S'M' \left| T_q^{(k)}(k_1, k_2, \tilde{k}_2, ..., k_{N-1}, (\tilde{k}_{N-1}), k_N) \right| (\tilde{S})SM \right\rangle \neq 0$
if and only if $|S - k| \leq S' \leq S + k$
and $M' - M = q$.
Both the Heisenberg-Dirac and biquadratic exchange are isotropic interactions. In fact, the corresponding Hamiltonians can be described by rank-0 tensor operators and thus have non zero matrix elements only with states with the same total spin quantum number S ($\Delta S = 0$ selection rule) and the same total spin projection M ($\Delta M = 0$ selection rule). The repesentative matrix can be decomposed into blocks depending only on the value of S and M. Differently, all anisotropic terms are described by rank-2 tensor operators which have non zero matrix elements between state with different total spin S ($\Delta S = 0, \pm 1, \pm 2$ selection rule). Therefore, their corresponding matrices can not be decomposed into blocks depending only on the value of the total spin S in account of the *S-mixing* between spin states with different values of S [38]. The single ion anisotropy can be written in terms of rank-2 single site ITO's. Nevertheless, if the rhombic term of crystal field anisotropy can be neglected, then the representative matrix of CF interaction results to be composed of blocks depending only on the value of the total spin projection M. This reflects the selection rules $\Delta S = 0, \pm 1, \pm 2$, $\Delta M = 0$. Finally, the antisymmetric exchange term is the sum of ITO's of rank $k = 1$, and its matrix elements are non zero only if $\Delta S = 0, \pm 1$.
The dimension of the matrices to be diagonalized for these systems increases dramatically by increasing the number of spin centers. In the next two sections two possible methods to solve this problem are described. Both methods take advantage from the

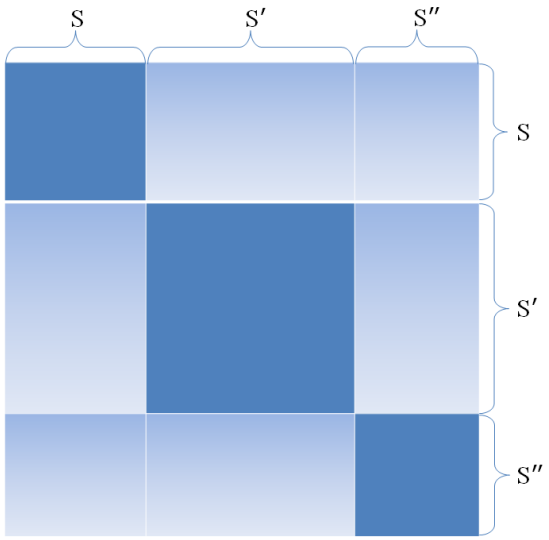

Figure 5: The full Hamiltonian matrix representing all the magnetic interactions. Diagonal blocks correspond to both isotropic and anisotropic terms with $\Delta S = 0$ selection rule within a given spin multiplet. The non diagonal blocks correspond to anisotropic interactions with $\Delta S = \pm 1, \pm 2$ selection rules.

obervation that in most magnetic molecules the Heisenberg-Dirac isotropic exchange is the dominant interaction.

2.3 Spin Hamiltonian: a perturbative approach

In the previous section we have seen how to describe a magnetic cluster with a matrix representing the different magnetic interactions. However, this kind of procedure is not always possible. In fact, when the number of magnetic ions increases, the system representative matrix can become too large for the eigenvalue problem to be solved exactly. As an example, the cluster named Cr_8Ni is composed by eigth ions Cr^{3+} with spin $s = 3/2$ and one Ni^{2+} ion with spin $s = 1$. The Hilbert spin space associated to the molecule has dimension $D = 196608$, beyond the computational power of most machines. In order to diagonalize the full matrix of this system, one should exploit alghoritms of parallel computing. Nevertheless, this would be quite unuseful since the information contained in the most of experimental data involves only levels thermally occupied at very low temperatures. Indeed, a perturbative approach can be applied since in magnetic molecules the isotropic exchange is almost always the dominant interaction. As a result, the problem can be solved by a two step procedure and this

was done in Cr_8 compound for the first time [39]. Initially, only the Heisenberg-Dirac Hamiltonian H_0 is considered. The eigenvalues and eigenvectors of the cluster are thus determined: the energy spectrum consists of several spin multiplets separated by the isotropic exchange. The eigenvectors of the isotropic exchange in terms of the basis vectors are:

$$|SM\rangle = \sum_{\tilde{S}} \left\langle (\tilde{S})SM \middle| SM \right\rangle \left| (\tilde{S})SM \right\rangle = \sum_{\tilde{S}} c_{S,(\tilde{S})} \left| (\tilde{S})SM \right\rangle . \tag{35}$$

It follows from the above expression that the generic matrix element (14) is:

$$\begin{aligned} &\langle S'M'| T^{(k)}(k_1, k_2, \tilde{k}_2, ..., k_{N-1}, (\tilde{k}_{N-1}), k_N) |SM\rangle = \\ &(-1)^{S'-M'} \sum_{(\tilde{S}'),(\tilde{S})} c_{S',(\tilde{S}')} c_{S,(\tilde{S})} \left\langle (\tilde{S}')S' \left|\left| T^k \right|\right| (\tilde{S})S \right\rangle \begin{pmatrix} S' & k & S \\ -M' & q & M \end{pmatrix} . \end{aligned} \tag{36}$$

In order to reduce the dimension of the system representative matrix, a cut in the energy diagram of H_0 can be performed: only eigenvectors of H_0 with corresponding eigenvalues with energy up to the decided cut-energy value are to be retained. Within this reduced spin subspace all magnetic interactions can be evaluated. In fact, by means of Eqs. (35) and (36) it is straightforward to calculate the matrix elements of anisotropic interactions between *any* of the eigenvectors of isotropic exchange. Finally, the second step of this procedure is to diagonalize the here determined complete spin Hamiltonian with all the anisotropic terms within the above-mentioned reduced spin subspace. The only approximation of this method consists in neglecting the *S-mixing* between levels of the reduced spin subspace and the other levels. This approximation can be always checked to produce an error smaller than the experimental error by a little increase of the reduced spin subspace dimension.

2.4 Strong exchange limit

When the Heisenberg-Dirac H_0 Hamiltonian is so much large that all other interactions can be treated as a perturbation of the isotropic exchange the strong exchange limit is achieved. This approximation has been intensively used, for instance, to develop the theory of quantum tunneling of magnetization [1] and to interpret inelastic neutron scattering experiments [40, 41].

The eigenvalues of H_0 are $(2S+1)$-fold degenerate and the energy separation between adjacent levels depends on the exchange integrals J_{ij} [see Eqs. (6) and (25)]. As a

result, the mixing between states of different S manifolds due to anisotropic interactions is expected to be small. This allows to work within a single spin multiplet S. The approximation consists in neglecting the matrix elements like $\langle \alpha SM \left| H \right| \alpha' S' M' \rangle$, where the $|\alpha SM\rangle$ are the eigenvectors of H_0. Within this assumption, the complete hamiltonian H is replaced with an effective Hamiltonian H_S written in the S manifold in terms of the total spin operator $\mathbf{S}$. For instance, up to second order:

$$H_S = \mathbf{S} \cdot \mathbf{D} \cdot \mathbf{S} = \sum_{q=-2}^{q=2} B_2^q O_2^q, \tag{37}$$

where O_k^q are the Stevens operator equivalents [1] defined in the total spin space of S manifold with B_k^q the corresponding parameters. In a reference frame where the traceless $\mathbf{D}$ tensor is diagonal, H_S reduces to $B_2^0 O_2^0 + B_2^2 O_2^2$, and with the common D and E parameters defined as $D = 3B_2^0$ and $E = B_2^2$. The strong exchange limit approximation holds since within the subspace of the S manifold the matrix elements of the full Hamiltonian H and the effective Hamiltonian H_S are proportional. For this purpose, let us focus on Eqs. (35), (36). If Eq. (36) is evaluated within a given state $|SM\rangle$ eigenvector of H_0 the generic matrix element reads as follows:

$$\begin{aligned} &\langle SM' | \, T^{(k)}(k_1, k_2, \tilde{k}_2, ..., k_{N-1}, (\tilde{k}_{N-1}), k_N) \, | SM \rangle = \\ &(-1)^{S-M'} \sum_{(\tilde{S}'),(\tilde{S})} c_{S,(\tilde{S}')} c_{S,(\tilde{S})} \left\langle (\tilde{S}')S \left|\left| T^k \right|\right| (\tilde{S})S \right\rangle \begin{pmatrix} S & k & S \\ -M' & q & M \end{pmatrix}. \end{aligned} \tag{38}$$

In the above equation, the second member is the product of three contributions in which the 3-j element depends on the quantum number M, while the sum is constant within the chosen spin multiplet S. Furthermore, the reduce matrix elements in the sum are the only terms which depend on the decomposition of $|SM\rangle$ in terms of $\left|(\tilde{S})SM\right\rangle$ and on $T_q^{(k)}$ in terms of single site operators. Information on the coupling schemes and on intermediate spins is contained only in reduced matrix elements. Besides, it has to be reminded that Stevens operator equivalents O_k^q can be expressed as linear combinations of tensor operators $\tilde{O}_k^q(S, S_z, S_\pm)$ which are diagonal in the total spin S, with $k > 0$ and $q > 0$ [42,43]. Within the considered spin multiplet, and exploiting the Wigner-Eckart theorem, the following equation can be found:

$$\langle SM' | \, \tilde{O}_k^q(S, S_z, S_\pm) \, | SM \rangle = (-1)^{S-M'} \left\langle S \left|\left| \tilde{O}_k \right|\right| S \right\rangle \begin{pmatrix} S & k & S \\ -M' & q & M \end{pmatrix}. \tag{39}$$

[1] As regards the definition of Stevens operator equivalents we refer to Refs. [6,33,34].

As can be easily seen, the two left sided members in Eqs. (36) and (39) are proportional with a coefficient Γ given by:

$$\Gamma(k,S) = \frac{\sum_{(\tilde{S}'),(\tilde{S})} c_{(\tilde{S}')} c_{(\tilde{S})} \left\langle (\tilde{S}')S \left|\left| T^{(k)} \right|\right| (\tilde{S})S \right\rangle}{\left\langle S \left|\left| \tilde{O}_k \right|\right| S \right\rangle}. \tag{40}$$

$\Gamma(k,S)$ depends only on the rank k of the considered tensor operator and on total spin S, but it is constant inside a S multiplet [38, 43].

Chapter 3

Spin dynamics in magnetic molecules: experimental techniques

The evolution of molecular observables can be reversible or irreversible in time. The former case occurs at short times: in this frequecy window inelastic neutron scattering (INS) technique constitutes a powerful tool in order to probe molecular dynamics. The latter case occurs at longer times when the coupling of the spins to other degrees of freedom causes decoherence of molecular observables and relaxation phenomena. This type of spin dynamics is probed by magnetic resonance techniques such as NMR or AC susceptibility or, at longer times, by magnetization measurements. In this chapter, a brief description of the INS and NMR techniques will follow.

3.1 Inelastic Neutron Scattering

Inelastic neutron scattering technique constitutes a very powerful tool for the aim of obtaining invaluable information about the structure, atomic motion and magnetic properties (magnetic order, phase transition, magnetic excitations) of materials. In fact, the magnetic moment of the neutron couples to those the unpaired electrons of magnetic materials, thus providing information about the magnetic properties. Furthermore, the neutron energy $E = h^2/m_n\lambda^2 = \hbar^2 k/2m_n$, where $k = 2\pi/\lambda$, is comparable to many excitation energies in condensed matter. The inelastic interaction of neutrons with the sample gives direct access to these excitation energies as well as to the structure of the eigenfunctions of the spin Hamiltonian representative of the magnetic system. In order to experimentally probe such excitation energies, neutron wavelengths between 1 and 10 Å are commonly used. During the scattering process, neutrons with initial energies

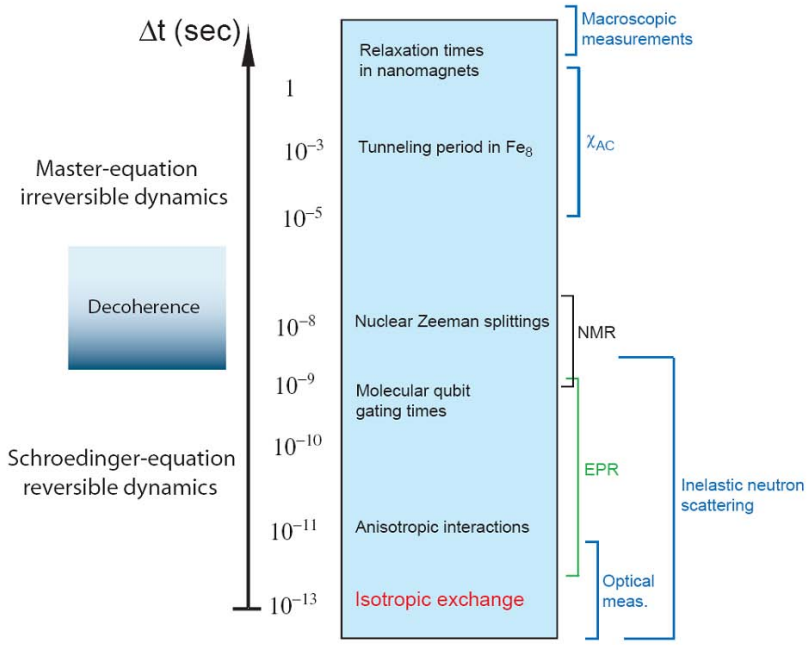

Figure 6: Typical time scales of spin dynamics in molecular nanomagnets. At short enough times, the spin dynamics evolves through Schrödinger equations and is time reversible. In this time window, high frequency techniques such as inelastic neutron scattering probe the spin dynamics. Differently, on longer timescales the system irreversibly evolves through master equations: decoherence and relaxation phenomena occur. This quasi-elastic part of spin dynamics is probed by low-frequency techniques such as NMR.

Properties of the neutron particle	
neutron mass	m_n=1.67×10^{-24}g
spin	1/2
electric charge	q_n=-0.4×10^{-21}e
magnetic moment	μ_n=1.91304275(45)μ_N

Table 1: The neutron mass m_n implies that its wave-length $\lambda = h/2m_n v$ (where the neutron velovity v varies in the range 200-3000 ms^{-1}) is of the order of interatomic distances in liquids and solids: structural and dynamics properties of materials can be probed by neutrons. Neutrons have no electric charge and thus highly penetrate materials, and because of their magnetic moments they can couple to magnetic nuclei and unpaired electrons in a sample. As regards the latter case, neutron energy $E = \hbar^2/2m_n\lambda^2$ is of the order of typical low-energy magnetic excitations in molecular nanomagnets: inelastic neutron scattering can give direct access to these excitations.

E_i and momentum $\mathbf{k}_i$ are scattered by the sample. After the scattering process, neutrons with final energy E_f and final momentum $\mathbf{k}_f$ will be collected by detectors. The energy and momentum conservation laws impose the following definitions:

$$\hbar\omega = E_f - E_0 = (\hbar^2/2m_n)(\mathbf{k}_f^2 - \mathbf{k}_0^2) \tag{41}$$

and

$$\mathbf{Q} = \mathbf{k}_f - \mathbf{k}_0, \tag{42}$$

where λ_0 and λ_f are the initial and final neutron wavelengths. In an inelastic neutron scattering experiment, the general expression for the double differential neutron cross-section is:

$$\frac{\partial\sigma}{\partial\Omega\partial\omega} = \frac{k_f}{k_0} b^2 S(\mathbf{Q},\omega) \tag{43}$$

where k_0 and k_f are the moduli of the initial and final neutron wave-vectors, b is the scattering length and $S(\mathbf{Q},\omega)$ is the scattering function, i.e. the time and space Fourier transform of the time-dependent spin-spin correlation function. In a time of flight spectrometer, the energy of the detected neutrons can be determined by their time of arrival, provided that the distance between the neutrons and the detectors is known. The spectrometers based on a time of flight (tof) technique can be set in a *direct geometry* or *inverse geometry* configuration. In a direct geometry spectrometer (see Fig. 7), the energy and wave-vector $\mathbf{k}_0$ of incident neutrons can be selected by a monochromator. The energy and wave-vector $\mathbf{k}_f$ of scattered neutrons is evaluated by time of flight technique. In an inverse geometry spectrometer, the incident neutron beam is polychromatic and the energy E_0 is determined by time of flight. After being scattered by the target sample, the neutrons reach the time-resolved detectors and the final energy E_f can be measured by means of a crystal. In a direct geometry configuration, once the incident wave-length has been fixed, the allowed transferred momenta are given by:

$$Q^2 = k_0^2 + k_f^2 - 2k_0k_f cos(2\theta), \tag{44}$$

or

$$\hbar^2Q^2/2m_n = E_0 + E_f - 2(E_0E_f)^{1/2} cos(2\theta), \tag{45}$$

where 2θ is the angle between the initial and final wave-vector (see Fig. 7). Finally, naming $\hbar\omega$ the energy transfer from the neutrons to the target sample ($\hbar\omega > 0$ energy gain and $\hbar\omega < 0$ energy loss for the sample), the above equation becomes:

$$\hbar^2Q^2/2m_n = E_0 + E_f - 2(E_0(E_0 - \hbar\omega))^{1/2} cos(2\theta). \tag{46}$$

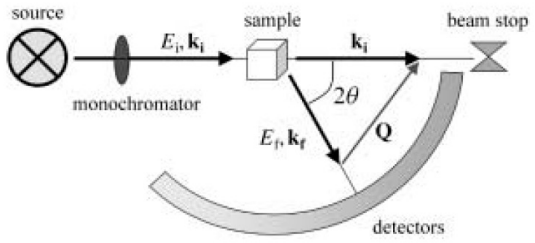

Figure 7: Representation of the experimental set up for a time of flight (*tof*) direct geometry spectrometer. The incident neutron beam coming from a reactor is polychromatic. A monochromator selects the desired neutron wave-length λ_0, therefore the energy E_0 and the wavevector $\mathbf{k}_0$. After being scattered by the sample, neutrons are collected by time-resolved detectors. The final energy E_f is determined by the time of arrival of the scattered neutrons. At the end, the final wave-vector $\mathbf{k}_f$ can be determined by the scattering angle 2θ and the $\mathbf{Q} = \mathbf{k}_f - \mathbf{k}_0$.

The trajectories defined in (Q, ω) space are recorded by time-resolved detectors, and constitute the so called *dynamic region* with the scattering angle 2θ assuming all the allowed values. In the particular case of magnetic scattering, the expression for the magnetic scattering cross-section is basically derived from first-order perturbation theory by using the Fermi's Golden rule with the assumption that the interaction of neutrons with unpaired electrons can be treated as a perturbation. In the case of a monoatomic system with spin-only moments, the partial differential cross-section for nonpolarized neutrons derived in Ref. [44] is:

$$\begin{aligned} \frac{d^2\sigma}{d\Omega dE} &= (\gamma r_0)^2 \cdot (\frac{k_f}{k_0}) \cdot \left[\frac{1}{2} g F(\mathbf{Q})\right]^2 \cdot exp(-2W(\mathbf{Q})) \times \\ &\sum_{\alpha,\beta} (\delta_{\alpha,\beta} - (\mathbf{Q}_\alpha \cdot \mathbf{Q}_\beta)/Q^2) \cdot S^{\alpha,\beta}(\mathbf{Q}, \omega), \end{aligned} \tag{47}$$

where $\gamma = -1.913$ is the gyromagnetic ratio, $r_0 = 2.818 \times 10^{-15}$ m is the classical radius of the electron, g is the Landé g factor, and $F(\mathbf{Q})$ is the magnetic form factor of the ion, which falls rapidly with $\mathbf{Q}$. Furthermore, $e^{-2W(\mathbf{Q})}$ is the Debye-Waller factor, which is usually neglected when dealing with magnetic scattering, since it is a slowly varying function of the scattering vector $\mathbf{Q}$. The factor $(\delta_{\alpha,\beta} - (\mathbf{Q}_\alpha \cdot \mathbf{Q}_\beta)/Q^2)$ implies that only the components of the magnetic moment perpendicular to the vawe-vector $\mathbf{Q}$ can couple to the neutron, being $\alpha, \beta = x, y, z$. $S^{\alpha,\beta}(\mathbf{Q}, \omega)$ is the so called scattering function. It is defined as the space and time Fourier transform of the time-dependent spin-spin correlation function. In the Schrödinger notation the scattering function is

given by:

$$S^{\alpha,\beta}(\mathbf{Q},\omega) = \sum_{i,j} exp(i\mathbf{Q}\cdot(\mathbf{R}_i - \mathbf{R}_j)) \times$$
$$\sum_{n,m} p_n \left\langle n \left| \tilde{s}_{\alpha_i} \right| m \right\rangle \left\langle m \left| \tilde{s}_{\beta_j} \right| n \right\rangle \delta(\hbar\omega - E_m + E_n), \tag{48}$$

where $\tilde{s}_{\alpha_i}$ is the α component of the spin operator on site i at position $\mathbf{R}_i$, $|n\rangle$ is the initial state with energy E_n, $|m\rangle$ is the final state with energy E_m, $p_n = \frac{e^{-\beta E_n}}{Z}$ is the Boltzman factor with Z the partition function. Finally, $\hbar\omega$ is the energy transfer between the neutrons and the spin system during the scattering process. It wise to remark that the scattering function contains all information about the magnetic strucure and spin dynamics. Its determination and knowledge is the main goal of any inelastic neutron scattering study. Eq. (47) can be extended to a number N_m of magnetic ions per unit cell. Besides, by exploiting the irreducible tensor operator technique, the partial differential cross-section for magnetic scattering by ions with spin-only moments can be averaged with respect to the possible orientations of the scattering vector $\mathbf{Q}$ [30,45]:

$$\frac{\delta^2\sigma}{\delta\Omega\delta\omega} = \frac{A}{N_m}\frac{k_f}{k_0}e^{-2W}\sum_{n,m}\frac{e^{-\beta E_n}}{Z} I_{nm}(Q)\delta(\hbar - E_m + E_n) \tag{49}$$

where A=0.29 barn, N_m is the number of magnetic ions. The function $I_{nm}(Q)$ is defined in terms of local spin matrices, magnetic form factors of metal ions $F(Q)$, and 0th, 2th order spherical Bessel functions $j_0(R_{ij}Q), j_2(R_{ij}Q)$, where $\mathbf{R}_{ij} = \mathbf{R}_i - \mathbf{R}_j$ is the vector defining the relative positions of ions i and j in the molecule [30,45]:

$$\begin{aligned} I_{nm}(Q) &= \sum_{i,j} F_i^*(Q)F_j(Q) \times \Big\{ \frac{2}{3}[j_0(QR_{ij}) + C_0^2 j_2(QR_{ij})]\tilde{s}_{z_i}\tilde{s}_{z_j} + \\ &\frac{2}{3}\Big[j_0(QR_{ij}) - \frac{1}{2}C_0^2 j_2(QR_{ij})\Big](\tilde{s}_{x_i}\tilde{s}_{x_j} + \tilde{s}_{y_i}\tilde{s}_{y_j}) + \\ &\frac{1}{2}j_2(QR_{ij})[C_2^2(\tilde{s}_{x_i}\tilde{s}_{x_j} - \tilde{s}_{y_i}\tilde{s}_{y_j}) + C_{-2}^2(\tilde{s}_{x_i}\tilde{s}_{y_j} + \tilde{s}_{y_i}\tilde{s}_{x_j})] + \\ &j_2(QR_{ij})[C_1^2(\tilde{s}_{z_i}\tilde{s}_{x_j} + \tilde{s}_{x_i}\tilde{s}_{z_j}) + C_{-1}^2(\tilde{s}_{x_i}\tilde{s}_{y_j} + \tilde{s}_{y_i}\tilde{s}_{z_j})]\Big\}, \end{aligned} \tag{50}$$

where

$$\begin{aligned} C_0^2 &= \frac{1}{2}\left[3\left(\frac{R_{ijz}}{R_{ij}}\right)^2 - 1\right] \\ C_2^2 &= \frac{R_{ijx}^2 - R_{ijy}^2}{R_{ij}^2} \\ C_{-2}^2 &= 2\frac{R_{ijx}R_{ijy}}{R_{ij}^2} \end{aligned}$$

$$C_1^2 = \frac{R_{ijx}R_{ijz}}{R_{ij}^2}$$
$$C_{-1}^2 = \frac{R_{ijy}R_{ijz}}{R_{ij}^2},$$

and

$$\tilde{s}_{\alpha_i}\tilde{s}_{\beta_j} = \langle n | s_{\alpha_i} | m \rangle \langle m | s_{\beta_j} | n \rangle ,$$

with $\alpha, \beta = x, y, z$.

Eq. (49) thus represents the partial differential neutron cross-section for unpolarized neutrons in the case of a powder sample with spin-only moments, and has been presented in Refs. [30, 45] for the first time. Eqs. (49) and (50) allow to gather very precise information about the energies of magnetic excitations in a magnetic molecule and the structure of spin eigenfunctions of the corresponding spin Hamiltonian. The former can be inferred by the magnetic peaks positions in the measured inelastic neutron cross sections. Moreover, detailed information about the latter can be obtained by the measured intensities under the inelastic peaks and their Q dependence.

3.2 Nuclear Magnetic Resonance

Nuclear moments are much smaller than electronic moments, being $\frac{\mu_B}{\mu_N} \sim 10^3$, where μ_B and μ_N are the Bohr and nuclear magnetons respectively. In fact, if the two-level system given by a single proton with $I = \frac{1}{2}$ is taken into account, the two states $m_I = +\frac{1}{2}$ and $m_I = -\frac{1}{2}$ are separated by an energy $\Delta E = g_N \mu_N B$, with g_N the proton gyromagnetic ratio, which is tiny. For a proton in a typical laboratory magnetic field $B_0 \approx 1$T the splitting between $m_I = +\frac{1}{2}$ and $m_I = -\frac{1}{2}$ would be $\approx 10^{-7}$ eV, which is equivalent to a temperature ≈ 1 mK. Therefore at room temperature and at magnetic fields of the order of 1T, the nuclei will show only a minute tendency to line up with the applied magnetic field on average, in account of the thermal randomizing energy, much greater than the alignment energy. As a result, any effect due to the magnetism of the nuclei requires a resonance technique such as NMR to be detected. One of the basic concepts underlying the NMR technique follows from the observation that the application of a magnetic field $\mathbf{B}$ to a magnetic moment can induce precession of that magnetic moment at an angular frequency given by $|\gamma B|$ where γ is the gyromagnetic ratio. The energy of a magnetic moment $\mathbf{M}$ in a magnetic field $\mathbf{B}$ is given by

$$E = -\mathbf{M} \cdot \mathbf{B}, \tag{51}$$

and it is minimized when the moment is aligned with the magnetic field. Besides, $\mathbf{B}$ will exert a magnetic torque on the magnetic moment $\mathbf{M}$:

$$\mathbf{G} = \mathbf{M} \times \mathbf{B}. \tag{52}$$

If the magnetic moment were not associated with any angular momentum, the torque $\mathbf{G}$ will tend to turn the magnetic moment towards the magnetic field, as in the case of the electric dipole [31]. However, since magnetic moments are associated with angular momentum -see the Einstein-de Haas or the Barnett effects- and because torque is equal to the rate of change of angular momentum, the previous equation can be rewritten as:

$$\frac{d\mathbf{M}}{dt} = \gamma \mathbf{M} \times \mathbf{B}. \tag{53}$$

As a consequence, in close analogy with the spinning of a gyroscope or a spinning top, the magnetic field causes the moment $\mathbf{M}$ to precess around $\mathbf{B}$ with frequency $|\gamma B|$, without changing the length of $\mathbf{M}$ vector. A system of magnetic moments in a magnetic field can thus absorbe energy at this frequency and a resonant absorption of energy from an electromagnetic wave tuned to the correct frequency may be observed [31, 33, 46]. In order to perform a NMR measurement, nuclei with non-zero nuclear spin, i.e. $I \neq 0$, are needed: ^{1}H (proton), ^{2}H (deuteron) and ^{13}C are commonly used. In a generic NMR experiment, a sample is placed inside a coil between the poles of a magnet which produces a uniform static magnetic field $\mathbf{B}_0$ along the z direction. The energy E of the magnetic nucleus in presence of $\mathbf{B}_0$ field is $E = -\mathbf{M} \cdot \mathbf{B}_0 = -g_N \mathbf{M}_N m_I B_0$, and this correspond to a ladder of equally spaced $2I + 1$ levels with mutual separation of $g_N \mathbf{M}_N m_I B_0$. To excite transitions between adjacent pairs of levels with a radiofrequency (RF) field one needs a field $\mathbf{B}_1$ applied orthogonally to $\mathbf{B}_0$, along the x direction, for instance. This leads to a perturbation to the system proportional to $B_1 I_x$, and consequently the matrix element of the perturbation is proportional to $\langle m'_I | I_x | m_I \rangle$. Therefore the selection rule imposed by this perturbation is $\Delta m_I = \pm 1$: only transitions between adjacent levels may occur. Besides, naming ΔE the energy difference between a pair of adjacent levels, the system will undergo a transition if $\hbar\omega = \Delta E$. For a deeper understanding of this process, let us consider a two-level spin system with - and + the lower and the higher level respectively. The probability per unit time of a transition between + and - is

$$|\langle + | I_x | - \rangle|^2 = |\langle - | I_x | + \rangle|^2, \tag{54}$$

and is independent of whether the transition is from the lower to the upper level or *vice versa*, and occurs at a rate W which is proportional to the size of the RF power used to

excite transitions. If $N_-(t)$ is the number of spins in the lower level at a time t, $WN_-(t)$ will be the spins excited per unit time to the higher level. A similar consideration can be done for the spins in the higher level thus having

$$\frac{dN_+(t)}{dt} = WN_-(t) - WN_+(t) \tag{55}$$

$$\frac{dN_-(t)}{dt} = WN_+(t) - WN_-(t). \tag{56}$$

By defining $n(t) = N_+(t) - N_-(t)$, the solution of the two equations above can be written as:

$$n(t) = n(0)e^{-2Wt}, \tag{57}$$

which means that an initial difference in population tends exponentially towards zero in account of a stimulated electromagnetic transition. At a time t the energy of the system is:

$$E(t) = N_-E_- + N_+(E_- + \hbar\omega), \tag{58}$$

and the rate of absorption is:

$$\frac{dE}{dt} = -W\hbar\omega n(t), \tag{59}$$

and will tend to zero with a time constant of $1/2W$, as the populations ot the upper and lower levels become progressively equalized. This implies that it is necessary to have a population difference for the system to absorb energy. After the absorption of energy, polarization may change. Nevertheless, since nuclear spins interact with the thermal motion and excitations of the sample, the polarization of the spin system will return back to the equilibrium value following a Boltzmann distribution:

$$\left(\frac{N_+}{N_-}\right)_0 = e^{-\hbar\omega/k_BT}. \tag{60}$$

By summaryzing, after the stimulated electromagnetic transitions has been switched off the system polarization will recover the equilibrium value in a time T_1. This T_1 is called *spin-lattice relaxation time* and measures the time constant of the interaction of the nuclei with the environment [31, 33, 46]. As a result, the polarization would tend to the Boltzmann distribution as

$$n(t) = n_0(1 - e^{-t/T_1}). \tag{61}$$

By putting together the relaxation process and the stimulated RF transitions, one obtains

$$\frac{d}{dt}n(t) = -2Wn(t) + \frac{n_0 - n(t)}{T_1}. \tag{62}$$

The equation above has a stationary solution when $dn(t)/dt = 0$. This leads to

$$n(t) = \frac{n_0}{1 + 2WT_1} \tag{63}$$

and

$$\frac{dE}{dt} = n(t)\hbar\omega W = n_0\hbar\omega\frac{W}{1 + 2WT_1}. \tag{64}$$

From Eq. (64) it follows that the rate of absorption is proportional to W, but for large perturbing RF fields becomes proportional to $1/T_1$ and independent of the precise value of W: this is known as saturation.

Let us focus on the relaxation process that can be monitored in a typical NMR experience. The weak polarization of nuclear spins produced by an applied magnetic field $\mathbf{B}_0$ -e.g. along z-axis- is destroied by the RF excitations. Once the RF field is switched off, the weak interactions of the nuclei with the surroundings will force the nuclear magnetization to the equilibrium value with a time constant T_1. As a consequence, we expect that

$$\frac{dM_z}{dt} = \frac{M_0 - M_z}{T_1}. \tag{65}$$

This T_1 relaxation must involve interactions with the lattice energy must be exchanged with it. In fact, a change of M_z implies that the nuclear magnetization $\mathbf{M}$ changes with respect to the applied field, and thus relaxing a spin along the z-direction requires an exchange of energy. As regards the in plane components of the magnetization M_x and M_y, they should be zero, but if they are not they will relax to zero in a time T_2 such that:

$$\frac{dM_x}{dt} = -\frac{M_x}{T_2}, \quad \frac{dM_y}{dt} = -\frac{M_y}{T_2}. \tag{66}$$

T_2 is the *spin-spin relaxation time* and causes differences in precession frequency due to interactions of the observed spin with the spins of its neighbours. It can also be due to inhomogeneities of the applied magnetic field $\mathbf{B}$ [31, 33, 46]. The change of M_x or M_y has no energetic consequences since $\mathbf{B}$ is along M_z.

The applied magnetic field also causes spin precession, so that the equations for M_x, M_y and M_z are

$$\frac{dM_x}{dt} = \gamma(\mathbf{M}\times\mathbf{B})_x - \frac{M_x}{T_2} \tag{67}$$

$$\frac{dM_y}{dt} = \gamma(\mathbf{M}\times\mathbf{B})_y - \frac{M_y}{T_2} \tag{68}$$

$$\frac{dM_z}{dt} = \gamma(\mathbf{M}\times\mathbf{B})_z - \frac{M_0 - M_z}{T_1}, \tag{69}$$

which are known as the *Bloch equations*.

For the purpose of experimentally determining T_2 the following technique can be used. In thermal equilibrium with B_1 switched off, there is a weak magnetization parallel to z. A short pulse of RF signal of duration τ, with the frequency $\omega/2\pi$ set to the resonance frequency of the spins, i.e. $\hbar\omega = \Delta E$, forces the spins to rotate by an angle $\gamma B_1\tau$, where B_1 is the amplitude of the RF signal. This angle can be properly varied by changing τ, the duration of the pulse. In particular, if $\tau = \pi/2\gamma B_1$ a *90° pulse* is produced, which means that the weak magnetization parallel to the static $\mathbf{B}_0$ field in thermal equilibrium with B_1 switched off is rotated such as to lie in xy plane. Depending on the amplitude and duration of the pulse, the magnetization precesses for a short period and rotates into xy plane. Being B_1 switched off, the magnetization precesses around $\mathbf{B}_0$ at a frequecy γB_0, producing an oscillation which is damped in account of T_2 relaxation processes (spin-spin relaxation). The oscillation relaxes thus allowing to measure the T_2 by exploiting the *spin echo technique*. Firstly, the application of a 90° pulse tips the spins in xy plane. Because of the steady field $\mathbf{B}_0$ along z-axis, the spins start to precess in xy plane at different rates in account of the inhomogeneities in the magnetic field. This involves the spins to dephase with respect to each other. A subsequent 180° pulse follows at a time $t = \tau$ along the x-axis. This implies that the spins will come back together at a time τ producing a spin echo signal. In this way the problem that the magnetic field is inhomogeneus and the spread in fields due to the chemical shift are removed. Indeed, the spin-spin relaxation mechanism can not be refocused and this causes the echo signal to be reduced in amplitude by an amount which depends on τ. The NMR intensity of the echo signal follows $I(2\tau) = I(0)e^{-2\tau/T_2}$ and a measurement of T_2 is possible. In an analogous way T_1 can be measured. This time a 180° pulse is applied first. As a result, the magnetization is rotated along $\hat{\mathbf{z}}$ to along $-\hat{\mathbf{z}}$. It then relaxes back to $\hat{\mathbf{z}}$ with a time constant T_1. The magnetization as a function of time τ after the 180° pulse is

$$\mathbf{M}(\tau) = M_0(\tau)\hat{\mathbf{z}} = M_0(1 - 2e^{-\tau/T_1})\hat{\mathbf{z}}. \tag{70}$$

After a time τ from the 180° pulse, a 90° pulse is applied: this rotates the magnetization on the xy plane where it now begins to a free indution decay with initial amplitude $M_z(\tau)$. Thus T_1 can be determined by measuring the initial amplitude $M_z(\tau)$ as a function of the time delay between the 180° pulse and the 90° pulse.

3.2.1 Perturbative treatment of the hyperfine dipolar interaction between nuclear and electronic spins

The spin dynamics in magnetic molecules can be probed by NMR. In fact, there exists a link between the electronic spin fluctuations and the measured longitudinal spin-lattice relaxation rate $1/T_1$ as derived by Moriya [47]. By treating the hyperfine dipolar interaction between the electronic and nuclear spins as a perturbation, we have the unperturbed hamiltonian given by

$$H_0 = H_e + H_N \tag{71}$$

where H_e is the molecular hamiltonian, while H_N is the hamiltonian of the nuclei with non-zero magnetic moment which are used as a probe for NMR measurements:

$$H_N = -\sum_i \hbar\omega_L I_{\zeta_i}, \tag{72}$$

where i index runs over all the nuclei which can be probed at ω_L angular Larmor frequency. Besides, ζ-axis defines the direction of the local magnetic field at the nucleus. The perturbation is given by

$$H' = \gamma_e\gamma_N\hbar^2 \sum_{i,l} r_{il}^{-3}\mathbf{I}\cdot\left(1 - 3\frac{\mathbf{r}_{il}\cdot\mathbf{r}_{il}}{r_{il}^2}\right)\cdot\delta\mathbf{S}_i, \tag{73}$$

where γ_e and γ_N are the gyromagnetic ratios of electrons and the probed nuclei, $\mathbf{r}_{il}$ is the vector which defines the relative position of the i electron with respect to the l nucleus, and finally $\delta\mathbf{S}_i = \mathbf{S}_i - \langle\mathbf{S}_i\rangle$. Within this theoretical framework and up to the first order in perturbation theory, the probabilities of transitions of a nuclear spin and thus the nuclear spin relaxation rate $1/T_1$ can be evaluated in terms of spin-spin correlation functions. By summaryzing, exploiting the Moriya formula [47], the NMR $1/T_1$ can be evaluated in absolute units using as inputs the positions of the magnetic ions and of the probed nuclei in the magnetic molecule:

$$\frac{1}{T_1} = \sum_{\substack{i,j=1,N\\ q,q'=x,y,z}} \alpha_{ij}^{qq'}\left(S_{s_i^q,s_j^{q'}}(\omega_L) + S_{s_i^q,s_j^{q'}}(-\omega_L)\right), \tag{74}$$

where the $\alpha_{ij}^{qq'}$ are geometric coefficients of the hyperfine dipolar interaction between magnetic ions and nuclei probed by NMR, while the $S_{s_i^q,s_j^{q'}}(\omega_L)$ are the Fourier transforms of the cross correlation functions calculated at the Larmor angular frequency $\omega_L = \gamma_N B$:

$$S_{s_i^q,s_j^{q'}}(\omega_L) = \frac{1}{2\pi\hbar}\int_{-\infty}^{\infty} dt e^{i\omega_L t}\left\langle s_i^q(t)[s_j^{q'}]^+\right\rangle \tag{75}$$

An expression for the $S_{s_i^q,s_j^{q'}}(\omega_L)$ functions will be given in Chapter 6 (see also Appendix A).

Chapter 4

Neutron spectroscopy and magnetization study of two spin segments: Cr_8Zn and Cr_8Cd compounds

In this chapter results of INS cross sections on Cr_8Zn and magnetization measurements on Cr_8Cd will be interpreted. The two compounds have not exactly the same chemical structure. Nonetheless they can be regarded as magnetically equivalent. In fact, both clusters were derived by insertion of a non-magnetic ion (Zn^{2+} or Cd^{2+}) in the ring-shaped structure of the well-known Cr_8 compound. The presence of the non magnetic ion prevents the exchange interaction between a couple of spins, thus causing a breaking of the ring symmetry. On the one hand, qualitative differences can be found in the energy level diagrams as inferred in magnetization measurements by the different set of level crossing fields from the open and the close version of the ring. On the other hand, it is the internal structure of the spin eigenstates, probed through the dependence of the neutron cross-section on the wave vector transfer, which allows to distinguish the close Cr_8 ring from the two derived spin segments at the microscopic level.

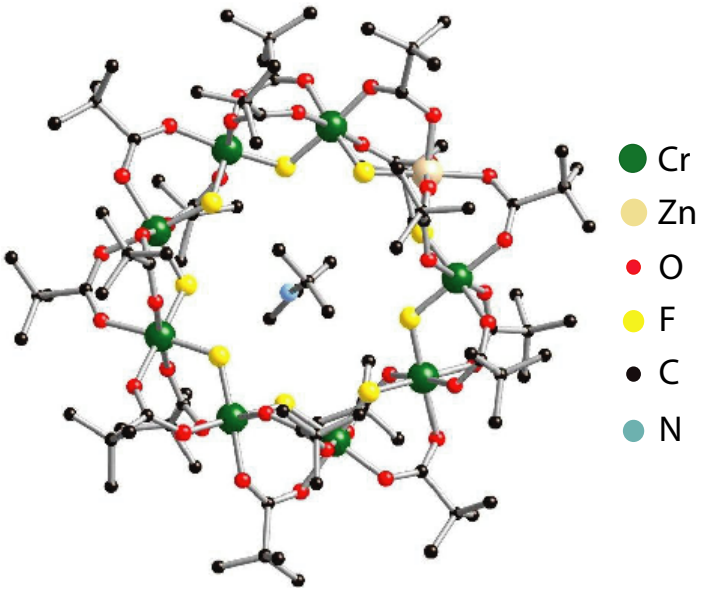

Figure 8: The structure of a Cr_8Zn molecule. The hydrogen atoms have been omitted for clarity.

4.1 Rotational band picture in rings and spin segments

A great variety of magnetic clusters have been synthesized in recent years. Of particular interest both for fundamental physics and for technological applications are antiferromagnetic (AF) ring-shaped clusters, formed by a set of N transition metal ions arranged in an almost cyclic planar structure. The possibility to chemically substitute metal ions in the cyclic structure allows to control microscopic exchange interactions and, as a consequence, the energy and spin wave functions of the low-lying states [30]. The Cr_8Zn cluster was derived by inserting a non magnetic Zn^{2+} ion in the ring-shaped structure of the well-known Cr_8 compound. This lowers the ideal ring symmetry by preventing exchange interaction between two of the spins. As a result, the Cr_8Zn molecule can be regarded as a finite spin segment and thus a model system for investigating magnetic properties and finite-size effects in the one-dimensional AF Heisenberg model.

Even-membered homonuclear AF rings present common features in the energy spectrum: due to the compensation of the N spins they have a singlet $S = 0$ ground state, whereas low-lying excited levels are arranged into rotational bands, with the lowest one (L-band) approximately following the so-called Landé rule $E(S) = 2JS(S+1)/N$ with J the exchange constant and S the total spin of the state [1,48,49]. If an external

magnetic field **H** is applied to the molecule, the spin ground state will sequentially change from $S = 0$ to $S = 1, 2, 3, ..., 12$ as H increases, but each of these states will always belong to the L-band. The second set of levels belongs to the so-called E-bands, which are also parabolic with respect to S but shifted to higher energies. In closed homometallic rings states can be classified according to the quantum number $k = 2\pi j/N$ ($j = 0, ..., N-1$) of the cyclic shift operator T, whose eigenvalues are e^{ik}. While the L-band states have wavevector $k = 0$ or π, for E-band states $k = 2\pi j/N$ with $j \neq 0, N/2$. The concept of rotational band has also been exploited to rationalize the low-temperature behavior of the complex Fe_{30} molecule, where three sublattices can be identified in its icosidodecahedron structure [10, 50, 51].

The energies of L-band states in the opened Cr_8 ring have already been investigated by macroscopic measurements on Cr_8Cd [7, 52]. Magnetization and heat capacity measurements showed deviations from the Landé rule, with a resulting different set of level crossing fields [7]. While these measurements provided information on the energy of the lowest (Landé) rotational band, the internal structure of eigenstates could not be directly probed. In addition, the higher-energy E-band states could not be directly accessed. In this paper, we exploit inelastic neutron scattering (INS) to probe the lowest-lying eigenstates of Cr_8Zn and we quantitatively analyze how the opening of the ring changes the structure of these eigenfunctions with respect to the closed version of the ring. In particular, we experimentally and theoretically show how the occurrence of disjoint quantum fluctuations of the total spin length of the two sublattices removes the sharp separation of the low-lying states in two distinct rotational bands.

4.2 Theory

The microscopic picture of the heteronuclear open-ring Cr_8Zn is based on the following spin Hamiltonian:

$$\begin{aligned} H &= J\sum_{i=1}^{7}\mathbf{s}(i)\cdot\mathbf{s}(i+1) + \sum_{i=1}^{8} d_i\left[s_z^2(i) - s_i(s_i+1)/3\right] \\ &+ \sum_{i>j} D_{ij}\left[2s_z(i)s_z(j) - s_x(i)s_x(j) - s_y(i)s_y(j)\right] \\ &+ \sum_{i=1}^{8} e_i\left[s_x^2(i) - s_y^2(i)\right] - \mu_B\sum_{i=1}^{8} g_i\mathbf{H}\cdot\mathbf{s}(i), \end{aligned} \tag{76}$$

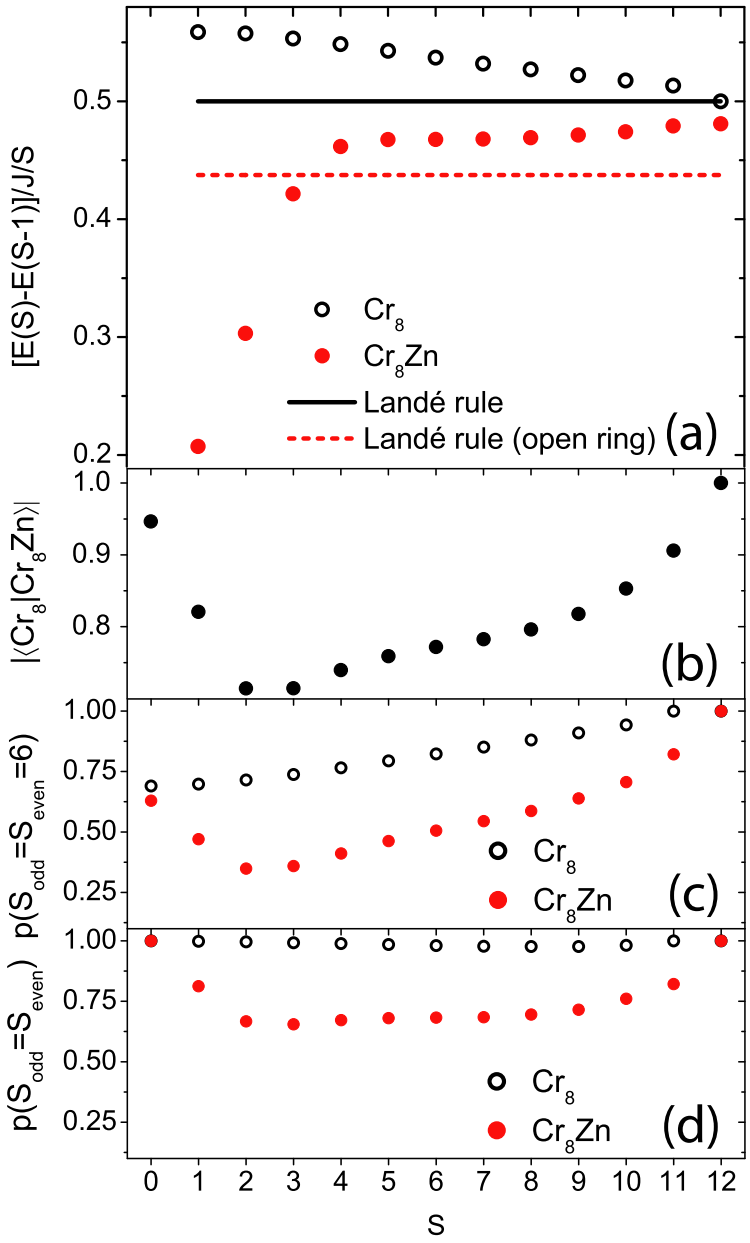

Figure 9: (a): Energy difference between two adjacent levels of the L-band for Cr_8 and Cr_8Zn. A deviation from the Landé rule can be seen for the open ring Cr_8Zn. (b): modulus of the scalar product between L-band states for the closed Cr_8 and the open Cr_8Zn rings. (c): weight of the Landé component (i.e., with $S_{odd} = S_{even} = 6$) in the L-band states of Cr_8 and Cr_8Zn. (d): weight of the component with $S_{odd} = S_{even}$ in the L-band states of Cr_8 and Cr_8Zn. This represents the probability of finding the same length for the total-spin of the two sublattices.

	Cr_8Zn	Cr_8
+	$\|L_{S=0}\rangle =$	$0.947\,\|L_{S=0}\rangle + ..$
-	$\|L_{S=1}\rangle =$	$0.821\,\|L_{S=1}\rangle - 0.243\,\|E^1_{S=1}\rangle - 0.242\,\|E^4_{S=1}\rangle + ..$
-	$\|E^1_{S=1}\rangle =$	$0.517\,\|L_{S=1}\rangle + 0.537\,\|E^1_{S=1}\rangle + 0.286\,\|E^4_{S=1}\rangle + ..$
+	$\|E^2_{S=1}\rangle =$	$0.468\,\|E^2_{S=1}\rangle + 0.689\,\|E^3_{S=1}\rangle - 0.318\,\|E^5_{S=1}\rangle + ..$
-	$\|E^3_{S=1}\rangle =$	$0.108\,\|L_{S=1}\rangle - 0.535\,\|E^1_{S=1}\rangle + 0.684\,\|E^4_{S=1}\rangle + ..$
+	$\|E^4_{S=1}\rangle =$	$0.778\,\|E^2_{S=1}\rangle - 0.372\,\|E^3_{S=1}\rangle + ..$
+	$\|E^5_{S=1}\rangle =$	$0.12\,\|E^2_{S=1}\rangle + 0.276\,\|E^3_{S=1}\rangle + 0.843\,\|E^5_{S=1}\rangle + ..$
-	$\|E^6_{S=1}\rangle =$	$0.356\,\|E^1_{S=1}\rangle - 0.77\,\|E^6_{S=1}\rangle + ..$

Table 2: Lowest-lying L- and E-like eigenstates of Cr_8Zn (left) in terms of eigenvectors of Cr_8 (right), see also Fig. 10. The states are classified according to their parity with respect to the C_2 symmetry operation (given in the first column). The degenerate (k, $-k$) E-band states of Cr_8 here have been combined in symmetric and antisymmetric superpositions having definite parity. Only dominant components on L and E states are shown. In Cr_8Zn, several $S = 1$ states have a non zero scalar product with the lowest $S = 1$ multiplet of Cr_8, and thus acquire a Landé-type contribution.

where $\mathbf{s}(i)$ is the spin operator of the the ith ion in the molecule ($s(i)$=3/2 for Cr^{3+} ions, and $s(i)$=0 for the non magnetic Zn^{2+} ion). Here we assume that the Zn^{2+} ion is in site $i = 9$. In the first term of the above equation, J represents the strength of the isotropic Heisenberg nearest neighbour exchange interaction. The second and third terms describe the axial anisotropic interactions (with the z axis perpendicular to the plane of the ring), i.e., local crystal-fields (CFs) and the axial part of the dipolar interaction. D_{ij} is calculated in the point dipole approximation. The fourth term accounts for small non-axial anisotropy. While the actual local CFs may be much more complex than assumed in Eq. (76), experimental data are nowhere near sufficient to fix more than two CF parameters. The last term represents the Zeeman coupling with an external field $\mathbf{H}$. We use the expression given in Ref. [30] in order to simulate the powder neutron scattering data.

Since isotropic exchange (H_{iso}) is the dominant interaction in (76), the energy spectrum is composed of total-spin multiplets split by local crystal fields. The mixing between different spin multiplets due to anisotropic interactions (S mixing) is small and does not affect the following discussion. As mentioned above, it is well known that in closed bipartite AF rings the lowest-lying multiplets are arranged in two bands (L and E) which can be approximately described by the effective three-rotor Hamiltonian

$$H_{rot} = J'\mathbf{S}_{odd} \cdot \mathbf{S}_{even} \tag{77}$$

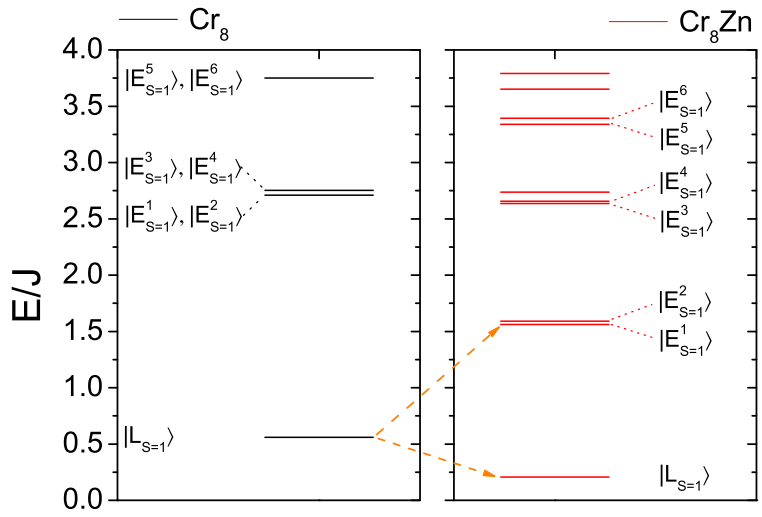

Figure 10: Energy of the low-lying triplet eigenstates of H_{iso} for Cr_8 and Cr_8Zn. For the latter, the labelling of states as L or E refers to the dominant component in the state.

with N the number of sites, $\mathbf{S}_{odd,even}$ the total spin of the two sublattices and $J' = \frac{4J}{N}$. The eigenvectors of (2) have the form $|\alpha S_{odd} S_{even} SM\rangle$, where α denotes additional quantum number specifying the internal structure of each sublattice. The corresponding eigenvalues are $2J/N(S(S+1) - S_{even}(S_{even}+1) - S_{odd}(S_{odd}+1))$. L-band multiplets are nondegenerate, have $k = 0$ or π and correspond to $S_{even} = S_{odd} = Ns/2$, whereas E-band states correspond to $|S_{even} - S_{odd}| = 1$ and $S_{even} + S_{odd} = (Ns - 1)$. The multiplet degeneracy is $N - 2$ and $k \neq 0, \pi$. The actual exchange hamiltonian $H_{iso} = H_{rot} + \Delta H$, where ΔH only connects states having the same value of k. Hence L- and E-band states do not mix in closed rings. To a very large extent, the effect of ΔH in L-band states is to add smaller components having $S_{odd} = S_{even} < Ns/2$, i.e., ΔH induces joint quantum fluctuations of the total spin length of the two sublattices (see Fig. 9). A similar situation of joint fluctuations occurs for E-band states, where the leading corrections have $S_{even} + S_{odd} < (Ns - 1)$, but still $|S_{odd} - S_{even}| = 1$. The E-band degeneracy $(N - 2)$ is partially lifted into $(N - 2)/2$ pairs of multiplets, each pair being characterized by a given value of $|k|$.

If the ring is magnetically opened, the rotational bands picture (with $J' = \frac{4(N-1)J}{N^2}$) breaks down (see Fig. 9). In fact, since the shift operator does not commute with H_{iso} anymore the wavevector quantum number is meaningless and only the parity with

respect to the remaining in-plane C_2 symmetry can be specified. Of course, this implies that the degeneracy of the k, $-k$ pairs in the E-band is removed. The resulting eigenstates therefore contain symmetric and antisymmetric combinations of the previously degenerate k and $-k$ states (called standing spin waves in [53]). However, the standing-spin-wave component is minoritary in most of the actual eigenstates (see Table I). Indeed, states having different value of $|k|$ are strongly mixed. In particular, ΔH directly mixes L-band states ($k = 0, \pi$) with E-band states having the same S and the same parity. The resulting states contain both components with $S_{even} = S_{odd}$ and components $S_{even} \neq S_{odd}$. Hence, in open rings quantum fluctuations of the total spin of the two sublattices do not occur jointly, not even at zero or low temperature. An exception is given by the ground $S = 0$ and the ferromagnetic $S = 12$ states, which remain very close to those of the closed ring. Indeed, if $S = 0$ or $S = 12$ there are no E-band states because necessarily $S_{even} = S_{odd}$.

The previous picture can be directly demonstrated by INS experiments. In fact, a mixing of L- and E-band states has characteristic consequences in the momentum-transfer dependence of the INS intensities and in the effective anisotropy and in the energy of the lowest-lying $S = 1$ states. These aspects will be discussed below, where the labelling of states as L or E is still used for simplicity and refers to the dominant component in the state.

4.3 Inelastic neutron scattering experiments

The INS experiments were performed using the time-of flight Disk Chopper Spectrometer at the NIST Centre for Neutron Research, Gaithersburg, MD (USA) [54]. For the INS experiment, 3.8 g of partially deuterated $[H_2N_{is}Pr_2][Cr_8ZnF_9\{O_2CC(CD_3)_3\}_{18}]$ microcrystalline samples (abbreviated Cr_8Zn) has been prepared according to a slightly modified literature procedure reported in [55] for $[H_2N_{is}Pr_2][Cr_8ZnF_9\{O_2CC(CD_3)_3\}_{18}]$ by dissolving chromium(III) fluoride trihydrate in a mixture of trimethyl-*d9*-acetic acid and diisopropylamine followed by addition an excess of the basic zinc carbonate. The preparation of trimethyl-*d9*-acetic acid starting from acetone-*d6* was adapted from standard methods [56]. Cr_8Zn-d was crystallized from toluene and then dried *in vacuo*. All procedures were performed under dried nitrogen atmosphere and all used solvents were anhydrous. Elemental analysis and the electrospray mass spectrometry confirmed the chemical compositions of this compound. The sample was packed into a hollow

aluminum cylinder (20 mm diameter and 0.7 mm sample thickness) and was inserted into a standard ILL cryostat to cool down to a base temperature of 1.5 K. Measurements were performed at different temperatures, ranging from 1.5 K to 15 K. The instrument was operated in the "low resolution" mode [54] and measurements were performed using four different incident neutron wavelengths, i.e. 3.8, 4.5, 6 and 7 Å. Measurements on an empty Al can were used for the background subtraction and a vanadium sample was used for detector calibration. The spectra were integrated over the whole detector bank. The transition from the S=0 ground state to the first S=1 excited state in the Landé band was probed with an incident wavelength of 7 Å (42 μeV full width at half maximum (FWHM) energy resolution at the elastic peak). At a base temperature of 1.5 K we observed two sharp transitions at about 0.2 and 0.3 meV energy transfer [Fig. 11(a)], a much lower energy than what was observed on the Cr_8 parent compound, where the equivalent transitions were observed at 0.7 and 0.9 meV respectively [39]. Higher energy transitions to the E-band could be observed using a lower incident wavelength $\lambda = 3.8$ Å (giving a FWHM 220 μeV at the elastic peak), as shown in Fig. 11(b).

The microscopic parameters of the spin Hamiltonian Eq. (76) have been varied in order to obtain the best fit of the calculated INS cross section to the neutron data. In the fitting procedure a Gaussian line shape is associated with each allowed transition, with the full width at half maximum fixed to the instrumental resolution and the area proportional to the calculated transition strength. Figure 11 shows the INS spectra collected at $\lambda = 7$ Å and $\lambda = 3.8$ Å. The solid lines represent the calculated INS intensity with parameters $J = 1.32$ meV, $d = -0.028$ meV, $|e| = 0.003$ meV [1]. In order to improve the fit a small next-nearest-neighbour exchange interaction has to be introduced, with exchange integral $J_{nnn} = -0.01$ meV. Alternatively, a set of slightly bond-dependent nearest-neighbour exchange constants can be assumed. The resulting simulations reproduce the experimental data very well. The uniaxial CF parameter obtained for Cr_8Zn is $d = -0.028$ meV, very close to the one reported for Cr_8 ($d = -0.029$ meV) [39]. The two peaks emerging in Fig. 11(a) at 0.2 meV and 0.3 meV correspond to the transition from the ground state $|L_{S=0}\rangle$ to the first-excited $|L_{S=1}\rangle$ multiplet, split by the single ion uniaxial CF terms. The in-plane anisotropy has been

[1] The axial dipole-dipole interaction has similar effects as the single ion axial anisotropy. Therefore, a very good agreement between calculated and measured INS spectra is once again obtained if the d parameter is suitably rescaled to the value of d=-0.036 meV, and understood as to include both the CF and the dipolar contributions.

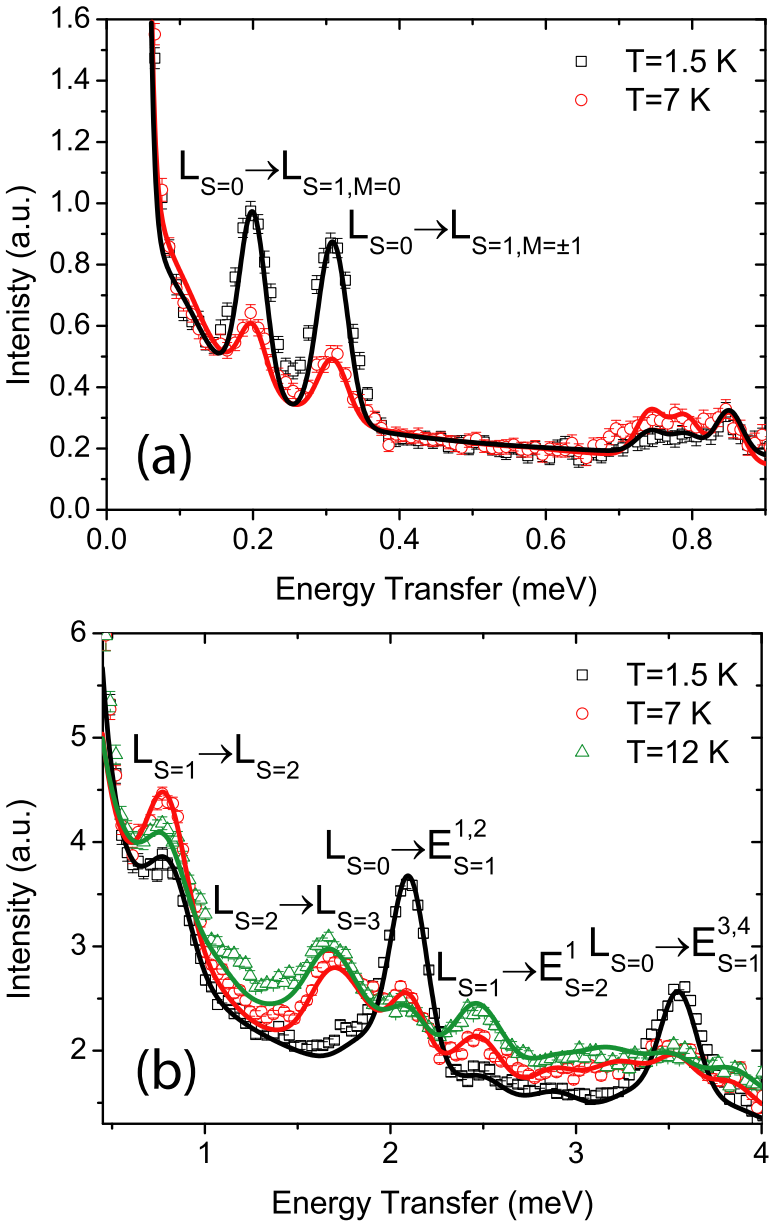

Figure 11: Cr_8Zn INS spectra at low energy collected with λ=7 Å at $T = 1.5$ K (squares) and $T = 7$ K (circles) in panel (a) and with λ=3.8 Å at T=1.5 K (squares), T=7 K (circles) and $T = 12$ K (triangles) in panel (b). Solid lines represent calculated spectra with INS cross section obtained in Ref. [30] and from eigenvalues and eigenvectors of Eq. (76) with the following set of parameters: $J = 1.32$ meV, $J_{nnn} = -0.01$ meV, $d = -0.028$ meV, $|e| = 0.003$ meV, where J_{nnn} is the the parameter of next nearest neighbours exchange interaction. The error bars in all the figures represent standard deviations in the measurement.

taken into account in order to reproduce the correct intensity of the second peak in Fig. 11(a) which involves two otherwise degenerate transitions $|L_{S=0}\rangle \rightarrow |L_{S=1}, M = \pm 1\rangle$. By reducing the incident wavelength it is possible to observe transitions involving higher-lying excited spin multiplets. In Fig. 11(b), the first peak in the spectrum at $T = 1.5$ K originates from the thermally-activated transition between the Landé states $|L_{S=1}\rangle$ and $|L_{S=2}\rangle$, while the other peaks are due to transitions from the ground state $|L_{S=0}\rangle$ to the excited $\left|E^{1,2}_{S=1}\right\rangle$ and $\left|E^{3,4}_{S=1}\right\rangle$ states. At higher temperatures, two further peaks emerge in the spectrum, corresponding to transitions between the L states $|L_{S=2}\rangle$, $|L_{S=3}\rangle$ and between $|L_{S=1}\rangle$ and the lowest E-type $S = 2$ multiplet. We have performed further measurements at intermediate wavelengths that are once again very well reproduced by theoretical simulations.

4.4 Discussion

Closed rings are characterized by the presence of a hierarchy of overall INS transition strengths: in decreasing order $L \rightarrow L$ (LL), $L \rightarrow E$ (LE) and $L \rightarrow$quasi-continuum (LQC). The above-discussed breakdown of the band picture in the open AF ring Cr_8Zn does not unambiguously show up in integrated INS intensities. However, it becomes apparent by inspecting the dependence of the INS intensity $I(Q)$ on the scattering wave vector Q, a quantity which more selectively senses the internal structure of eigenfunctions. The behavior of $I(Q)$ can be understood by expressing the eigenstates of the Cr_8Zn isotropic exchange Hamiltonian in terms of those of Cr_8 (see Table 2), and by taking into account that for the latter molecule inter-band INS transitions are less intense than intra-band ones. The first-excited $S = 1$ state of Cr_8Zn ($|L_{S=1}\rangle$ in Fig. 10) has a dominant contribution from the Landé-band $|L_{S=1}\rangle$ state of Cr_8. Therefore, for the transition between the ground $|L_{S=0}\rangle$ state and $|L_{S=1}\rangle$, $I(Q)$ is similar to that of the corresponding transition of Cr_8 (reported in [39,49]). A remarkable difference with respect to Cr_8 is expected for the unresolved transitions between the ground $|L_{S=0}\rangle$ state and states $|E^1_{S=1}\rangle$ and $|E^2_{S=1}\rangle$. In fact, in the open ring $|E^1_{S=1}\rangle$ acquires a large component of the Landé $|L_{S=1}\rangle$ state of Cr_8. Since a LL transition has much more INS intensity than an LE or an LQC transition, most of the scattering for the unresolved $|L_{S=0}\rangle \rightarrow |E^1_{S=1}\rangle$, $|E^2_{S=1}\rangle$ transitions is produced by the Landé component in $|E^1_{S=1}\rangle$. Thus, $I(Q)$ for these transitions should be close to $I(Q)$ for the $|L_{S=0}\rangle \rightarrow |L_{S=1}\rangle$ transition. This picture is confirmed by the agreement between calculated and experimental $I(Q)$ in Fig. 12(a): the shape of $I(Q)$ is similar for energy transfers around 0.25 and

2 meV. This proves the presence of the Landé-type contribution ($S_{odd} = S_{even}$) to the lowest E-state of Cr_8Zn (see Table 2). Since all remaining E states contain at most a small fraction of the $|L_{S=1}\rangle$ state of Cr_8, $I(Q)$ for the corresponding $|L_{S=0}\rangle \rightarrow |E_{S=1}\rangle$ transitions is markedly different and recalls that of the $|L_{S=0}\rangle \rightarrow |E_{S=1}\rangle$ transitions of Cr_8 [Fig. 12(b)].

Another consequence of the breakdown of the band picture is the decrease of the effective axial anisotropy of the $|L_{S=1}\rangle$ multiplet for Cr_8Zn with respect to Cr_8. As we have stressed above, the microscopic axial CF parameter d is almost the same in Cr_8 and Cr_8Zn. However, the way such anisotropy terms project onto the $|L_{S=1}\rangle$ multiplet to split it into a singlet $M = 0$ state and a quasi-doublet $M = \pm 1$ depends on the internal structure of the multiplet. Indeed, the presence of sizeable E components in the $|L_{S=1}\rangle$ multiplet of Cr_8Zn almost halves its effective anisotropy. The reason is that for the E-states of Cr_8, each of the eight local CF terms yields much smaller contributions to the effective anisotropy than for L-states of the same S. This effective-anisotropy reduction is directly evidenced by the energy difference between the two peaks at 0.2 and 0.3 meV in Fig. 11(a), which is half the difference observed in Cr_8 [39].
The lowering of the gap between $|L_{S=0}\rangle$ and $|L_{S=1}\rangle$ in Cr_8Zn [Figs. 10 and 11(a)] with respect to Cr_8 [39] again reflects the presence of E-components in $|L_{S=1}\rangle$, i.e., the appearance of disjoint quantum fluctuations of the total spins of the two sublattices. In fact, the ground-state energy in the open ring is nearly $(N-1)/N$ times the ground-state energy of the closed ring as the associated wavefunctions $|L_{S=0}\rangle$ almost coincide (Table I). On the other hand, $|L_{S=1}\rangle$ in the open ring can be written as $|L_{S=1}\rangle = c_a |a\rangle + c_b |b\rangle$, where $|a\rangle$ and $|b\rangle$ are two orthogonal states characterized respectively by having $S_{odd} = S_{even}$ and $S_{odd} \neq S_{even}$. By considering only the Heisenberg isotropic exchange, the energy $E(L_{S=1}) = \langle L_{S=1}| H_{Heis} |L_{S=1}\rangle = c_a^2 \langle a| H_{Heis} |a\rangle + c_b^2 \langle b| H_{Heis} |b\rangle + c_a c_b [\langle a| H_{Heis} |b\rangle + \langle b| H_{Heis} |a\rangle]$. For Cr_8Zn the gap is $E(L_{S=1}) - E(L_{S=0}) \approx 0.21J$ [Figs. 10 and 11(a)], much smaller than the gap of $\approx 0.56J$ of Cr_8. The origin of this decrease can be understood by forcing to zero the contribution of the configurations with $S_{odd} \neq S_{even}$, i.e., imposing $c_a = 1$ and $c_b = 0$. The resulting gap becomes $\approx 0.59J$, even larger than in Cr_8. This shows that the decrease of the gap is not due to a change in the Landé-type ($S_{odd} = S_{even}$) component $|a\rangle$, but rather to the presence of the E-type ($S_{odd} \neq S_{even}$) contributions.

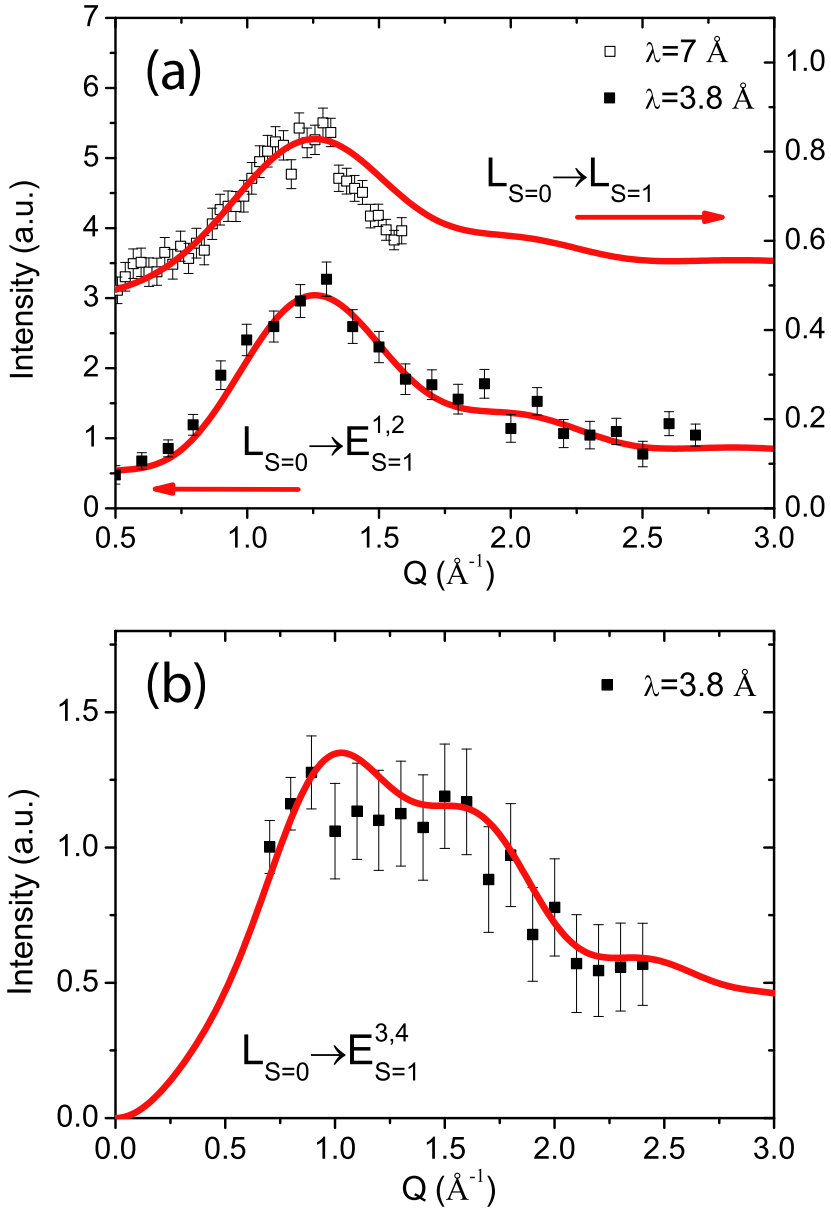

Figure 12: INS spectra as a function of the scattering vector amplitude Q obtained with incident wavelength λ=7 and 3.8 Å and sample temperature $T = 1.5$ K. Calculations are represented by continuous lines.

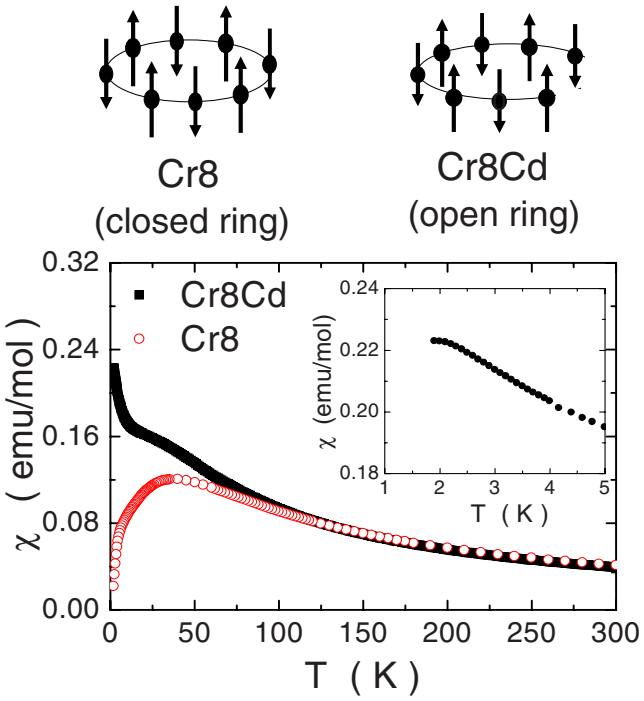

Figure 13: (Top) schematic views of Cr_8 (closed ring) and Cr_8Cd (open ring). (Bottom) Temperature dependence of magnetic susceptibility of Cr_8 (open circles) at H=1.28 T and Cr_8Cd (closed squares) at H=1.0 T. The inset shows the T dependence of χ for Cr_8Cd in low-temperature region.

4.5 Magnetization study of Cr_8Cd

In this section, a comprehensive study of the magnetic properties of the "open" ring Cr_8Cd and "closed" ring Cr_8 revealed by high-field magnetization measurements at very low temperatures is reported. The observed magnetization processes are well reproduced by theoretical calculations and the differences in the two systems can be explained entirely by the different topology of the magnetic interactions. The polycrystalline samples of $(Me_2CH_2)NH_2[Cr_8CdF_9(O_2C\,C(CH_3)_3]_{18}$ and $[Cr_8F_8(O_2CC(CH_3)_3)_{16}]$ $0.25C_6H_{14}$ were prepared as described in Refs. [55] and [57] respectively. The temperature dependence of the magnetic susceptibility was measured in a temperature range of T=1.8-300 K using a superconducting quantum interference device (SQUID) magnetometer (Quantum Design MPMS-7T). The magnetization curve was measured using a pulsed magnet up to 57 T and at a temperature below 1 K utilizing ^{3}He-^{4}He dilution refrigerator at the ISSP of the University of Tokyo. The duration of the pulsed magnetic field is about 6 ms. The temperature dependence of the magnetic susceptibility

for Cr_8Cd is shown in the bottom part of Fig. 13, together with the one of Cr_8 for comparison. The T dependence of Cr_8 agrees with the one reported previously [57]. The broad maximum around 40 K is due to the antiferromagnetic interactions between the Cr^{3+} spins. The χ tends to zero at low temperatures, reflecting the spin singlet ground state. At high temperature, above ∼100 K, where each Cr^{3+} spin fluctuates independently, the susceptibility of both rings coincides with each other very well. With decreasing T, χ for Cr_8Cd starts to deviate from that of Cr_8 below ∼70 K and keeps increasing down to 2 K with a shoulder around ∼40 K. The χ in the open ring seems to display a maximum around 2 K as shown in the inset of Fig. 13. Figures 14(a) and 14(b) show the magnetization (M) curves for Cr_8Cd (T=0.5 K) and Cr_8 (T=0.15 K) respectively, for increasing magnetic field. In both systems, a clear step-wise increase in magnetization is observed. At low magnetic field, M is observed to be zero for both systems. This is a direct evidence of a singlet ground state for the "open" ring Cr_8Cd as well as for the "closed" ring Cr_8. Thus the χ of Cr_8Cd is expected to decrease below 2 K and will go to zero at low temperatures due to the singlet ground state. The M rapidly increases step by step with plateaus of ∼2 μ_B, ∼4 μ_B, ∼6μ_B, ..., at the transition fields H_n ($n = 1, 2, 3, \ldots$). The H_n's were determined by the peak positions of dM/dH curves which are shown by orange lines in Figs. 14(a) and 14(b) for Cr_8Cd (T=0.5 K) and Cr_8 (T=0.15 K) respectively. The magnetization curves are nearly the same with no evident hysteresis for the up and down magnetic-field processes. On the other hand, we observed butterfly-type hysteresis in magnetization curves for both systems for increasing and decreasing magnetic field at T=1.3 K. The hysteresis behavior of the magnetization for Cr_8 is shown in Fig. 15, as an example. The observation of the hysteresis behavior of the magnetization originates from nonequilibrium conditions because of the use of a pulsed magnetic field with a few milliseconds duration. Similar hysteresis of the magnetization curve measured utilizing a pulsed magnet have been observed for several magnetic nanomagnets [58, 59, 60] and discussed in terms of phonon bottle-neck effects and/or magnetic Föehn effects [61, 62]. It is also interesting to point out in Fig. 14(b) the small increase in M for Cr_8 around the middle point in each plateau. This originates from level crossings at excited energy levels. The detailed analysis of the hysteresis behavior observed at T =1.3 K and magnetization jump due to the excited energy level crossings will be reported elsewhere [9]. The most striking difference between closed ring and open ring is found in the transition fields. The first level crossing field from S=0 to S=1 is ∼7.3 T for Cr_8 and 2.3 T for Cr_8Cd. The difference cannot be explained by a small difference of the exchange coupling constants. In

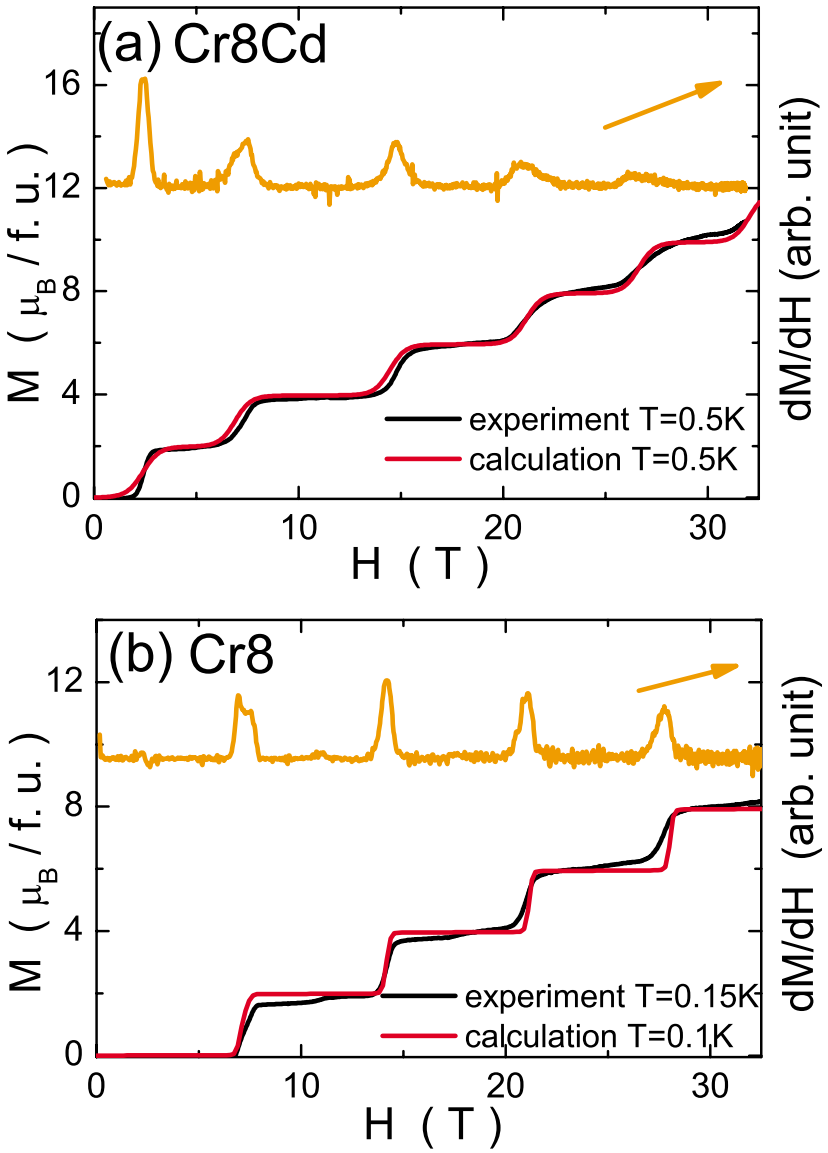

Figure 14: (a) Magnetization curve of Cr_8Cd measured at T=0.5 K. The red line shows the theoretical calculated result for T=0.5 K with the set of parameters: J_{Cr-Cr} =15.2 K, d_{Cr}=-0.3 K, and g_{Cr}=1.98. The orange line shows the experimental dM/dH curve. (b) Magnetization curve for Cr_8 at T=0.15 K. The red line is the theoretical calculated result for T=0.1 K and parameters: J_{Cr-Cr}=16.9 K d_{Cr}= -0.3 K, and g_{Cr}=1.98. The orange line shows the experimental dM/dH curve.

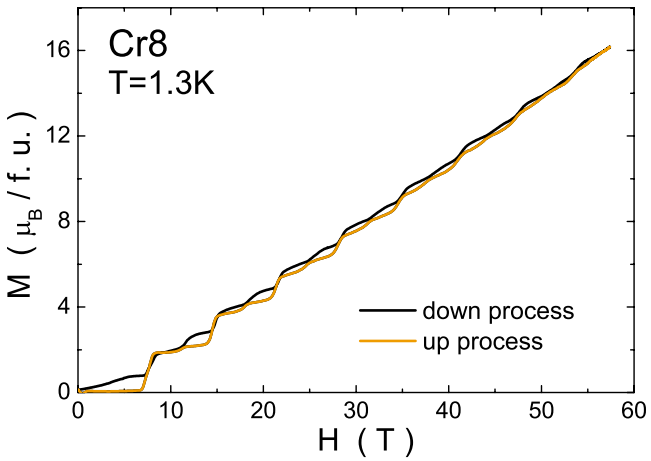

Figure 15: Magnetization curves at T=1.3 K for Cr_8. The orange and black lines are for increasing and decreasing field respectively.

addition, the separation of magnetic fields between the level crossing fields defined as $\Delta H_n = H_n - H_{n-1}$ (where H_0 is zero) is also different as shown in Fig. 16. ΔH_n for Cr_8 slightly decreases from 7.3 T for n=1 to ~6.6 T with increasing n. On the contrary, for Cr_8Cd, ΔH_n initially increases from 2.3 T (n=1) to 7.2 T (n=3) then decreases to 5.4 T (n=5). Another interesting feature expected from the topological effects is the magnetic moment redistributions in the magnetic ground state. In a closed ring, the excitation energy does not depend on the position so that one can expect uniform spin moment distributions in the magnetic ground state. In other words, the excited magnon (so-called triplon) delocalizes in the ring. On the other hand, in the case of the open ring, as the excitation energy depends on the position, the spins at the edge position would be polarized easier than in other positions. This can be regarded as a localization of the magnons at the edge position. Thus the magnetic moments depend on the position in the open ring system. To make the above idea more quantitative, we have carried out theoretical calculations for the Cr-based ring system where each magnetic ion has s=3/2. The starting spin Hamiltonian describing the AF ring-shaped clusters is

$$H = J\sum_{m-1}^{i=1}\mathbf{s}_i\cdot\mathbf{s}_{i+1} + J'\mathbf{s}_8\cdot\mathbf{s}_1 + \sum_{i=1}^{m} d_{Cr}\left[s_z^2(i) - \frac{1}{3}s_i(s_i+1)\right] - g_{Cr}\mu_B\sum_{i=1}^{m}\mathbf{H}\cdot\mathbf{s}_i \qquad (78)$$

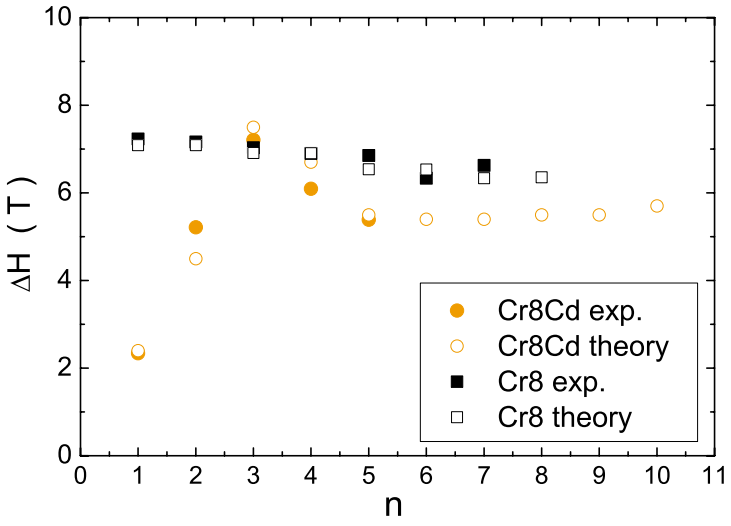

Figure 16: ΔH_n as a function of n. The closed and open symbols show experimental and theoretical results respectively. The experimental data are taken from the experimental results shown in Fig. 14.

where m is the number of magnetic ions. The first and second terms are the isotropic nearest-neighbor Heisenberg interaction. J' is equal to J for Cr_8 while J is assumed to be zero for Cr_8Cd because the Cd ions have no magnetic moment. We also assume that the small next-nearest-neighbour interaction is neglected. The third term describes local crystal fields (d_{Cr} represents a uniaxial anisotropy) and the fourth term represents the Zeeman interaction (g_{Cr} is g-factor for the Cr^{3+} ions). The Hamiltonian is diagonalized by following a perturbative procedure described in Refs. [39, 63, 64]. Calculated eigenstates and eigenvalues have been used to evaluate the magnetic-field dependence of the thermal averaged magnetization and the local magnetic moments. Since we used polycrystalline samples, calculations are powder-averaged. With a set of parameters of J_{Cr-Cr}=16.9 K, d_{Cr} =-0.3 K and g_{Cr}=1.98, the magnetization curve for the Cr_8 is well reproduced by the calculations [see Fig. 14(b)]. The n dependence of ΔH_n is also well reproduced by the theory as seen in Fig. 16. The theoretical estimate of ΔH_n is done by determining H_n from the peak positions of dM/dH for the calculated powder-averaged M. The experimental results for Cr_8Cd are also well reproduced by the calculations with the set of parameters: J_{Cr-Cr}=15.2 K, d_{Cr}=-0.3 K, and g_{Cr} =1.98, as shown by the red line in Fig. 14(a). Interestingly, the peculiar behavior of ΔH_n in Cr_8Cd is almost perfectly reproduced by the calculations as shown by orange open circles in Fig. 16. As expected, a large difference of distributions for

the magnetic moments on different Cr sites in the closed and open nanomagnets is evidenced by the theoretical calculation. In the case of the closed ring Cr_8, the magnetic moment on the Cr ions is zero in S=0 ground state below the first level crossing field of ∼7.3 T. Above the crossing field, the Cr ions have a uniform local magnetic moment of 1/4 μ_B for each ion in the S=1 state, as shown by the dotted line in Fig. 17. This can be interpreted as a consequence of the delocalized traveling triplon with S=1. On the contrary, the breaking of the ring symmetry in the open ring Cr_8Cd leads to redistributions of magnetic moments with a staggered spin structure as a consequence of the localized triplon on the edge sites. The site dependence of the magnetic moments on Cr ions is shown by solid lines in the figure. Cr ions near the Cd ions possess the largest magnetic moment, while the magnetic moment on Cr ions decreases with increasing distance from the Cd ions. Note that spins in Cr_8Cd align not uniformly (ferromagnetically) as in Cr_8 but staggeringly (antiferromagnetically). These results indicate that the microscopic spin structure in the magnetic ground states is different in the two systems, although the macroscopic total magnetic moment is the same. To confirm the spin moment distribution from the experimental point of view, a nuclear magnetic resonance (NMR) measurement is one of the most powerful tools. For example, local magnetic moment for each Cr ion has been revealed by ^{53}Cr-NMR in an odd numbered "open" ring nanomagnet Cr_7Cd [65]. The ^{53}Cr-NMR measurements for Cr_8 and Cr_8Cd are currently in progress. In conclusion, the magnetic properties of two different antiferromagnetic ring-shaped nanomagnets Cr_8 and Cr_8Cd have been investigated experimentally and theoretically. Different magnetic couplings in the "closed" ring Cr_8 and "open" ring Cr_8Cd nanomagnets give us opportunities to investigate the role on magnetic properties of spin topology. The spin singlet ground state and several excited levels in Cr_8Cd as well as in Cr_8 are probed directly from high-field magnetization measurements below 57 T using a nondestructive pulse magnet in conjunction with a dilution fridge. The energy level structures for quantum total spin states for both systems are directly determined by observation of very clear step-wise increase in the magnetizations. The striking difference of energy structure for the total quantum spin states in the two systems is well understood in terms of topology (in other words, different periodic boundary conditions) and was well reproduced by theoretical calculations based on a spin Hamiltonian including single-ion anisotropy contributions.

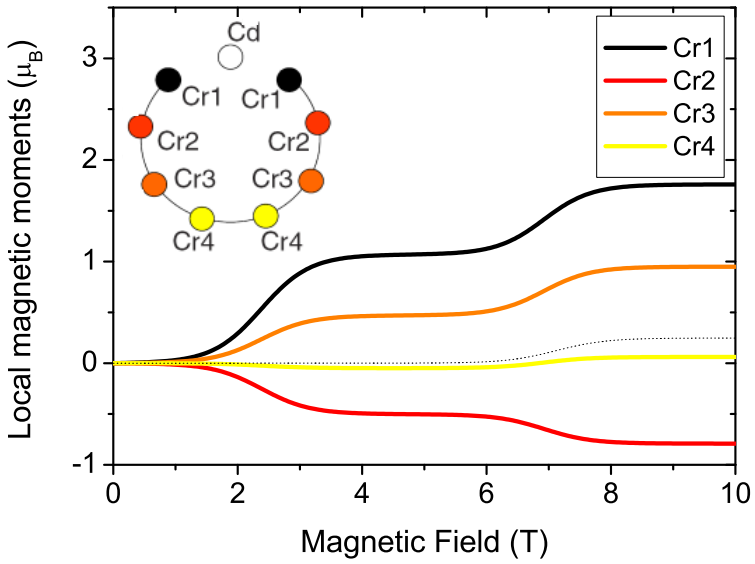

Figure 17: Magnetic-field dependence of thermal averaged local magnetic moments for Cr_8 (dotted line) and Cr_8Cd (solid lines) for T=0.5 K calculated from Eq. (78). The numbering of Cr sites for Cr_8Cd is shown in the inset.

4.6 Conclusions

We have investigated the consequences of the breaking of the ring symmetry in Cr_8Zn and Cr_8Cd spin segments taking the closed Cr_8 ring as reference. Firstly inelastic neutron scattering experiments have been performed in the spin segment Cr_8Zn. This has allowed to determine the set of isotropic exchange and CF interactions parameters necessary to describe the magnetic excitations with energy below about 4 meV by comparing the experimental cross sections with theoretical predictions. The most relevant effect of the ring opening has been found in the structure of eigenstates of the Heisenberg isotropic exchange interaction: the appearance of disjoint quantum fluctuations of the total spin length of the two sublattices causes the usual classification of low-lying states into distinct rotational bands to fail. These fluctuations show up in the measured INS intensity as a function of the scattering wave vector Q, and produce the large decrease of the effective anisotropy with respect to the closed ring. Another consequence is the decrease of the gap between ground- and first-excited multiplets. We have then focused on this last point by analysis of magnetization measurements on Cr_8Cd (open ring) and Cr_8 compounds. In both clusters the magnetization M as a function of applied magnetic field shows a clear staircase structure. By determining the peak positions of dM/dH it is possible to demonstrate that Cr_8Cd shows a more

prominent deviation from Landé rule with respect to Cr_8 due to the ring opening.

Chapter 5

Macroscopic measurements in Cr_7Ni and Cr_8Ni heterometallic rings

In this chapter attention will be focused on two heterometallic compounds named Cr_7Ni and Cr_8Ni derived from the well-known Cr_8 ring. One Ni^{2+} ion (s=1) replaces a Cr^{3+} ion (s=3/2) to have Cr_7Ni, whilst it is inserted in the ring-shaped structure of the eigth chromiums in order to have a Cr_8Ni cluster. Due to the dominant antiferromagnetic (AF) exchange interactions and the even number of magnetic ions Cr_7Ni shows a Kramers doublet $S = 1/2$ ground state. This is one of the reasons for which Cr_7Ni has been considered to be suitable in the field of quantum computation [13]. As regards Cr_8Ni compound, it represents the first example of AF ring with an odd number of magnetic ions, with the exception of spin triangles [9, 66]. Contrary to what occurs in odd-membered rings with half integer spins this cluster has a non magnetic $S = 0$ ground state. Nevertheless, Cr_8Ni is a frustrated spin systems since all AF interactions can not be simultaneously satisfied [67]. Magnetization measurements on both compounds allow to demonstrate how the spin Hamiltonian approach proves to be suitable even at very high fields, exploring spin multiplets no accessible to other experimental techniques (e.g. inelastic neutron scattering).

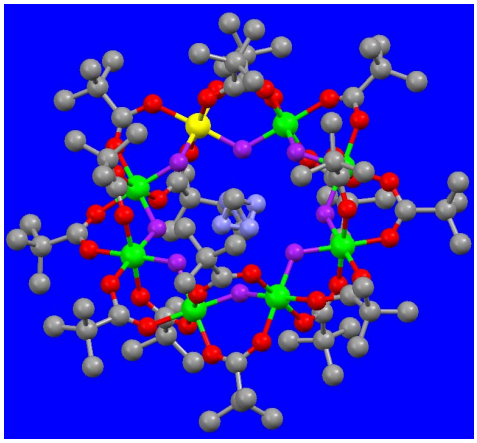

Figure 18: View of the structure of a Cr_7Ni molecule. Green spheres represent the Cr^{3+} ions, while the yellow one represents the Ni^{2+} ion.

5.1 The Cr_7Ni heterometallic ring

The magnetic molecule has been theoretically analyzed within a spin Hamiltonian approach, with the Hamiltonian given by:

$$\begin{aligned} H &= \sum_{i>j} J_{ij}\mathbf{s}(i)\cdot\mathbf{s}(j) + \sum_i d_i\left[s_z^2(i) - s_i(s_i+1)/3\right] \\ &\quad + \sum_{i>j}\mathbf{s}(i)\cdot\mathbf{D}_{ij}\cdot\mathbf{s}(j) - \mu_B\sum_i g_i\mathbf{H}\cdot\mathbf{s}(i), \end{aligned} \tag{79}$$

where $\mathbf{s}(i)$ is the spin operator of the the ith ion in the molecule ($s(i)$=3/2 for Cr^{3+} ions, and $s(i)$=1 for the Ni^{2+} ion). The first term of the above equation is the dominant nearest neighbour Heisenberg exchange interaction. The second and the third terms describe the uniaxial local crystal fields and anisotropic intracluster spin-spin interactions respectively (with the z axis assumed perpendicular to the plane of the ring). The last term represents the Zeeman coupling with an external field $\mathbf{H}$. The parameters of the above Hamiltonian were determined by inelastic neutron scattering (INS) experiments [30, 68]. In order to corroborate the microscopic description of the Cr_7Ni from INS data, a detailed study of high field magnetization is very powerful. In fact, with high pulsed fields up to almost 60 T, spin multiplets not accessible to a standard INS experiment can be explored. In Fig. 19(a) the magnetization curve as a function of the magnetic field $\mathbf{H}$ is reported. A clear staircase structure with plateaus at $\approx 1\mu_B$, $\approx 3\mu_B$ and odd multiples of μ_B reflects the change in the ground state due to the external field at the level anticrossing fields H_n. An hysteresis of the measured magnetization curves has been observed. The effect arises from the non-equilibrium

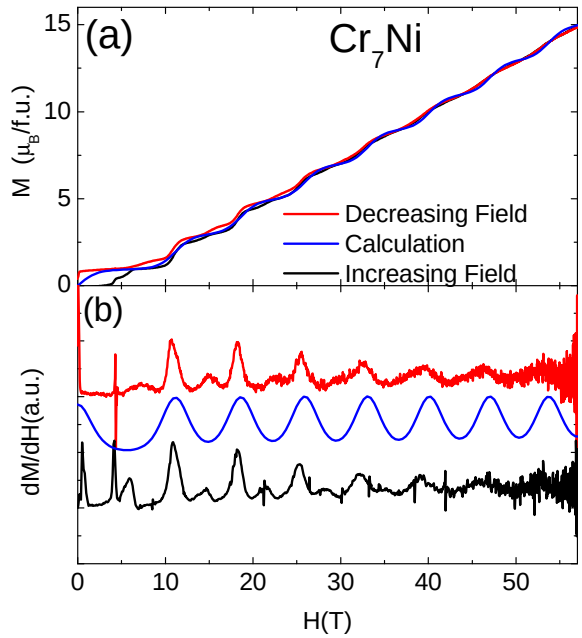

Figure 19: Magnetization curve of Cr_7Ni (top) and derivative dM/dH (bottom) at T=1.3K. Red and black lines represent the down and up experimental magnetic field processes respectively. The dashed blue lines represent the theoretical calculation mediated on powders with the following set of parameters: J_{Cr-Cr}=16.9 K, J_{Cr-Ni}=19.6 K, d_{Cr}=-0.3 K, d_{Ni}=-4 K, g_{Cr}=1.98, g_{Ni}=2.2.

condition due to the high pulsed magnetic field with a few millisecond duration [7] and has been discussed in terms of phonon bottle-neck and magnetic Foehn effects [61]. There is a very good agreement between the measured and calculated magnetization curves. This is clearly visible in Fig. 19(b) where the positions of the main peaks of the calculated and measured dM/dH matches correctly. The smaller peaks in the experimental dM/dH are due to level anticrossings between excited energy levels. The effects are caused by the non-equilibrium exeperimental conditions and are not included in equilibrium calculations reported in Fig. 19 [7]. These results confirm that the microscopic picture derived from INS experiments [30, 68] perfectly holds even at very high applied magnetic fields.

5.2 The Cr_8Ni heterometallic ring

In Chapter 4 the magnetic properties of AF even numbered rings have been shown in order to clarify the effect of the breaking of the ring symmetry. For this purpose the

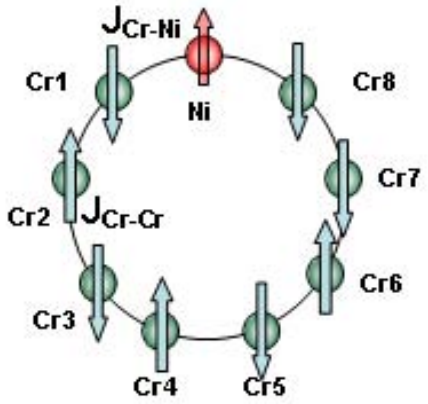

Figure 20: Schematic view of Cr_8Ni compound.

well-known Cr_8 ring and the spin segments Cr_8Zn, Cr_8Cd have been taken into account, where Zn^{2+} and Cd^{2+} are two non magnetic ions. If the ion inserted in the ring-shape structure is magnetic, an AF ring with an odd number N of magnetic ions is obtained. In the case of odd-membered AF rings, magnetic properties are expected to be changed drastically due to the spin frustration effects. The simplest AF ring with N odd is a system with three spins s=1/2 antiferromagnetically coupled: within this regard V_{15} [69] and Cu_3 [70] molecular magnets are good examples. In these frustrated triangular AF spin systems the ground state is a magnetic $S = 1/2$ [69]. Other odd-membered AF rings with $N > 3$ have been more difficult to synthesize. Quite recently a new family of odd-membered AF rings with N=9 has been created with the synthesis of a heterometallic Cr-based ring-shaped AF magnet $(C_6H_{11})_2NH_2[Cr_8NiF_9(O_2CC(CH_3)_3)_{18}]$ (in short, Cr_8Ni) by Winpenny and co-workers [66, 71, 72]. The Cr_8Ni is the first odd-membered AF ring with $N > 3$. The cluster shows spin frustration effects because all antiferromagnetic interactions can not be simultaneously satisfied. For this reason, Cr_8Ni molecule can be regarded as a magnetic analogue of the Möbius strip [66,71]. Due to the odd number of spins it is impossible to align all nearest neighbour spins antiparallel to each other. The region where the spins are not antiparallel can be considered as a knot of the Möbius strip. The precursor of Cr_8Ni is a well known even membered AF ring $[Cr_8F_8(O_2CC(CH_3)_3)_{16}]0.25C_6H_{14}$ (in short, Cr_8) whose ground state is spin singlet S=0 state due to AF interaction ($J_{Cr-Cr} \approx$16.9 K) between nearest neighbor Cr^{3+} (s=3/2) spins [39]. The Cr_8Ni is basically obtained by inserting a Ni^{2+} (s=1) ion into the Cr_8 ring. The metal ions are bridged by one fluoride and two $(CH_3)3CCO_2$ radicals [66, 71]. The antiferromagnetic interactions between Cr^{3+} ions and between Cr^{3+} and Ni^{2+} ions are reported to be J_{Cr-Cr}=16 K and J_{Cr-Ni}=70 K respectively.

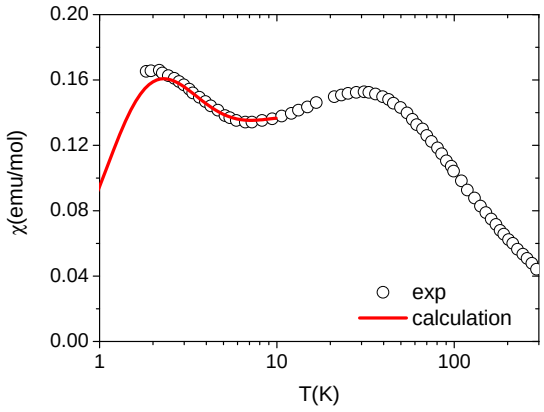

Figure 21: Measured (scatters) and calculated (line) temperature dependence of magnetic susceptibility *chi* in Cr_8Ni. The fall of χ at $T \approx 0$ strongly support the occurence of a non magnetic ground state. Experimental data are taken from Ref. [66].

These values were obtained by a fit of the temperature dependence of the magnetic susceptibility χ which shows two peaks around 2K and 25K (see Fig. 21) [66,71]. From the fitting of the magnetic susceptibility in the temperature range T =1.6-300 K it is also inferred that the ground state is a singlet $S = 0$ and that the first excited state is a $S = 1$ at 3.7 K from the ground state. This fit was based on a spin Hamiltonian with only the isotropic Heisenberg exchange term. The presence of a singlet ground state in this frustrated ring is quite interesting and requires more direct experimental evidence. In order to obtain more information on the ground state of the Cr_8Ni system from an experimental point of view, it is important to investigate the magnetic properties at low temperature, i.e. well below the lowest energy gap temperature. However, there are no experimental studies of magnetic properties on this cluster at low temperatures below 1 K up to now. The magnetization and NMR experiments performed on Cr_8Ni clearly show evidence of a spin singlet ground state and allows to establish the energy separation of the low-lying quantum magnetic states. The experimental results are in good agreement with predictions from theoretical calculations. Interestingly, the width of the steps in the field-dependence of the magnetization and the lack of sharp minima in the field-dependence of the specific heat show that sizeable Dzyaloshinski-Moriya (DM) interactions are present and lead to anticrossings between states of different total spin.

Fig. 22(a) shows the magnetization curves for Cr_8Ni at T=0.1 K for increasing (decreasing) magnetic fields: a clear step-wise increase (decrease) of magnetization is observed. The magnetization curves are nearly the same with no striking hysteresis

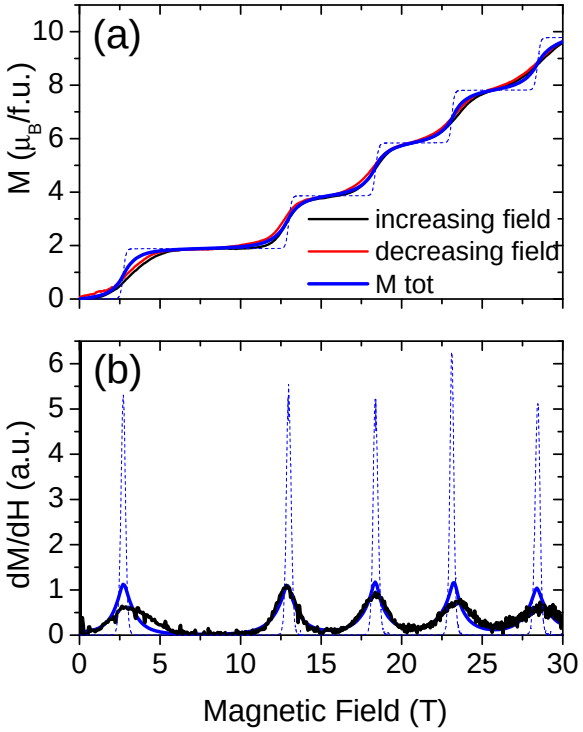

Figure 22: Magnetization curve of Cr_8Ni measured at T=0.1 K. Blue line shows the theoretical calculated results for T=0.1 K with the following parameters: J_{Cr-Cr}=14.7 K, $JCr-Ni$=85 K, d_{Cr}=-0.42 K and d_{Ni}=-4.9 K. (b) dM/dH curve at T=0.1 K. Blue line shows the theoretical calculated results for T=0.1 K.

for the up and down magnetic process at this temperature. The magnetization rapidly increases step by step with plateaus at $\approx 2\mu_B$, $\approx 4\mu_B$, $\approx 6\mu_B$, $\approx 8\mu_B$, $\approx 10\mu_B$ between the transition fields H_n (n=1,2,...). The H_n is determined by the peak positions of dM/dH curves [see Fig. 22(a)] to be 2.81, 12.8, 18.3, 23.5, and 28.5T, for n=1, 2, 3, 4, and 5, respectively. Line width (δH) defined at half amplitude for each peak in dM/dH is estimated to be 3.07, 1.61, 1.69, 2.15, and 2.06 T for n=1, 2, 3, 4, and 5, respectively. These values are larger than an expected thermal width 0.26 T for T=0.1 K estimated from an equation of $\delta H = 3.53 k_B T/g\mu_B$ with an assumption of $g \approx 2$. As discussed below, the broadening is also too large to be attributed merely to the distribution of level crossing fields H_n in the powder sample, and it is thus an indication of the presence of level anticrossing effects. If the ground state of system were magnetic, one should observe Brillouin function-like increase for the initial magnetization. The observed convex downward magnetization curve clearly proves a nonmagnetic ground

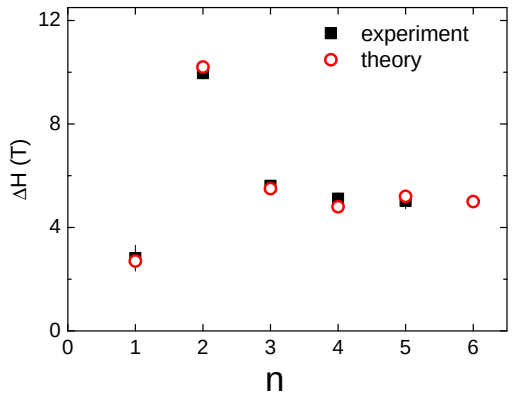

Figure 23: H-dependence of ΔH. Closed and open symbols show experimental and theoretical results respectively.

state. Thus the H_n are the level crossing fields between the S=0 ground state and the first excited S=1 for n=1, between S=1 and S=2 for n=2 and so on. The difference between adiacent level crossing fields defined as $\Delta H = H_n - H_{n-1}$ (where H_0 is zero) as a function of n is shown in Fig. 23. The n-dependence of ΔH for Cr_8Ni does not follows the Landé's rule which predicts that ΔH is independent of n. Fig. 24 shows the H-dependence of the specific heat C_{total} at T=0.5 K while the inset shows the temperature dependence of the specific heat C_{total} under zero magnetic field. The measured specific heat is the sum of a magnetic contribution and a lattice contribution, i.e. $C_{total} = C_{mag} + C_{lattice}$. However, as we will discuss later, the observed specific heat at T=0.5 K can be considered mainly due to the magnetic contributions C_{mag}. A single broad peak is observed around the first level crossing H_1=2.82 T. At the second level crossing, one can resolve two peaks at 12.1 and 13.7 T with a small dip around 13.0 T. In presence of a level crossing one should indeed observe two peaks with a dip in the middle. This is due to a Schottky-type anomaly as it was observed in even membered AF rings Fe_6 [73] and Cr_8 [63]. The two-level Schottky model predicts

$$C_s = (\Delta(H)/k_BT)^2 \times exp(\Delta(H)/k_BT)/(1 + exp(\Delta(H)/k_BT))^2$$

a behavior which yields a maximum when $\Delta(H)$ ≈2.5 k_BT. Near a level crossing field, the energy separation $\Delta(H)$ between two lowest-lying states can be expressed approximately as $\Delta(H) \approx g\mu_B|H_n - H|$ and thus two maxima are expected at $|H - H_n|$=2.5 $k_BT/g\mu_B$ with a dip at H_n where $\Delta(H)$ is smallest. In presence of a pure level crossing the dip between the two Schottky-like peaks should go down to zero since at level crossing $\Delta(H)$=0 while in presence of a level repulsion (level anticrossing) the dip

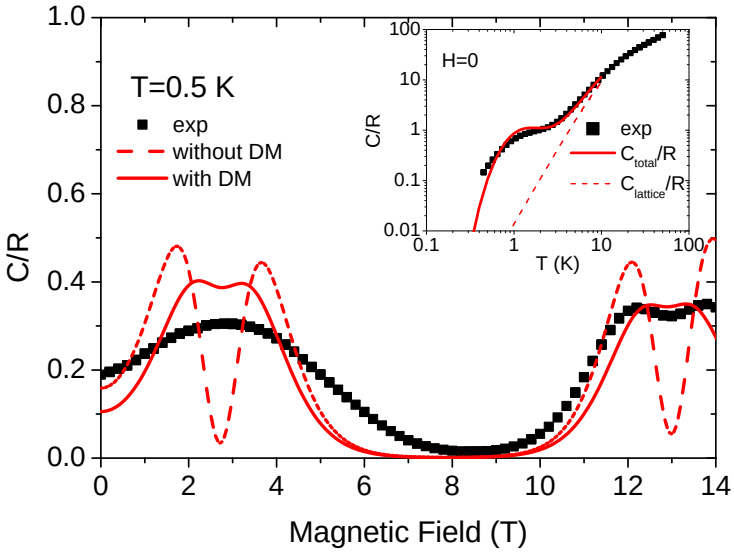

Figure 24: H-dependence of the specific heat at T=0.5 K. Solid line is theoretical calculated results for T=0.5K. The inset shows temperature dependence of specific heat measured under zero magnetic field. Red and broken lines in the inset show calculated C_{total} and $C_{lattice}$, respectively. $C_{lattice}$ is calculated from the Eq. (82) with this set of parameters: r=343, Θ_D=180 K and d=0.27

can be much less pronounced and it gives a measure of the gap at the anticrossing [63]. As shown in Fig. 24 a small dip superimposed on a broad maximum is observed only at the second level crossing. The broadening of the peaks cannot be ascribed to the distribution of the level crossing fields in a powder sample as will be demonstrated below in the discussion of the broadening of the magnetization steps. Thus one can conclude that at both the first and second level crossing a sizeable gap exists between the two crossing levels (level anticrossing).

The spin singlet ground state in Cr_8Ni is also revealed by proton NMR spectrum measurements at H=0.2 T. We observed a single narrow line of ^{1}H-NMR as shown in the inset of Fig. 25. The full width at half amplitude (FWHA) decreases from ≈62 kHz (≈15 Oe) at T=1 K on lowering temperature and becomes almost independent of T (≈42 kHz (≈10 Oe)) below ≈0.6 K as shown in Fig. 25. The FWHA≈10 Oe can be explained by nuclear-nuclear dipolar interactions. In fact the nuclear dipolar field between two protons is of the order of $\gamma_n\hbar/r^3$ ≈8.3 Oe when one assumes an internuclear distance r = 1.5 Å (γ_n is the gyro magnetic ratio of a proton). Thus we may conclude there is no magnetic broadening in the spectrum due to the Cr and/or Ni spin moments. This is consistent with a total spin S=0 ground state and also with a zero expectation

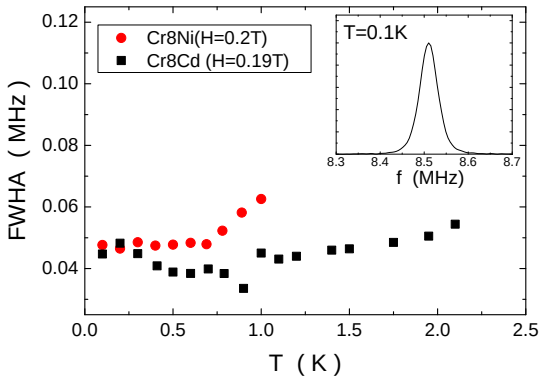

Figure 25: Temperature dependence of full width of half amplitude (FWHA) of ^{1}H-NMR spectra in Cr_8Ni (closed circles) at H=0.2 and Cr_8Cd (closed squares) at H=0.19 T. The inset shows a typical ^{1}H-NMR spectrum in Cr_8Ni at T=0.1K

value for the local spin component at each ion site. To check this conclusion, we have measured the FWHA of ^{1}H-NMR spectrum at nearly the same magnetic field H=0.19 T in a similar odd membered Cr-based AF ring $Me_2NH_2[Cr_8CdF_9(O_2CCMe_3)_{18}]$ (in short, Cr_8Cd) which has a spin singlet ground state with a first excited spin triplet state at ∼3 K above the ground state [7,52]. As shown in Fig. 25, the FWHA for both compounds coincide at low temperatures within our experimental uncertainty, indicating that the FWHA of about 10 Oe originates from the nuclear dipolar interaction, which is the same for isostructural Cr_8Ni and Cr_8Cd. We turn now to a quantitative comparison of the experimental results with the theoretical calculations. The starting spin Hamiltonian for the odd membered AF ring is

$$\begin{aligned} H &= J_{Cr-Ni}(\mathbf{S}_8 \cdot \mathbf{S}_{Ni} + \mathbf{S}_{Ni} \cdot \mathbf{S}_1) + J_{Cr-Cr} \sum_{i=1}^{7} \mathbf{S}(i) \cdot \mathbf{S}(j) \\ &+ d_{Cr} \sum_{i=1}^{8} \left[S_z^2(i) - S_{Cr}(S_{Cr}+1)/3 \right] + d_{Ni} \left[S_{z,Ni}^2 - S_{Ni}(S_{Ni}+1)/3 \right] \\ &- g_{Cr}\mu_B \sum_{i=1}^{8} \mathbf{H} \cdot \mathbf{S}_i - g_{Ni}\mu_B \mathbf{H} \cdot \mathbf{S}_{Ni}, \end{aligned} \tag{80}$$

where i labels the eight Cr ions (spins). The first and second terms describe the dominant isotropic Heisenberg interaction. Here we assume two differente exchange costants, one between Cr and Ni spins (J_{Cr-Ni}) and another between Cr spins (J_{Cr-Cr}). The third and fourth terms describe local crystal fields, where d_{Cr} and d_{Ni} represent the uniaxial single ion anisotropy for Cr and Ni ions, respectively. Finally, the fifth and sixth terms represent the Zeeman interactions. The two exchange parameters

have been determined to be J_{Cr-Cr}=14.7 K and J_{Cr-Ni}=85 K by fitting magnetization and susceptibility data. Reasonable values of d_{Cr} an d_{Ni} turn out to produce tiny effects in the powder properties. Hence we assume d_{Cr}=-0.42 K as in the parent Cr_8Zn compound [8] and the same ratio of d_{Cr} to d_{Ni} as in Cr_7Ni [68], yielding d_{Ni} =-4.9 K. The Hamiltonian is diagonalized by following the procedure described in Ref. [39]. The calculated eigenstates and eigenvalues have been used to evaluate the H-dependence of the thermal averaged magnetization and specific heat (C_{mag}) as well as the T-dependence of χ and C_{mag}. Since we used polycrystalline samples, all calculated results are powder averaged so that they can be directly compared with the experimental observations. By using g_{Cr}=1.98 and g_{Ni}=2.2, the T-dependence of χ (see the solid line in the Fig. 21) and the positions of the observed values of H_n are well reproduced [see Fig. 23(c)]. The n dependence of ΔH is also well reproduced by the theory as shown in Fig. 23. On the other hand, the width of the calculated peaks is much smaller than the experimental results as shown in Fig. 22(b). The origin of the broadening of the magnetization steps is likely to be the same as the origin of the broadening of the specific heat peaks and is discussed after the presentation of the specific heat results. The temperature dependence of the calculated specific heat C is shown by a line in the inset of Fig. 24. The temperature dependence of the calculated specific heat $C_{total}(= C_{mag} + C_{lattice})$ is shown by a red solid line in the inset of Fig. 24. C_{mag} was calculated from the following equation [39]:

$$\frac{C_{mag}}{R\beta^2}\frac{\sum_i E_i^2 exp(-\beta E_i)\sum_i exp(-\beta E_i) - [E_i exp(-\beta E_i)]}{[\sum_i exp(-\beta E_i)]}, \tag{81}$$

where E_i are the eigenvalues obtained from Eq. (80), and $\beta = (k_B T)^{-1}$. The lattice contribution to C has been estimated from a phenomenological model [74];

$$C_{lattice}/R = 234 r T^3/(\Theta_D + \delta T^2)^3 \tag{82}$$

where r is the number of atoms per molecule, and Θ_D and δ are parameters. For Cr_8Ni, we used a set of parameters: r=343, Δ_D=180 K and δ =0.27 whose values are very similar to those reported for the isostructural AF ring Cr_8Cd [52]. The broken line in the inset shows the calculated $C_{lattice}$. The specific heat at low temperatures (below 1 K) is dominated by the magnetic contribution (C_{mag}). The result is in good agreement with the experimental data as in the inset of Fig. 24. It should be noted that we did not use any scaling factors to fit the experimental data by the calculation. On the other hand the calculated C_{mag} at T=0.5 K as a function of H, shown by a dashed line

in Fig. 24, is not in good agreement with the experiments. The problem is the remarkable broadening of the peak in the experimental specific heat at level crossings, which should have the same origin as the broadening in the magnetization steps [see Fig. 22(a)] and which is not reproduced by calculations based only on Eq. (80). We have already introduced reasonable single-ion terms in the calculations, hence the broadening effects in the experiment cannot be simply attributed to a distribution of H_n due to the random direction of crystal-field anisotropy axes in a powder sample. In principle, a distribution of exchange parameters from molecule to molecule resulting from disorder (J-strain) might produce a broadening. For instance, in Cr_7Ni, a distribution with standard deviation of the order of 2.5% was found [68]. However we find that an unrealistically large value for the standard deviation has to be assumed to account for the entity of the observed effects. In addition, the effect of J-strain on the minimum in C at 2.7 T is much smaller than that on the minimum at 13 T, whereas in experimental data the broadening is of the same entity in the two minima. On the other hand, if the level crossings (LCs) are not true crossings but level anticrossings(ACs), C_{mag} does not vanish at H_n because $\Delta(H)$ remains finite. By considering only the lowest multiplet for each value of S, even-S and odd-S multiplets belong to different irreducible representations of the ideal spin permutational symmetry of Eq. (80). Hence, crossings can be turned into ACs only by including in the Hamiltonian terms which break this symmetry (for instance site-dependent Cr crystal fields). However, this sort of symmetry lowering would not significantly affect the first crossing at 2.7 T. In fact, only a DM interaction can directly mix the S=0 and S=1 multiplets because it is the only term (beside the Zeeman term which does not break spin permutational symmetry) which is described by rank-one complex tensor operators T^1_Q and because if $K > 1$ $\left\langle S=0 \left| T^K_Q \right| S=1 \right\rangle = 0$. Hence, the absence of a minimum in $C(H)$ at 2.7 T provides strong evidence of the presence of DM interactions in the microscopic Hamiltonian. The most likely sources of this interaction are the two Cr-Ni bonds because the inversion symmetry is maximally broken and the exchange interaction is the strongest. In addition, the orbital degrees of freedom which are besides the DM interaction are much less quenched in Ni^{2+} than in Cr^{3+} ions. To investigate the effect of DM interactions, we have made calculations assuming the simplest possible choice for their form:

$$H_{DM} = \mathbf{D} \cdot (\mathbf{S}_8 \times \mathbf{S}_{Ni}) + \mathbf{D} \cdot (\mathbf{S}_{Ni} \times \mathbf{S}_1) \tag{83}$$

where we assume the two DM vectors to be equal and parallel to the z axis. The actual DM vectors are very likely to be different than in Eq. (83), but our aim is not to look

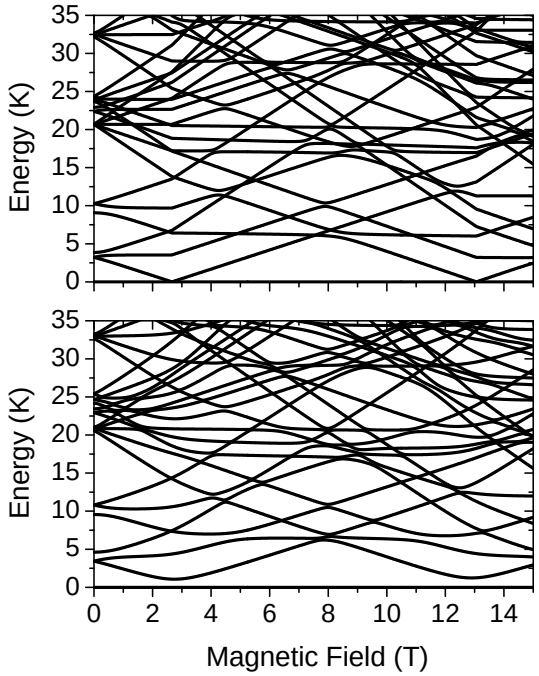

Figure 26: Magnetic-field dependence of the low-lying energy levels of Cr_8Ni without (top) or with (bottom) DM interactions described by Eq. (83). The fields makes an angle of 45 degrees with the z axis. For each value of H the ground-state energy has been set to zero.

for a best fit of the data but merely to assess whether the DM interaction is a realistic mechanism to explain the observed behavior or not. We assume for the modulus of **D** the typical value D= 0.1 J_{Cr-Ni}. The resulting spectrum is compared with that obtained for D=0 in Fig. 26. Sizeable ACs open up at H_n whose amplitude depends on the angle between the applied field and the z axis. The effect on C is shown by the continuous line in Fig. 24. The DM interactions remove the sharp minima at H_n in agreement with the experimental results. In addition, the width of steps in the calculated field-dependence of M is in very good agreement with experimental data [see the blue line in Figs. 22(a) and 22(b)]. Having established the main interactions appearing in the microscopic Hamiltonian we can study the properties of the resulting ground state for $H = 0$. Since isotropic exchange is the dominant interaction we focus on the ground state of the cluster Hamiltonian (80), neglecting crystal-field and DM interactions which do not qualitatively affect the ground state properties. While classical calculations yield an infinite number of degenerate lowest-energy configurations, quantum mechanically the ground state is an S=0 singlet in agreement with exper-

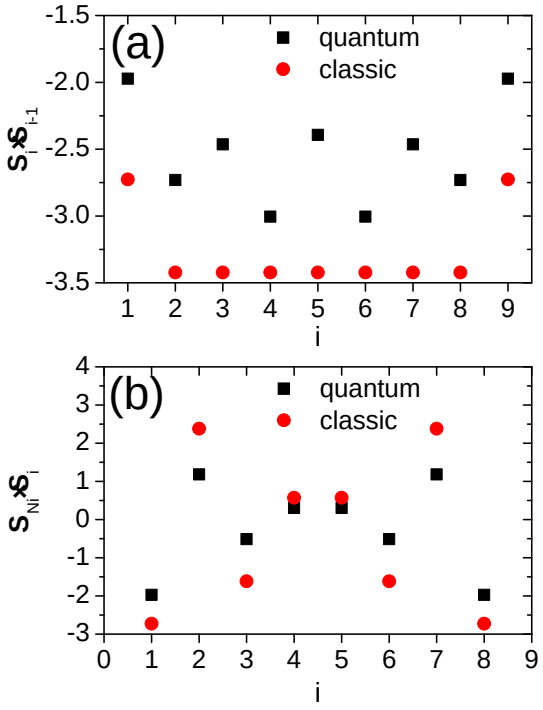

Figure 27: Quantum and classic correlation functions nearest neighbours $< \mathbf{S}_i \cdot \mathbf{S}_{i-1} >$ type in panel (a) (where $i-1=9$ if $i=1$) or $< \mathbf{S}_{Ni} \cdot \mathbf{S}_i >$ type in panel (b).

imental observations. In order to investigate the structure of the ground state and, in particular, how this is affected by frustration, we have used the following coupling scheme $|S_{18}, S_{189}, S_{27}, S_{36}, S_{2736}, S_{45}, S_{273645}, S>$ [32] where $S_{ijk}\ldots$ are quantum numbers for the modulus of $\mathbf{S}_i+\mathbf{S}_j+\mathbf{S}_k+\cdot+\ldots$. The Nickel ion is assumed to be in site 9. We have found that the S=0 ground state (and the lowest multiplet for each value of S up to S=11) is formed by states with S_{18}=3, S_{189}=2 for about the 95%. This indicates that the Cr spins on sites 1 and 8 are practically locked antiparallel to the Ni spin and parallel to each other.This originates from the much larger value of J_{Cr-Ni}=85 K with respect to J_{Cr-Cr}=14.7 K. Thus these three spins behave as an effective spin-2 degree of freedom antiferromagnetically coupled to the two neighboring Cr spins. To characterize the magnetic alignment of the spins in the ground state, we have calculated static zero-temperature two-site correlations $\langle \mathbf{S}_i \cdot \mathbf{S}_j \rangle$ and the corresponding quantities for the classical Hamiltonian corresponding to Eq. (80). For the latter the spins are classical vectors of length $\sqrt{s_i(s_i+1)}$. We focus in particular on correlations of the eight Cr spins with the Ni spin, shown in Fig. 27(a), and on nearest-neighbor correlations shown in Fig. 27(b). Correlations $< \mathbf{S}_{Ni} \cdot \mathbf{S}_1 >$ and $< \mathbf{S}_{Ni} \cdot \mathbf{S}_8 >$ reflect the

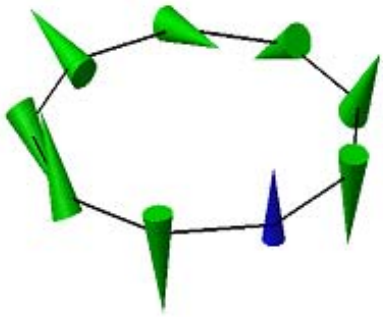

Figure 28: This figure reports one of the degenerate configurations corresponding to an $S = 0$ ground state calculated for the classical version of the model of Cr_8Ni. The blue cone represents the Nickel ion. Within this reference frame, the angle between spin 4, 5 (whose bond is opposite to the Nickel site) and the spin of the Ni ion along z is $\approx$78°, while the angle between spin 4 and 5 is $\approx$156°, being z the axis perpendicular to the plane of the ring. Therefore the knot is delocalized in the eight Cr ions with the sites 4 and 5 having the same z component. The classic picture of the ground state holds most of the main features of the quantum $S = 0$ ground state obtained from exact diagonalization of the isotropic Heisenberg term in Eq. (80).

above-mentioned locking of the three spins in an $S = 2$ state. The meaning of the remaining $< \mathbf{S}_{Ni} \cdot \mathbf{S}_i >$ correlations can be understood by inspecting the vector structure of the classical ground state (see Fig. 28), which shows a pattern of correlations similar to that of the quantum ground state: classically, the spins are oriented in a noncollinear fashion due to spin frustration. For instance, the Cr spins at sites 4 and 5 are almost lying in a plane perpendicular to the Ni spin which corresponds to nearly vanishing correlations $< \mathbf{S}_{Ni} \cdot \mathbf{S}_4 >$ and $< \mathbf{S}_{Ni} \cdot \mathbf{S}_5 >$ as shown in Fig. 27(b). On the other hand, quantum mechanically, the S=0 ground state approximately resonates among the infinite classical configurations. Hence, local magnetic moments vanish at low temperature due to quantum fluctuations, which is directly revealed by present NMR measurements.

5.3 Conclusions

In this chapter we have carried out analysis of high field magnetization at low temperatures in two heterometallic antiferromagnetic ring-shaped molecules Cr_7Ni and Cr_8Ni. In both cases a clear step-wise increase of magnetization with increasing field is observed. The very good agreement of high field magnetization measurements up to almost 60 T with calculations shows the spin Hamiltonian approach to be suitable even

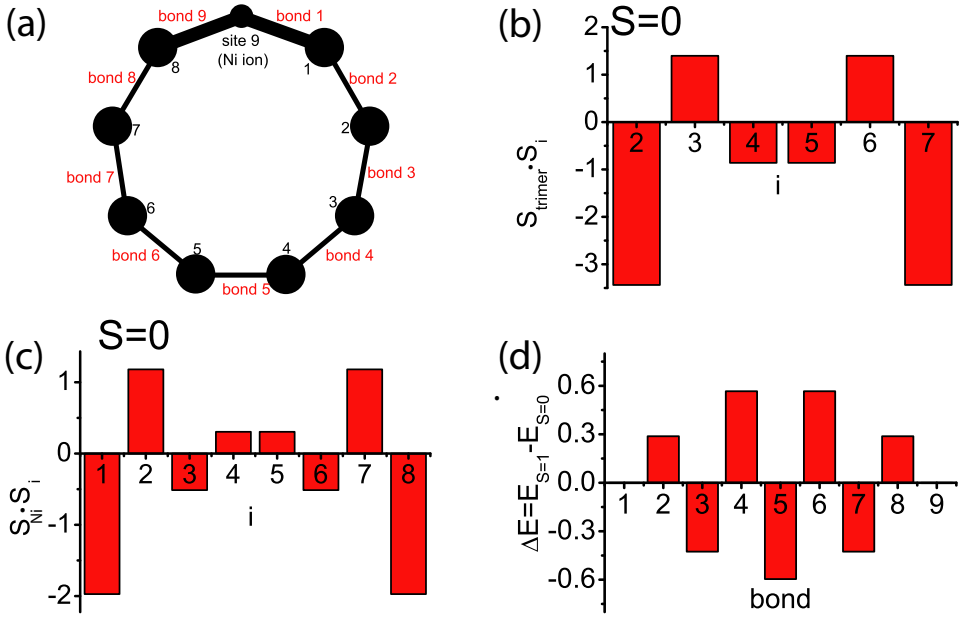

Figure 29: (a) Schematic structure of the Cr_8Ni cluster with the enumeration of bonds and spin sites. (b) Scalar products $\mathbf{S}_{trimer} \cdot \mathbf{S}_i$ show how frustration is distributed in magnetic sites from 1 to 7, being $S_{trimer} = S_{18} + S_9$. (c) Scalar product $\mathbf{S}_{Ni} \cdot \mathbf{S}_i$. Assuming the Nickel spin in position 9 to be aligned along z-axis, $\mathbf{S}_{Ni} \cdot \mathbf{S}_i$ reflects the non uniform distribution of local moments in the ground $S = 0$ state. (d) Excitation energy of the first excited state $S = 1$ with respect to the ground state $S = 0$ as a function of the exchange bonds. It is straightforward to note that bonds 1 and 9 do not cooperate to the first excitation. This occurs since $J_{Cr-Ni} >> J_{Cr-Cr}$ and thus the trimer is blocked in a $S_{trimer} = 1$ state.

at very high fields. In particular, in Cr_7Ni these results confirm that the microscopic picture derived from INS experiments [30,68] at zero field perfectly holds even for spin multiplets not accessible to the INS tecnique. Besides, in Cr_8Ni high field magnetization together with specific heat measurements at low temperatures(below 1K) give clear evidence for a spin singlet ground state at zero magnetic field in agreement with theoretical calculations based on an Hamiltonian including Heisenberg, crystal field and Dzyaloshinski-Moriya interactions. In particular, the field-dependence of the specific heat and the widths of the magnetization steps provide strong evidence of the presence of level anticrossings due to antisymmetric terms in the Hamiltonian. The proton NMR measurements confirm the above results indicating that the local spin density is zero in the ground state as a result of quantum fluctuations among frustrated local spins configurations [9].

Chapter 6

Relaxation dynamics in magnetic molecules

In the present chapter the theory of relaxation of molecular observables developed in the following section and derived in Ref. [20] will be applied to several types of magnetic molecules. The Mn_{12}, Fe_8 nanomagnets, the Fe_{30} icosidodecaedron, the V_{12} antiferromagnetic cluster containing ions with spin 1/2 and the Cr_7Ni heterometallic ring will be taken into account and investigated as regards their spin dynamics. Irrespective of the different topology, local ions and microscopic interactions, all studied molecules show similar relaxation mechanisms. In many cases we will show how the NMR technique can provide useful information about the relaxation dynamics in magnetic molecules.

6.1 Decoherence and relaxation phenomena in magnetic molecules

The interaction of electronic spins with other degrees of freedom such as phonons causes decoherence in the time evolution of molecular observables, thus leading to relaxation dynamics. This is reflected in the irreversible evolution of the density matrix $\rho_{st}(t)$, evaluated in the basis of exact eigenstates of the cluster Hamiltonian $[H\,|s\rangle| = E_s\,|s\rangle]$. Since we are interested in relaxation phenomena characterized by time scales much longer than the free evolution periods of the system $2\pi\hbar/(E_s - E_t)$, the evolution of the diagonal matrix element $\rho_{ss}(t) = p_s(t)$ can be decoupled from that of the off-diagonal ones $\rho_{s\neq t}(t)$ [secular approximation]. This allows a clear separation of quasi-elastic (QE) and inelastic (IE) spectral contributions in frequency domain. The former can

be detected by low-frequency experimental techniques such as AC suceptibility and NMR, while the latter are determined by the lifetimes of the involved pair of levels and can be probed by means of higher frequency techniques such as INS and electron spin resonance (or ESR).

Exploiting the so called secular approximation, the populations of the molecular eigenstates evolve, $p_t(t)$ through the well known rate master equations

$$\dot{p}_s(t) = \sum_t W_{st} p_t(t), \tag{84}$$

where W_{st}, the st element of the rate matrix $\mathbf{W}$, represents the probability per unit time that a transition involving $|s\rangle$ and $|t\rangle$ levels occurs because of the interaction of the system with the heat bath ($W_{ss} = -\sum_t W_{ts}$). In the range of temperatures of our interest, dechoerence and relaxation phenomena are caused by the interaction of electronic spins with phonons. In magnetic molecules with local spin $s > 1/2$ the main contributions to this coupling come from modulation of the local rank-2 crystal fields (CFs) $\sum_i \sum_q b(i)_2^q O_2^q(\mathbf{s}_i)$, with $O_2^q(\mathbf{s}_i)$ Stevens operator equivalents for spin i and $b_2^q(i)$ CF parameters. This leads to the following spin-phonon coupling potential:

$$V = \sum_{i=1,N} \sum_{Q=0,1,2} \sum_{\mathbf{k},\sigma} C_Q(i,\mathbf{k},\sigma), T_2^Q(\mathbf{s}_i)(c_{\mathbf{k}\sigma} + c^+_{-\mathbf{k}\sigma}), \tag{85}$$

where N is the number of ions in the cluster, $C_Q(i,\mathbf{k},\sigma)$ is the coupling constant between the Q-type electric quadrupole on ion i and the phonon modes of wave vector $\mathbf{k}$ and branch σ. Adopting a Debye model for phonons and choosing coupling coefficients $C_Q(l,\mathbf{k})$ independent of l and Q we obtain the following transition rates W_{st} between levels s and t (in first order perturbation theory):

$$W_{st} = \gamma\pi \left| \langle t| \sum_{i=1,N} \sum_{Q=0,1,2} O_2^Q(\mathbf{s}_i) |s\rangle \right|^2 \Delta_{st}^3 n(\Delta_{st}) \tag{86}$$

with $n(x) = (e^{\beta\hbar x} - 1)^{-1}$, $\Delta_{st} = (E_s - E_t)/\hbar$. In this simple model, γ is the unique free parameter: it represents the spin-phonon coupling strength. Another possible choice for the magnetoelastic coupling leads to the following expression:

$$W_{mn} = \gamma\pi^2 \Delta_{mn}^3 n(\Delta_{mn}) \sum_{\substack{i,j=1,N \\ q_1,q_2=x,y,z}} \langle m| O_{q_1,q_2}(\mathbf{s}_i) |n\rangle \times \langle n| O_{q_1,q_2}(\mathbf{s}_j) |m\rangle , \tag{87}$$

where $O_{q_1,q_2}(\mathbf{s}_i) = (s_{q1,i}s_{q2,i} + s_{q2,i}s_{q1,i})/2$ are quadrupolar operators which give rise to a spherically symmetric magnetoelastic (ME) coupling for the transition metal ions in

a cluster with $s > 1/2$ and $q_1, q_2 = x, y, z$ [75]. In Section 6.4 we will investigate the relaxation dynamics in a molecule containing $s = 1/2$ ions. In this case, we recall that phonons are assumed to cause the modulation of next neighbours anisotropic exchange, since there are no local crystal field terms for ions with spin 1/2.

In order to understand the mechanisms which governs the spin dynamics in magnetic molecules, the Fourier transform $S_{\mathcal{A},\mathcal{B}}(\omega)$ of the cross correlation function $\langle \Delta\mathcal{A}(t)\Delta\mathcal{B}(0)\rangle$, where $\mathcal{A}$ and $\mathcal{B}$ are two generic molecular observables, has to be evaluated. First of all, the fluctuation dissipation theorem allows to relate the imaginary part of the generalized susceptibility $\chi''_{\mathcal{A},\mathcal{B}}(\omega)$, the real part of the Laplace transform $\tilde{R}'_{\mathcal{A},\mathcal{B}}(z)$ of the relaxation function $R_{\mathcal{A},\mathcal{B}}(t)$ and the $S_{\mathcal{A},\mathcal{B}}(\omega)$ together:

$$S_{\mathcal{A},\mathcal{B}}(\omega) = \frac{2k_BT\chi''_{\mathcal{A},\mathcal{B}}(\omega)}{\omega} = 2k_BT\tilde{R}'_{\mathcal{A},\mathcal{B}}(\omega) \tag{88}$$

The relaxation function is defined as $\lim_{\epsilon\to 0}(\langle\mathcal{A}(t)\rangle - \langle\mathcal{A}\rangle^{eq})/\epsilon$, with a small perturbation ϵB switched off at $t = 0$. Acting inside the well established framework developed in [76,77], we are able to calculate the $R_{\mathcal{A},\mathcal{B}}(t)$ by first-order perturbation theory. Being H_0 the unperturbed Hamiltonian of our spin system and $|n\rangle$ and $E_n^{(0)}$ its eigenvectors and eigenvalues respectively, at $t < 0$ we introduce the small perturbation $\epsilon\mathcal{B}$ (e.g. a small magnetic field which couples with the observable $\mathcal{B}$). As a result, retaining only first-order terms in $\epsilon\mathcal{B}$, at $t = 0$ the density matrix reads as follows:

$$\begin{aligned}
\rho(t=0) &= \sum_{\tilde{n}} \frac{e^{-\beta E_{\tilde{n}}}}{Z} |\tilde{n}\rangle\langle\tilde{n}| \\
&= \sum_n p_n^{(eq)} |n\rangle\langle n| + \epsilon p_n^{(eq)}\beta(\mathcal{B}_{nn} - \langle\mathcal{B}\rangle)|n\rangle\langle n| - \\
&\quad -\epsilon p_n^{(eq)} \sum_{q\neq n} \left(\frac{\mathcal{B}_{qn}}{E_n^{(0)} - E_q^{(0)}} |q\rangle\langle n| + \frac{\mathcal{B}_{nq}}{E_n^{(0)} - E_q^{(0)}} |n\rangle\langle q| \right)
\end{aligned} \tag{89}$$

where $|\tilde{n}\rangle$ and $E_{\tilde{n}}$ are respectively the eigenvectors and eigenvalues of the complete Hamiltonian, $p_n^{(eq)} = e^{-\beta E_n^{(0)}}/Z_0$ is the nth diagonal density matrix element at equilibrium, being Z_0 the partition function of the unperturbed spin system. According to the theory presented in [77] for the irreversible evolution of the density matrix, the QE and IE part of $\rho(t)$ at times $t > 0$ can be determined separately:

$$\rho_{nn}(t) = \sum_m \nu_{nm}(t)\rho(t=0)_{mm} \tag{90}$$

$$\rho_{mn}(t) = \Gamma_{nm}(t)\rho_{mn}(t=0) \tag{91}$$

where

$$\nu(t) = e^{Wt} \tag{92}$$

is the propagator which gives the time evolution of the QE part of the density matrix, while

$$\Gamma_{nm}(t) = e^{i\Delta_{nm}t}e^{-t/\tau_{nm}} \tag{93}$$

is the IE propagator of ρ. Here $\tau_{nm} = -\frac{1}{2}(\Gamma_{mm}+\Gamma_{nn})$ is the average of the the lifetimes of levels n and m, and represents the time after which the phase coherence is lost [77]. Since we are interested in the QE part of spin dynamics, we calculate the evolutions of molecular observables neglecting the off-diagonal terms of the density matrix. As a result, we obtain:

$$\begin{aligned} R_{\mathcal{A},\mathcal{B}}(t) &= lim_{\epsilon\to 0}\frac{\langle A(t)\rangle - \langle\mathcal{A}\rangle_{eq}}{\epsilon} \\ &= \beta\sum_{m,n} p_m^{(eq)}\left(\mathcal{B}_{mm} - \langle\mathcal{B}\rangle_{eq}\right)\nu_{nm}(t)\left(\mathcal{A}_{nn} - \langle\mathcal{A}\rangle_{eq}\right). \end{aligned} \tag{94}$$

Finally, we have to take the real part $\tilde{R}'_{\mathcal{A},\mathcal{B}}(i\omega)$ of the Laplace transform of $R_{\mathcal{A},\mathcal{B}}(t)$:

$$\begin{aligned} \tilde{R'}_{\mathcal{A},\mathcal{B}}(i\omega) &= \beta\sum_{m,n} p_m^{(eq)}\left(\mathcal{B}_{mm} - \langle\mathcal{B}\rangle_{eq}\right)\times \\ &\quad \times Re\left\{\left(\frac{1}{i\omega - W}\right)_{nm}\right\}\left(\mathcal{A}_{nn} - \langle\mathcal{A}\rangle_{eq}\right). \end{aligned} \tag{95}$$

If we consider Eqs. (88) and (95) it should be noted that the QE part of the Fourier transform of the cross correlation function $S_{\mathcal{A},\mathcal{B}}(\omega)$ involves only the diagonal elements of observables $\mathcal{A},\mathcal{B}$ [20, 21]. Thus, the Fourier transform for the QE part of a general spin-spin correlation functions is:

$$\begin{aligned} S_{\mathcal{A},\mathcal{B}}(\omega) &= \sum_{q,t}(\mathcal{B}_{tt} - \langle\mathcal{B}\rangle_{eq}) \\ &\times \quad (\mathcal{A}_{qq} - \langle\mathcal{A}\rangle_{eq})Re\left\{p_t^{eq}\left(\frac{1}{i\omega - \mathbf{W}}\right)_{qt}\right\}, \end{aligned} \tag{96}$$

where $p_t^{(eq)}$ is the equilibrium population of the t-th level, $\mathcal{B}_{tt} = \langle t|\mathcal{B}|t\rangle$ and $\mathbf{W}$ is the so-called rate matrix. Furthermore, since we are mainly interested in the dynamics of magnetization we take $\mathcal{A} = \mathcal{B} = S_z$ and write Eq. (96) as:

$$S_{S_z,S_z}(\omega,T,B) = \sum_{i=1,N} A(\lambda_i,T,B)\frac{\lambda_i(T,B)}{\lambda_i(T,B)^2+\omega^2} \tag{97}$$

where $\lambda_i(T,B) = 1/\tau_{QE}^{(i)}$ are the eigenvalues of $-\mathbf{W}$. As a consequence, the autocorrelation of magnetization is given by a sum of lorentzians centered at zero frequency and

with width $\lambda_i(T,B)$, and decays as a sum of exponentials with characteristic times $\tau_{QE}^{(i)}$. Here the $A(\lambda_i,T,B)$ coefficients represent the weights of the N possible lorentzians, N being the dimension of the Hilbert spin space of the molecule. Each $\tau_{QE}^{(i)}$ refers to a particular spin-bath relaxation channel, given by the corresponding eigenstate $|w_i\rangle$ of $\mathbf{W}$: the composition of $|w_i\rangle$ in terms of the molecular eigenstates gives the complete relaxation path. Further information on the spin-bath dissipation channels is contained in the N level lifetimes $\tau_{life}^{(i)}$ defined as $\tau_{life}^{(i)} = [-W_{ii}]^{-1} = [\sum_j W_{j\leftarrow i}]^{-1}$: this is the inverse of the sum of all transition rates between the considered i level and all other ones according to the selection rules imposed by spin-bath interaction. The two sets of $\tau_{QE}^{(i)}$ and $\tau_{life}^{(i)}$ times contain complementary information on the QE part of relaxation dynamics.

The electronic dynamic properties of magnetic molecules can be probed by NMR. In fact, the measured longitudinal relaxation rate $1/T_1$ is given by a linear combination of local spin correlation functions through the Moriya formula [47]:

$$\frac{1}{T_1} = \sum_{i,j=1,N} \sum_{q,q'=x,y,z} \alpha_{ij}^{qq'} \left(S_{s_i^q,s_j^{q'}}(-\omega_L) + S_{s_i^q,s_j^{q'}}(\omega_L) \right) \tag{98}$$

where N is the number of magnetic ions in the cluster, $\alpha_{ij}^{qq'}$ are the geometric coefficients which depend on the positions of ions i and j and the probed nuclei, while $S_{s_i^q,s_j^{q'}}(\omega_L)$ is the Fourier transform of the cross correlation function calculated at the Larmor frequency of hydrogen nucleus $\omega_L = \gamma B$, being γ the proton gyromagnetic ratio and B a magnetic field applied along z [see Eq. (97)]. Since far from level crossings $\omega_L << \Delta_{mn} = \hbar/(E_m - E_n)$, with E_m, E_n eigenvalues of the cluster Hamiltonian, only the QE part of $S_{s_i^q,s_j^{q'}}(\omega_L)$ contributes to $1/T_1$, i.e. that calculated by means of Eq. (96). Furthermore, as long as anisotropy can be neglected, $\langle t|s_x(i)|t\rangle = \langle t|s_y(i)|t\rangle = 0$ since from Eq. (96) it follows that only $\alpha = \beta = z$ terms are non zero. In addition for a magnetic ring $\langle t|s_z(i)|t\rangle = \langle t|s_z(j)|t\rangle = 1/N\langle t|S_z|t\rangle$ where S_z is the z component of the total spin operator $\mathbf{S}$. Thus Eq. (98) reduces to:

$$\frac{1}{T_1} = G S_{S_z,S_z}(\omega_L), \tag{99}$$

where G is a geometric scale factor which accounts for the positions of hydrogens probed by NMR. This results holds also in the case of nanomagnets with easy-axis anisotropy, provided that the magnetic field is applied along the easy-axis direction. As a consequence the NMR techinque constitutes a probe of the dynamics of magnetization in most of magnetic molecules [20]. The results we will see in this chapter well reproduce

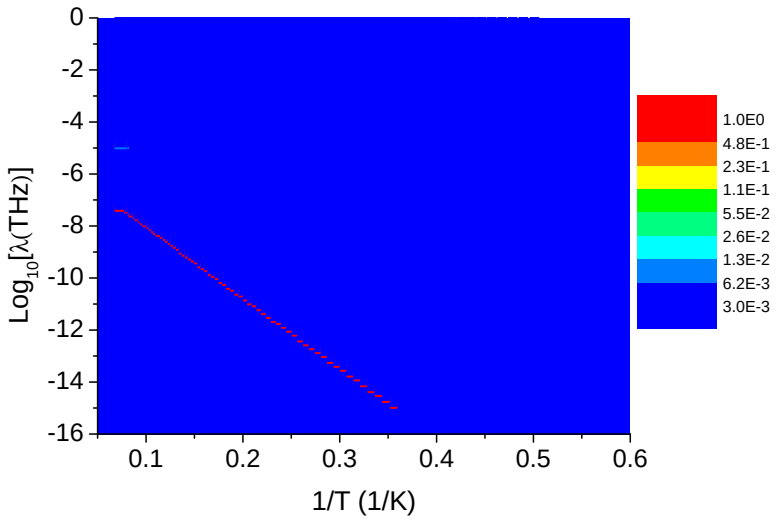

Figure 30: Calculated frequency weights $A(\lambda, T, B)$ of the magnetization autocorrelation function *vs* $1/T$. The y axis represents $Log_{10}(\lambda)$. The color maps $Log_{10}[A(\lambda, T, B)/(\chi T)]$. The spectrum have been normalized by χT, since χT determines the size of equilibrium fluctuations. The red line in the spectrum represents the dominant frequency in the spectrum and follows the Arrhenius law. The parameters for Mn_{12} spin Hamiltonian were derived by inelastic neutron scattering experiments [22].

the experimental curves and indicate that the T-dependence of NMR $1/T_1$ may or may not show any sharp peak. This can be understood noting that in agreement with previous studied molecules [11, 10, 20] the frequency spectrum of a given molecule at low T is dominated by a single lorentzian of characteristic frequency λ_0. In fact, as long as there is a λ_0 with appreciable weight, from Eq. (97) it can be argued that *only* when $\lambda_0 = \omega_L$ $1/T_1(T)$ should peak. Therefore, the NMR technique can probe the characteristic times of the spin dynamics in magnetic molecules.

6.2 The Mn_{12} and Fe_8 nanomagnets

In this section we will focus on a novel relaxation mechanism of magnetization peculiar of well-known molecular nanomagnets such as Mn_{12} and Fe_8. Mn_{12} contains eight Mn^{3+} ions (s=2) and four Mn^{4+} ions (s=3/2) magnetically coupled in such a way that at low T it behaves as an effective $S = 10$ state in presence of a strong double well potential [1, 22]. In the Fe_8 molecule the competing antiferromagnetic (AFM) interactions among the eight Fe^{3+} centers (s=5/2) lead to a $S = 10$ ground state [40, 41, 78]. As already mentioned in Chapter 1, Mn_{12} and Fe_8 show slow relaxation

dynamics at low T. The thermally activated mechanism of relaxation occurs through multi-step Orbach processes. Let us perturbe the magnetic system, for instance by the application of a magnetic field. When the magnetic field is removed the magnetization has to overcome the overall energy barrier to relax back to equilibrium. The time of this relaxation process follows the so called Arrhenius law:

$$\tau = \tau_0 exp(\frac{\Delta}{k_B T}),$$

where Δ/k_B is the height of the energy barrier for the reorientation of magnetization: Δ/k_B $\approx$61 K for Mn_{12} [1] and Δ/k_B $\approx$22 K for Fe_8 [78]. At temperatures $T > 1$ K relaxation and decoherence phenomena are mainly due to the coupling of magnetic spins with phonons [20,79]. In the previous section we have derived a general expression for the quasi-elastic (QE) part of the spin-spin correlation function [see Eqs. (96), (97)]. As already demonstrated [11, 10, 20, 79] in most classes of magnetic molecules there exists a quite wide range of temperatures and applied fields for which the magnetization fluctuations spectrum [see Eq. (97)] is dominated by a single lorentzian, i.e. a single time τ_{QE} characterizes the QE component of spin dynamics. In Fig. 30 a typical spectrum of magnetization fluctuations for Mn_{12} is shown in which the single time dynamics is apparent. In fact, the red line in the spectrum represents the frequency $\lambda_0 = 1/\tau_{QE}$ corresponding to the dominant lorentzian in Eq. (97). It is worth to stress that the calculated time τ_{QE} corresponds to a relaxation time measured by means of low frequency techniques such as AC susceptibility and NMR. On the other hand, the relaxation time defined as $max_i\{\tau_i = 1/\lambda_i\}$ corresponds to a relaxation time measured in a magnetization experiment. Nevertheless, as it can be seen in Fig. 31, the here calculated τ_{QE} well reproduces the relaxation time experimentally probed by a magnetization measurement only up to a given magnetic field $H' \sim 1.04$ T. Beyond H' the calculated τ_{QE} becomes orders of magnitude smaller than the corresponding measured relaxation time: if an AC susceptibility experiment were feasible, it would detect a relaxation time different from the one probed by a magnetization measurement and thus a different relaxation mechanism. It is possible to understand this peculiar behaviour in more detail by inspecting the dynamics of the Fe_8 nanomagnet. The microscopic parameters of the following spin Hamiltonian of Fe_8 were determined by inelastic neutron scattering experiments in Ref. [41]:

$$H = B_0^2 O_0^2 + B_2^2 O_2^2 + B_0^4 O_0^4 + B_2^4 O_2^4 + B_4^4 O_4^4, \tag{100}$$

and in K unit are reported to be $B_0^2 = -9.75 \times 10^{-2}$, $B_2^2 = -4.66 \times 10^{-2}$, $B_0^4 = \times 10^{-6}$, $B_2^4 = 1.2 \times 10^{-7}$, $B_4^4 = 8.6 \times 10^{-6}$. By assuming a spherically symmetric ME coupling

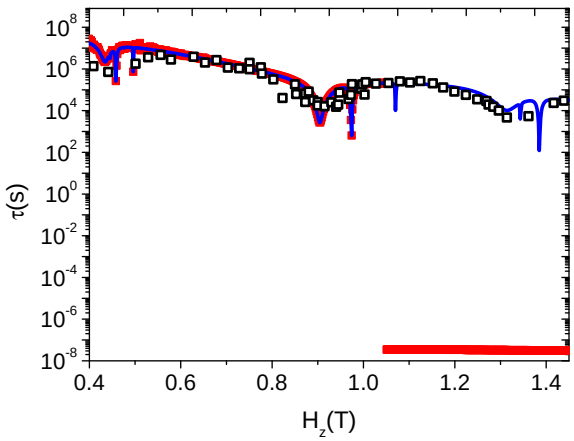

Figure 31: Relaxation time in the Mn_{12} cluster as a function of the field H_z applied along z-axis, assumed to be the easy axis of anisotropy. An angle of $\theta = 1^\circ$ defines the direction of the magnetic field **H** with respect to z. Open scatters represents the measured relaxation time as in Ref. [80]. Blue line represents the calculated relaxation time as $\tau_{QE} = max_i\{1/\lambda_i\}$, the longest time characterizing the dynamics of magnetization in Mn_{12}, i.e. the outcoming of a magnetization measurement. The red closed scatters represent the calculated relaxation time of magnetization corresponding to the dominant lorentzian in the spectrum of magnetization fluctuations [see Eq. (97)], i.e. the outcoming of an AC susceptibility experiment. These times have been calculated by taking the Hamiltonian contained in Ref. [80] and a spherically symmetric ME coupling with a constant $\gamma = 2 \times 10^{-10}$ THz^{-2}.

with a constant $\gamma = 0.9 \times 10^{-9}$ THz^{-2}, the relaxation time of magnetization can be evaluated as shown in Fig. 32(b). The calculated τ_{QE} follow an Arrhenius law with an energy barrier for the reversal of magnetization of ∼23 K, very close to the experimental value inferred from AC susceptibility measurements reported in Ref. [78]. Interestingly, with an applied field $H_z = 1$ T, for instance, the calculated magnetization relaxation time abruptly decreases for T <3.5 K showing a strong deviation from the Arrhenius law (see Fig. 33). This means that at $T < 3.5$ K another relaxation mechanism becomes predominant. In fact, if the magnetic field along z is strong enough, the two lowest levels can be those with $\langle S_z \rangle \cong 10$ and $\langle S_z \rangle \cong 9$ [1]. In addition, if temperature is low enough that the lowest state of the other well, i.e. with $\langle S_z \rangle > \cong -10$, is not appreciably populated, the cluster magnetization relaxes through a direct process involving the two lowest levels $\langle S_z \rangle \cong 10$ and $\langle S_z \rangle \cong 9$ instead of overcoming the

[1] In Fe_8 cluster the projection M of the total spin S along the z-axis is not a good quantum number. This is due to the presence of a strong in plane anisotropy term. Nonetheless, the molecule eigenstates can be labelled by the expectation value of S_z operator.

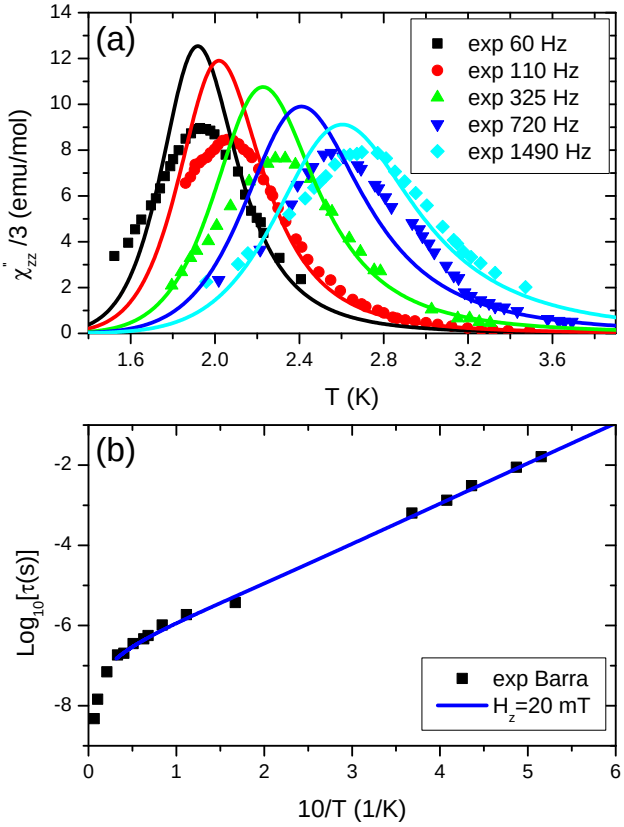

Figure 32: (a) Measured and calculated out-of-phase susceptibility as a function of T. Experimental data are taken from Ref. [78]. From the peak positions of χ'' at different angular frequencies the T-dependence of the relaxation time τ of magnetization can be inferred. (b) Calculated τ well reproduces the experimental values following an Arrhenius law with τ_0=1×10^{-7} s and Δ/k_B=23.1 K.

overall energy barrier through multi-step Orbach processes. Therefore, the dominant relaxation process occurs within the right well of the potential energy barrier and does not follow the Arrhenius law. The occurence of this fast relaxation process depends on both magnetic field and temperature, as it can be noted in Fig. 34. Besides, it is wise to remark that the relaxation time gets faster also for fields H_z ∼0.4 T, ∼0.8 T, ∼1.3 T and ∼1.7 T. In fact, for instance levels $\langle S_z\rangle >\cong -10$ and $\langle S_z\rangle >\cong 8$ produce an anticrossing at ∼ 0.4 T due to the presence of non-axial term in the cluster hamiltonian [see Eq. (100)]. In correspondence of this anticrossing field, an efficient relaxation path opens up for a quantum tunneling process between the quasi-degenerate levels. The fast relaxation mechanism has not been detected up to date but a measurement of χ'' as a function of the magnetic field applied along z at two different temperatures would

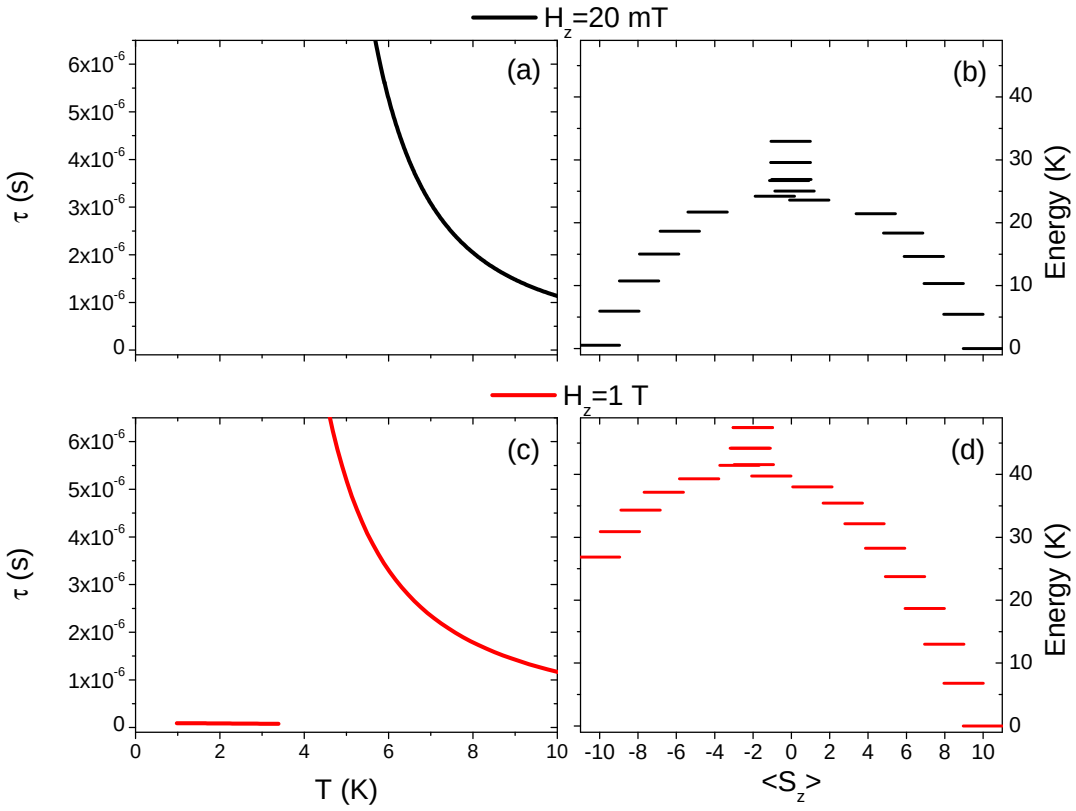

Figure 33: Calculated τ as a function of T for H_z=20 mT [in panel (a)] and for H_z=1 T [in panel (c)]. At $T < 3.5$ K for $H_z = 1$ T τ abruptly decreases: the cluster magnetization relaxes mainly through a thermally activated intra-well mode. This occurs through a direct relaxation process between the two lowest levels, $< S_z > \cong 10$ and $< S_z > \cong 9$. Thus the Arrhenius law is broken. Levels of Fe_8 with $H_z = 20$ mT [panel (b)] and with $H_z = 1$ T [panel (d)]. Due to the presence of sizeable non axial terms in Fe_8 hamiltonian, the cluster eigenstates can not be labelled with M, since it is not a good quantum number.

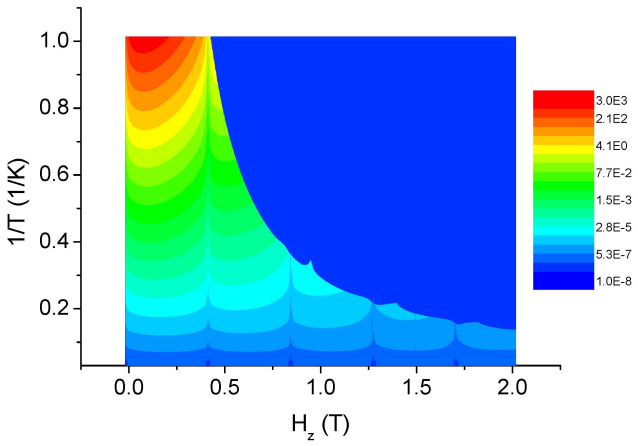

Figure 34: Dominant relaxation time in the Fe_8 molecule as a function of H_z (x-axis) and $1/T$ (y-axis). The color maps $Log_{10}[\tau(s)]$. The fast relaxation process at low T occurs for H_z >0.4 T. Moreover, at certain values of H_z a couple of quasi-degenerate levels allows a QTM process: at these fields τ gets smaller (clear vertical paths at ∼0.4 T, ∼0.8 T, ∼1.3 T and ∼1.7 T.)

allow to detect the direct intra-well relaxation process. In fact, by calculating χ'' *vs* H_z at 2.5 and 5 K, it can be argued that the decrease of χ'' calculated at $T = 2.5$ K *vs* H_z, where the fast relaxation mechanism is dominant at H_z=1 T, is more prominent than at $T = 5$ K, where the relaxation time again follows the Arrhenius law. This is a direct consequence of the crossover between slow multi-step Orbach processes and a fast intra-well direct process which occurs at $T < 3.5$ K for $H_z = 1$ T. In fact, due to the latter relaxation mechanism the system is much closer to resonance at $T = 5$ K than at $T = 2.5$ K [see Fig. 35(d)]. This causes χ'' *vs* H_z to decrease more rapidly at $T = 2.5$ K with respect to $T = 5$ K. By summarizing, in a nanomagnet with a double well potential the application of a strong enough magnetic field can speed up the relaxation dynamics with decreasing the sample temperature, thus causing the breakdown of the Arrhenius law.

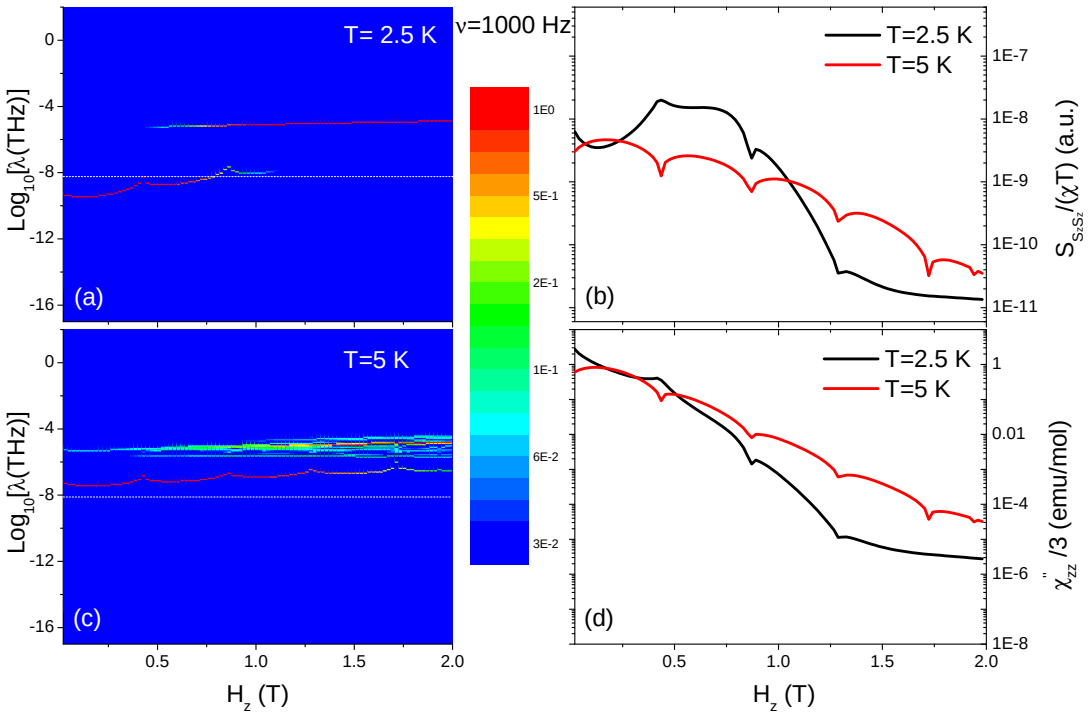

Figure 35: (a) and (c): Calculated frequency weights $A(\lambda, T, B)$ of the magnetization autocorrelation function *vs* H_z. The y axis is $Log_{10}(\lambda)$. The color maps $Log_{10}[A(\lambda, T, B)/(\chi T)]$. The spectra have been normalized by χT, since χT determines the size of equilibrium fluctuations. In each spectrum the red line is the dominant frequency in the spectra. (b): Effects of the fast intra-well relaxation mechanism in calculated $S_{S_z S_z}/(\chi T)$ *vs* H_z at 2.5 and 5 K for a frequency of 1000 Hz. The decrease of $S_{S_z S_z}/(\chi T)$ *vs* H_z is more prominent at $T = 2.5$ K than at $T = 5$ K. This reflects the presence of a fast relaxation mechanism which activates at $T < 3.5$ K if $H_z = 1$ T [see Fig. 33(c)]. (d): The effect of the fast relaxation process can be also seen in calculated χ''.

6.3 The Fe_{30} mesoscopic molecule

In this section our attention will be focused on the relaxation dynamics of one of the largest molecules synthetized so far known as Fe_{30}. Recent synthetic strategies [81, 82] have led to the preparation of this new kind of highly symmetric polyoxomolybdate compound that opens up the possibility for such giant paramagnetic clusters, something that might not be straightforward using traditional bridging ligands. Thus, thanks to its huge dimensions, Fe_{30} offers the possibility of investigating the crossing from quantum to bulk cooperative behaviour. The compound $[Mo_{72}Fe_{30}O_{252}(Mo_2O_7(H_2O))_2(Mo_2O_8H_2(H_2O))(CH_3C\,OO)_{12}(H_2O)_{91}]\cdot 150H_2O$, hereafter $Mo_{72}Fe_{30}$, is paradigmatic among these new *keplerates*. The 30 Fe^{3+} (s = 5/2) ions in this material occupy the vertices of an icosidodecahedron embedded in a framework of $\{(Mo)Mo_5\}$ groups that act as an effective superexchange pathway despite the large nearest-neighbor Fe–Fe distance (6.4 Å) [83], leading to a relatively strong antiferromagnetic coupling (J = 1.57 K [84]) and a ground state with net spin S_T = 0. The system behaves as a simple paramagnet down to about 20 K, where the susceptibility departs from a simple Curie-Weiss law before reaching a plateau at 1 K. On first approximation, the magnetism of $Mo_{72}Fe_{30}$ can be qualitatively described by a classical Heisenberg model [85, 86] that, based on the possibility of decomposing the icosidodecahedron (composed by 20 corner-sharing triangles) into three sublattices, argues that the system adopts the same ground state spin arrangement as the classical AFM triangle; that is, with nearest-neighbour spins at a relative angle of 120°. The model correctly predicts the quasi-linear field dependence of the magnetization up to a critical field H_c = 17.7 T, at which it saturates [84]. As an alternative, a simplified quantum model based on a rotational band picture of the low-lying excitation spectrum has been proposed. This also accounts for the overall low-T behavior in this material. The concept of rotational bands (i.e. $E \propto S(S+1)$, where E is the energy of each discrete level), noted experimentally to approximate the low energy states of molecular ring structures with an even number of AFM-ly coupled Heisenberg spins [39, 87, 88, 89], has been shown to apply to all finite Heisenberg systems with AFM exchange, including non-bipartite, frustrated lattices such as the icosidodecahedron [48]. Thus, by considering an effective Hamiltonian that accounts for the three sublattices in $Mo_{72}Fe_{30}$, Schnack and co-workers derive an excitation spectrum whose lower part is formed by a set of parallel rotational bands, with the gap between the two lowest bands being $5J$ (∼8 K) [48, 50]. Experimentally, the observed temperature

and field dependences of the magnetization are also consistent with the existence of the first quadratic band [50, 84]. Evidence for higher order bands has been provided by a recent neutron scattering study, which shows a main mode centered at 0.6 meV (∼8 K), interpreted as arising from transitions between the two lowest bands [51]. The details of the spectrum, especially its field dependence at base T, are not, however, entirely consistent with the model of Schnack and co-workers. Theoretical calculations of the nuclear spin-lattice relaxation rate $1/T_1$ are performed within the framework of the threesublattice quadratic-band model. We find that $1/T_1$ probes the decay of the fluctuations of the total molecular magnetization produced by the magnetoelastic coupling with the phonon heat bath. At low T, this decay is mainly determined by a single type of relaxation process involving multi-step Orbach paths passing through the first-excited rotational band. Therefore, these data provide further support for the three-sublattice quadratic-band model and highlight the possibility of obtaining the interband gap by studying the temperature behaviour of the experimental NMR relaxation rates.

6.3.1 Nuclear magnetic resonance measurements

^{1}H NMR measurements were performed on $Mo_{72}Fe_{30}$ powders in the temperature range $1.5 \leq T \leq 300$ K at several magnetic field values using a standard Fourier-transform pulse spectrometer. The ^{1}H NMR spectrum consists of a single line with no peculiar structure, the width being due to the nuclear dipolar interaction [90]. The data referring to the temperature behaviour of its full width at half maximum are reported in Ref. [91]. The nuclear spin-lattice relaxation rate (NSLR, T_1^{-1}) was measured from the recovery of the nuclear magnetization obtained with a Hahn-echo sequence, following a series of saturating radio-frequency pulses. As already reported in previous work on this material [91, 92], this recovery deviates from a single exponential behavior due to the number of different inequivalent protons in the molecule, each with its own relaxation rate. The reported T_1^{-1}'s are, therefore, average values, estimated from the initial slope of the recovery curve following the common practice in these cases [93]. The thermal evolution of the relaxation rates for B =1.18 and 2.75 T is presented in Fig. 36. Here, the solid lines represent the fits performed following the model presented in the following paragraph. As for other molecular magnets [91, 94, 95], $1/T_1(B, T)$ is characterized by a low-T maximum which shifts to higher T and reduces its intensity with increasing magnetic field.

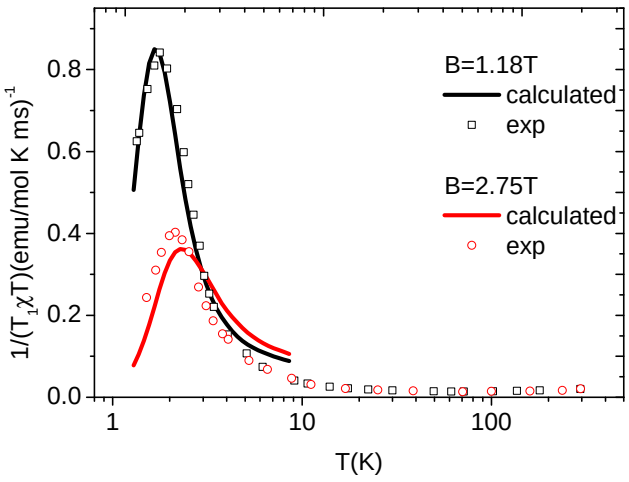

Figure 36: $1/T_1/(\chi T)$ vs T curves for two different values of the applied magnetic field B. The empty circles and squares are experimental data, while the solid and dashed lines are calculations (see text).

6.3.2 Theoretical analysis and discussion

Each Fe_{30} magnetic molecule can be described by the spin Hamiltonian

$$H = \sum_{i>j} J_{ij}\mathbf{s}_i \cdot \mathbf{s}_j + \sum_i \sum_{k,q} b_k^q(i) O_k^q(\mathbf{s_i}) + \sum_{i>j} \mathbf{s}_i \cdot \mathbf{D}_{ij} \cdot \mathbf{s}_j - g\mu_B \mathbf{B} \cdot \mathbf{S} \quad (101)$$

where $\mathbf{s}_i$ are spin operators of the i^{th} magnetic ion in the molecule. The first term is the isotropic Heisenberg exchange interaction. The second term describe the interactions with local crystal-fields (CFs), with $O_k^q(\mathbf{s_i})$ Stevens operator equivalents for the i-th ion [33] and $b_k^q(i)$ CF parameters. The third term represents the dipolar anisotropic intra-cluster spin-spin interactions. The last term is the Zeeman coupling with an external field $\mathbf{B}$ ($g = 1.974$ [85]), with $\mathbf{S}$ the total spin. Unfortunately, the dimension of the Hilbert space for Fe_{30} is huge (6^{30}) and precludes the numerical diagonalization of H on any computer. Recently, an approximate three-sublattices model has been proposed and exploited to analyze inelastic neutron scattering results [50, 51]. By naming $\mathbf{S}_A$, $\mathbf{S}_B$ and $\mathbf{S}_C$ the total spin of the three sublattices, the low-energy spin dynamics of Fe_{30} is approximately described by

$$H_{eff} = J(\mathbf{S}_A \cdot \mathbf{S}_B + \mathbf{S}_A \cdot \mathbf{S}_C + \mathbf{S}_B \cdot \mathbf{S}_C)/5 - g\mu_B \mathbf{B} \cdot \mathbf{S}, \quad (102)$$

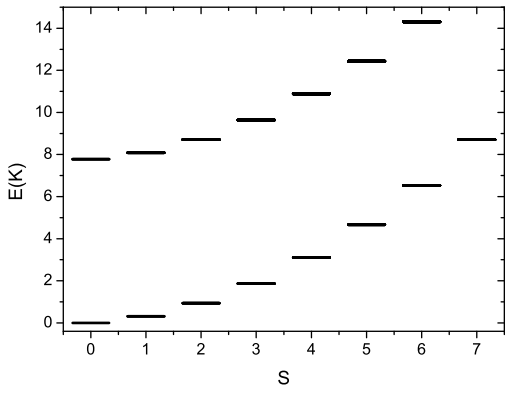

Figure 37: The two lowest bands of energy levels calculated in zero-field from the three-sublattices model [50, 51].

where $J = 1.55K$ is the nearest-neighbor exchange constant and $\mathbf{S}$ is the molecular total spin. Eigenvalues of H_{eff} can be analytically calculated

$$\begin{aligned} E(S_A, S_B, S_C, S, M) &= J(S(S+1) - S_A(S_A+1) \\ &\quad -S_B(S_B+1) - S_C(S_C+1))/10 - g\mu_B BM, \end{aligned} \tag{103}$$

with M the eigenvalue of the z component of the total spin. The system has a nonmagnetic $S = 0$ ground state whereas the low-lying excited states form a set of parabolic rotational bands (see Fig. 37). The lowest rotational band, for which $S_A = S_B = S_C = 25$ is composed by 132651 levels, while the second rotational band, characterized by having $S_A = 24, S_B = S_C = 25$ and permutations thereof, contains 3441123 states. The eigenvalues in Eq. (103) are degenerate with respect to the intermediate quantum number $\mathbf{S}_{AB} = \mathbf{S}_A + \mathbf{S}_B$. Further degeneracy arises because of the internal spin structure of each giant spin S_A, S_B, S_C when $S_{A,B,C} \leq 24$. As a result, the degeneracies for $S \leq 24$ are $D_1 = d_1(S)(2S+1)$ for the lowest, and $D_2 = d_2(S)(2S+1)$ for the first excited rotational band. Here $d_1(S) = 2S+1$ and $d_2(S) = 27(2S+1)$ are the S-degeneracy factors for the two lowest bands [51]. Since the Fe^{3+} ions are arranged on the vertices of an icosidodecahedron, Fe_{30} offers the possibility to study the relaxation dynamics of a highly frustrated system.

The low-frequency quasi-elastic (QE) spin dynamics of Fe_{30} is calculated as in Ref. [20]. The interaction with the phonon heat bath leads to the expression of Eq. (96) for the Fourier transform of the time autocorrelation function for equilibrium fluctuations of two generic observables $\mathcal{A}$, $\mathcal{B}$ as derived in Section 6.1. The QE frequency-spectrum is therefore a sum of n lorentzians centered at zero frequency whose widths λ_i are the

eigenvalues of $-\mathbf{W}$ (n being the dimension of the molecule spin Hilbert space). As noted in [20], these n $\tau_{QE}^{(i)}$ are different from the n level lifetimes $\tau_{life}^{(s)}$.
The main contribution to the spin-phonon coupling potential V comes from the modulation of rank-2 intramolecular anisotropic interactions by elastic waves. On the one hand, experimental information is by far insufficient to assess the specific form of V. Moreover, even if V was known, it would be impossible to calculate the W_{st} matrix elements. In fact, transitions between spin levels induced by the spin-phonon interaction can be divided into two groups: intra- and inter-band transitions. The former involve states having the same sublattices total-spin quantum numbers ($S_A,\ S_B,\ S_C$) while in the latter the involved states differ for one total-spin quantum number at least. The calculation of the matrix elements of V for inter-band transitions requires assumptions on the structure of spin eigenstates which are beyond the simple approximate three sublattices model. Indeed, this model does not provide information on the complex composition of each eigenstate in terms of local spin states. In view of this, the most unbiased choice is to assume $v = |\langle t|V|s\rangle|^2 = 1$ if the selection rules $|\Delta S| = 0, 1, 2$, $|\Delta S_A| = 0, 1, 2$, $|\Delta S_B| = 0, 1, 2$, $|\Delta S_C| = 0, 1, 2$, $|\Delta S_{AB}| = 0, 1, 2$ and $|\Delta M| = 0, 1, 2$ are satisfied, and $v = 0$ otherwise ($\mathbf{S}_{AB}$=$\mathbf{S}_A$+$\mathbf{S}_B$). This sort of approximation is analogous to that used in [51] for the interpretation of neutron spectroscopy data. By adopting a Debye model for phonons, this leads to

$$W_{st} = \gamma\pi v\Delta_{st}^3 n(\Delta_{st}), \tag{104}$$

with

$$n(x) = (e^{\beta\hbar x} - 1)^{-1}, \Delta_{st} = (E_s - E_t)/\hbar. \tag{105}$$

The free parameter γ describes the spin-phonon coupling strength, and is determined by comparison with experimental data. Even within this approximation, calculating the relaxation spectrum [Eq. (96)] by including all the states belonging to the two lowest bands is unfeasible because of the huge dimension of the resulting Hilbert space (3573774 states). Therefore, in order to calculate the relaxation dynamics of Fe_{30}, we have exploited two further approximations. First, we have limited our calculations to low temperature, thus including levels with energy only up to 11.1 K (9.3 K) from the (field dependent) ground state for B=1.18 T (=2.75 T), and higher-lying levels of the two lowest bands connected to these by V. For each of these eigenstates of the second band, there are eight further degenerate eigenstates having the same set of quantum numbers ($S_A, S_B, S_C, S_{A,B}, S, M$). To further reduce the dimension of the spin Hilbert

space, we have considered only one representative state (out of nine), and we have multiplied interband transition probabilities by 9. We have checked that if both these approximations are relaxed, results do not change qualitatively.

Important information on the relaxation dynamics of Fe_{30} can be obtained through NMR measurements of the nuclear spin-lattice relaxation rate $1/T_1$ [20]. The latter is given by a linear combination of the Fourier transforms of electronic spins correlation functions evaluated at the Larmor frequency [47]. By considering only the Heisenberg and Zeeman terms in the Hamiltonian [see Eq. (101)], Eq. (98) becomes:

$$\begin{aligned} 1/T_1 \quad \propto \quad & \sum_{i,j=1,N} \alpha_{ij}(S_{s_i^z,s_j^z}(\omega_L) + S_{s_i^z,s_j^z}(-\omega_L)) + \\ & \beta_{ij}(S_{s_i^+,s_j^-}(\omega_L) + S_{s_i^+,s_j^-}(-\omega_L) + \\ & S_{s_i^-,s_j^+}(\omega_L) + S_{s_i^-,s_j^+}(-\omega_L)), \end{aligned} \tag{106}$$

and represents the spin lattice relaxation rate of a magnetic nucleus of Larmor frequency ω_L interacting with a molecule composed of N spins. Here α_{ij} and β_{ij} are geometrical coefficients of the dipolar interaction between nuclear and electronic spins, and $S_{\mathcal{A},\mathcal{B}}(\omega)$ is the Fourier-transform of the time correlation function. Since far from level crossings $\omega_L << \Delta_{st}$, only the QE part of the $S_{\mathcal{A},\mathcal{B}}$ in the above formula contributes to $1/T_1$ [2]. Then, for Fe_{30} Eq. (96) implies that only zz terms are nonzero in Eq. (106) because in the lack of anisotropy $\langle s|s_i^{\pm}|s\rangle = \langle t|s_i^{\pm}|t\rangle = 0$. Since far from level crossings $\omega_L \ll \Delta_{st}$, only the QE part of the $S_{A,B}(\omega)$ in the above formula contributes to $1/T_1$. In addition, within the three sublattices model $\langle s|s_{i,z}|s\rangle \propto \langle s|S_z|s\rangle$. Therefore, within the present model the nuclear spin-lattice relaxation rate is proportional to the Fourier transform of the autocorrelation function of S_z,

$$1/T_1 \propto S_{S_z,S_z}(\omega_L). \tag{107}$$

Hence, in Fe_{30} a measure of $1/T_1$ allows to directly extract information on the decay of the autocorrelation the molecular magnetization. Therefore, in the following we focus on the spectrum of fluctuations of the molecular magnetization by Eq. (97). In general, many different relaxation frequencies $\lambda_i(T,B)$ can contribute to this spectrum:

$$S_{S_z,S_z}(\omega,T,B) = \sum_{i=1,n} A(\lambda_i,T,B)\frac{\lambda_i(T,B)}{\lambda_i(T,B)^2+\omega^2}.$$

[2] Direct incoherent transitions between degenerate levels have been neglected due to the vanishing phonon density of states.

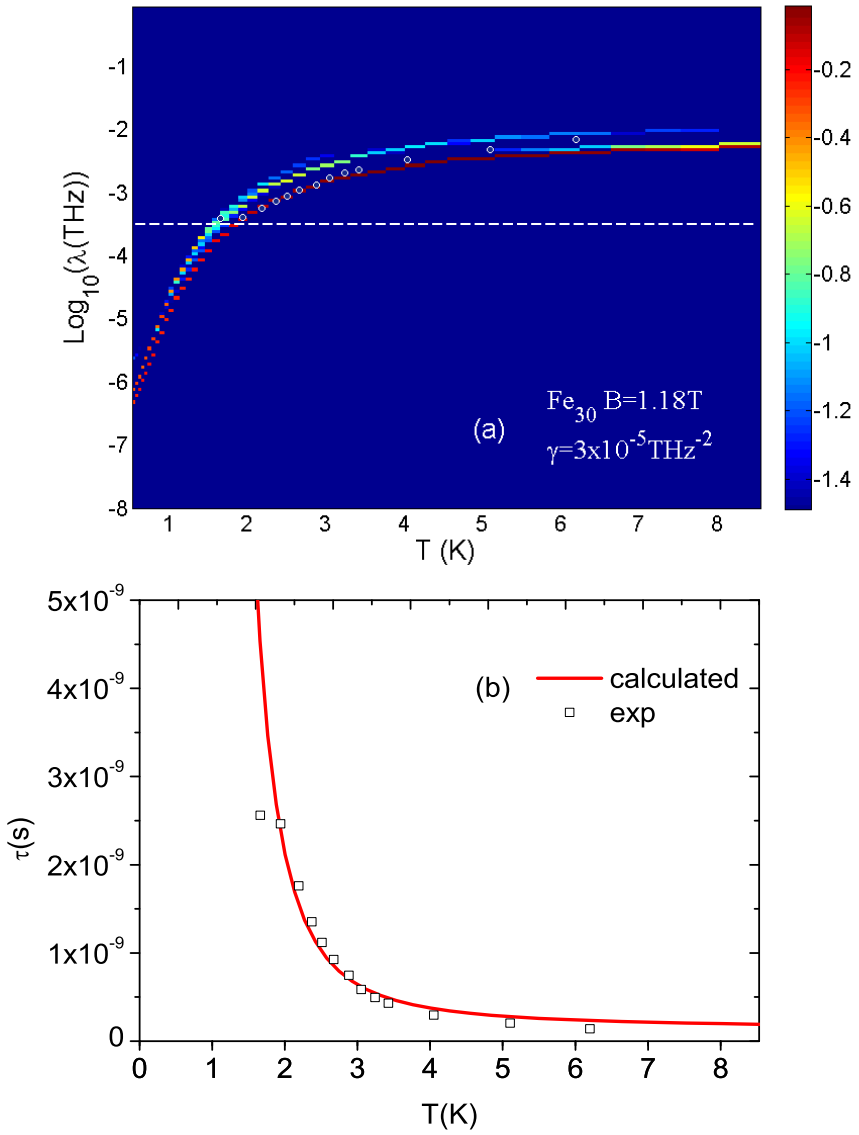

Figure 38: (a): Calculated frequency spectra $A(\lambda_i, T, B)$ of the magnetization auto-correlation $S_{S_z,S_z}(\omega)$ as function of T. The color maps $\text{Log}_{10} A/\chi T$ and gives the weight of each lorentzian to the spectrum of fluctuation of S_z. For each value of T, the ω-integrated weight equals the size of equilibrium fluctuations, proportional to χT. The white dashed line represents the ^1H Larmor angular frequency ω_L, and the white points are the characteristic frequency $\lambda_0(T)$ extracted from experimental NMR data [see panel (b)]. The graphic shows only the frequency weights larger than 3%. (b): Calculated (red line) and measured (squares) relaxation time τ_0^{mag} for $B = 1.18T$. The red line corresponds to the dominant frequency λ_0 in panel (a). The T-dependence of τ_0^{mag} follows an Arrhenius law with a gap $\Delta/k_B \approx 7.2K$.

Fig. 38(a) shows logarithmic intensity plots of the frequency weights $A(\lambda_i, T, B)$ as function of temperature T. The free parameter $\gamma = 3 \times 10^{-5}$ Thz^{-2} has been estimated by fitting the position of the peaks observed in the T-dependence of $1/T_1$ (see below). The precise value of γ does not change the spectra qualitatively, but merely sets the frequency range. Surprisingly, *a single lorentzian* of characteristic frequency λ_0 dominates the relaxation spectrum of S_z for a fairly wide ranges of values of T and B. By exploiting linear response theory, the dynamical structure can be approximately rewritten as

$$S_{S_z,S_z}(\omega, T, B) \propto \chi T \frac{\lambda_0(T,B)}{\lambda_0(T,B)^2 + \omega^2}. \tag{108}$$

The single dominating decay-time $\tau_{QE}^{(mag)} = \lambda_0^{-1}$ is different from the lifetime of any thermally-populated level. Our calculations indicate that in the *single-lorentzian* regime the decay of fluctuations of the molecular magnetization is mostly due to inter-band Orbach-like processes. In particular, the dominant relaxation time $\tau_{QE}^{(mag)}$ follows at low T an Arrhenius law $\tau \propto \exp(-\frac{\Delta}{k_B T})$ with $\Delta/k_B \approx 7.2K$ (for $B = 1.18T$) [Fig. 38(b)], which is close to the energy gap between the two lowest energy bands. Direct intra-band transitions do not appreciably affect the relaxation behavior due to the small associated gaps.

Since there is only a single frequency with appreciable weight in the spectrum of fluctuations, Eq. (107) implies (see Fig. 36) that $1/T_1/(\chi T)(T)$ displays a sharp peak at the temperature T_0 for which $\lambda_0(T_0) = \omega_L$, i.e. where the white dashed line intersects the red one in Fig. 38(a). In spite of the unavoidable approximations made in the calculation, the agreement between theoretical and experimental results in Figs. 6b and 4 is very good and provides strong support to our picture of relaxation dynamics in Fe_{30}. In particular, a single thermally-activated Orbach process sets the decay of S_z, just as found in AF rings, AF grids and high-anisotropy nanomagnets [20]. This in spite of the very different spectrum of the highly frustrated Fe_{30} molecule.

In the mesoscopic molecule Fe_{30} we have found that in the intermediate temperature regime (above 1K), the NMR relaxation rates show a unique dominating correlation time characterized by a thermally activated behavior with an activation energy roughly equivalent to the gap between the lowest rotational bands of this material. These results are consistent with our theoretical calculations, which show that a single interband Orbach process dominates the low-E excitation spectrum in this regime.

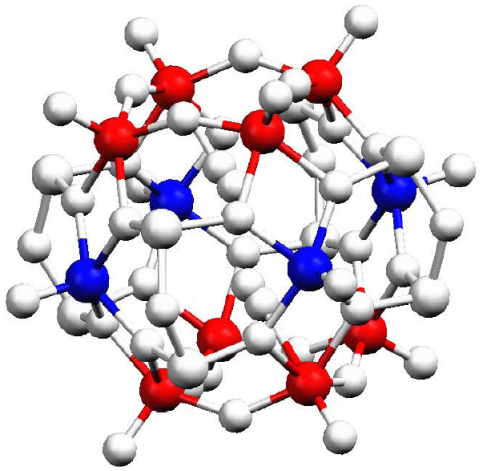

Figure 39: Schematic representation of the V_{12} cluster. The red and blue spheres are the Vanadium ions in the two outer V_4 squares and in the central V_4 square respectively.

6.4 The antiferromagnetic cluster V_{12} containing ions with spin 1/2

In this section, we consider the case of the so-called V_{12} molecule. This cluster contains twelve Vanadium ions organized in three squares (see Fig. 39). It has been shown that low-temperature (T <300 K) magnetic properties of this molecule are the result of exchange interaction of the four central $s = 1/2$ Vanadium ions. The latter are antiferromagnetically coupled [96,97], giving a $S = 0$ ground state. The remaining eight Vanadium ions are so strongly antiferromagnetically coupled within each square that the thermodynamic and magnetic properties of the cluster are explained in terms of the only four inner ions up to room temperature. Here we calculate the electronic relaxation dynamics of V_{12} which has been experimentally probed by NMR $1/T_1$ measurements [97]. Being $s = 1/2$ ions unaffected by the crystal field and its modulation by phonons, we assume the main contribution to the spin-phonon coupling to arise from modulation of the two-ion anisotropic exchange interaction. As in the previous section, here we investigate the molecular magnetization M through the approach presented in Section 6.1. In this case phonons are assumed to cause the modulation of nearest neighbours anisotropic exchange, since there are no local crystal field terms for ions with spin 1/2.

Thus, a simple choice for the magnetoelastic coupling yields [98]

$$W_{mn} = \gamma\pi \left| \langle n| \sum_{\substack{i=1,N \\ Q=0,1,2}} c(i) T_2^Q(i) \, |m\rangle \right|^2 \Delta_{mn}^3 n(\Delta_{mn}) \tag{109}$$

where $N = 4$ is the the number of bonds, $n(x) = (e^{\beta\hbar x} - 1)^{-1}$, $\Delta_{mn} = \frac{E_m - E_n}{\hbar}$ the gap between the eigenstates $|m\rangle$ and $|n\rangle$ of the molecule. Here the $T_2^Q(i)$ are combinations of rank-2 complex tensor operators describing the anisotropic exchange on bond $i, i+1$ [35, 98]:

$$\begin{aligned} T_2^0(i) &= T_0^2(11|i, i+1), \\ T_2^1(i) &= \left[T_{-1}^2(11|i, i+1) - T_1^2(11|i, i+1)\right], \\ T_2^2(i) &= \left[T_2^2(11|i, i+1) + T_{-2}^2(11|i, i+1)\right]. \end{aligned} \tag{110}$$

γ is the unique free parameter of the theory, which sets the frequency scale and reflects the strength of the magnetoelastic coupling causing relaxation. The $c(i)$ are numerical coefficients whose specific choice does not influence results qualitatively, provided γ is properly rescaled [3]. Eq. (97) shows that the spectrum of the fluctuations is a sum of 16 lorentzians, each characterized by a frequency λ_i. Our calculations show that only a few relaxation frequencies significantly contribute to $S_{S_z,S_z}(\omega, \mathbf{B}, T)$ in the investigated range of $\mathbf{B}$ and T. It has been demonstrated that in ring-shaped molecules with small anisotropy, $1/T_1 \propto S_{S_z,S_z}(\omega_L)$, $1/T_1$ being the nuclear spin-lattice relaxation rate [20]. The proton $1/T_1$ can be evaluated in absolute units by exploiting the Moriya formula [47] using as input the positions of the V-ions and of the hydrogens of the molecule.

In previously studied rings [20, 79, 98] only a single frequency λ_0 has appreciable weight. In this case, Eq. (97) implies that $1/T_1(T)$ sharply peaks at the temperature T_0 for which $\lambda_0(T_0) = \omega_L$. However our calculations indicate that in V_{12} the dominant frequency does not intersect ω_L [see Fig. 40(a)]. This is reflected in the T-dependence of $1/T_1$ shown in Fig. 40(b). Indeed, the calculated $1/T_1$ reaches an almost constant value without showing any sharp peak, in excellent agreement with the experimental NMR data.

[3] The available experimental information is by far insufficient to deduce the exact form of the magnetoelastic hamiltonian

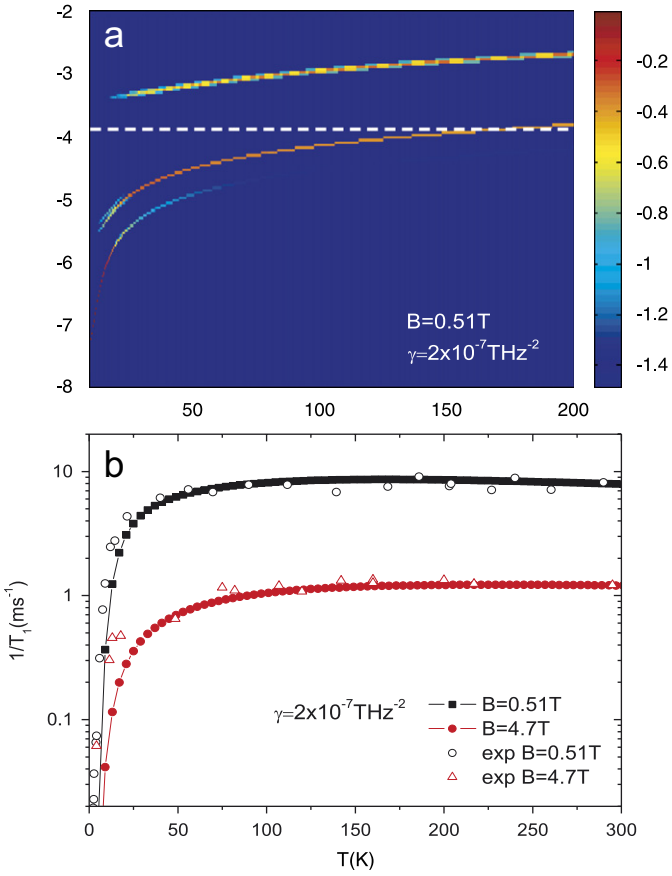

Figure 40: Top: Spectral weights $(A(\lambda_i, T, \mathbf{B}))$ as a function of temperature T [see Eq.(97)]. The y-axis is $log_{10}(\lambda)$ (in THz). The color maps $log_{10}A/\chi T$ and gives the weight of each lorentzian to the spectrum of the fluctuations of **M** and the white dashed line represents the ^1H Larmor frequency ω_L. The graphic only shows frequency weights larger than 3%. Bottom: The calculation of proton NMR $1/T_1$ for two values of the applied magnetic field **B**. Experimental points are taken from Ref. [97].

6.5 The antiferromagnetic ring Cr_7Ni

The Chromium-based heterometallic ring named Cr_7Ni was taken into account in chapter 5 as regards its static magnetic properties. In this section we want to focus on the spin dynamics of Cr_7Ni cluster. In fact, a major obstacle to the proposed technological applications of magnetic molecules is constituted by phonon-induced relaxation. Molecular observables, e.g. the magnetization, are deeply affected by the interaction of the spins with other degrees of freedom such as phonons [20]. Here we investigate the molecular spin-spin correlations through the approach described in Section 6.1 and already applied for the Mn_{12} and Fe_8 nanomagnets, the Fe_{30} mesoscopic molecules and the antiferromagnetic cluster V_{12}.

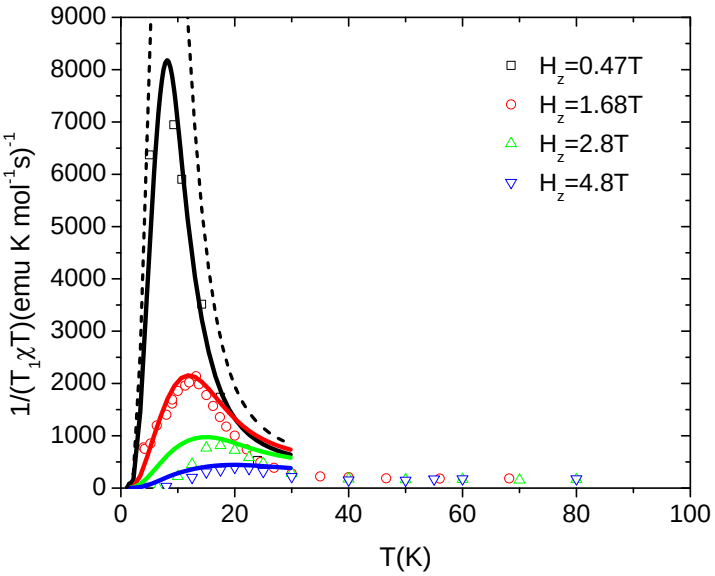

Figure 41: Experimental data (scatters) and calculations (lines) of reduced proton NMR $1/T_1/(\chi T)$ for different values of the applied field along z (parallel to the ring axis). The dashed line represents the calculations for $H_z = 0.47$ T considering the same set of hydrogens used to produce the curves with $H_z = 1.68, 2.8$ and 4.7 T. The consequences of the so called wipe-out effect [99] are apparent.

In the following we will assume a spherically symmetric ME coupling as in Ref. [75] [see Eq. (87)]. γ still represents the spin-phonon coupling strength, which can be determined by comparing the theoretical results with experimental data. In fact, the nuclear spin-lattice relaxation rate $1/T_1$ probes the fluctuations of molecular observables, thus giving information on the relaxation dynamics [20]. Exploiting the Moriya formula [47], the proton NMR $1/T_1$ can be evaluated in absolute units using as inputs the positions of the Cr and Ni ions and of the hydrogens of the molecule by means of Eq. (98). The occurence of a peak in the proton NMR $1/T_1$ has been clearly explained in homonuclear ring-shaped molecules with small anisotropy such as Cr_8 [20]. In fact, in this case $1/T_1 \propto S_{S_z,S_z}(\omega_L)$, where $S_{S_z,S_z}(\omega, \mathbf{H}, T)$ is the Fourier transform of the autocorrelation function of M [20]: $S_{S_z,S_z}(\omega, T, \mathbf{H}) = \sum_{i=1,N} A(\lambda_i, T, \mathbf{H})\lambda_i(T, \mathbf{H})/[\lambda_i(T, \mathbf{H})^2 + \omega^2]$. This equation shows that the spectrum of fluctuations of M is given by a sum of N Lorentzians, where N represents the dimension of the Hilbert spin space associated to the molecule. Each lorentzian has characteristic frequency λ_i, given by the eigenvalues of $-\mathbf{W}$. For a wide range of $\mathbf{H}$ and T in these systems only a single relaxation frequency λ_0 significantly contributes to $S_{S_z,S_z}(\omega, T, \mathbf{H})$. As a result, if the dominant frequency λ_0 intersects the Larmor angular frequency, i.e. when $\lambda_0(T_0) = \omega_L$, at the

temperature T_0 the proton NMR $1/T_1$ shows a sharp peak [20, 94]. Being an heterometallic ring, this explanation does not hold for Cr_7Ni and Eq. (98) has to be used. Nevertheless, our calculations show that a peak in the reduced $1/T_1/(\chi T)$ occurs in agreement with experimental data (see Fig. 41). By fitting the observed peak position we have obtained $\gamma = 0.8 \times 10^{-7}$ THz^{-2} [100]. This value turns out to be quite reasonable since it can be further obtained by reproducing the experimental proton NMR $1/T_1/(\chi T)$ data in the parent Cr_8 compound as shown in Fig. 42 [4] [20, 79]. A ME coupling strength similar in the two Cr-based rings should be expected, even though the presence of a Ni ion in Cr_7Ni could in principle cause the ME constant to augment. In fact, the ME constant of each magnetic ion is proportional to the square of the CF magnitude, and in Cr_7Ni the rate of the Chromium and Nickel CF parameters, d_{Cr} and d_{Ni} respectively, has been found to be d_{Ni}/d_{Cr} ∼12. Nonetheless, since the experimental information is by far insufficient to fix more than one ME constant, it has been chosen to reabsorbe the greater Nickel ME constant in a unique ME constant equal for each magnetic ion. Apart from the similarities in the ME coupling strength, the spin dynamics in the two parent compounds is quite different. In fact, in Cr_8 the occurence of peaks in the proton NMR $1/T_1/(\chi T)$ can be well explained in terms of cluster magnetization dynamics by means of Eq. (97) [20, 79]. On the other hand, in heterometallic ring Cr_7Ni $1/T_1/(\chi T)$ is proportional to a linear combination of local spin-spin correlation functions as shown in Eq. (98). Thus the positions and intensities of the peaks can be understood by inspecting the behaviour of $\alpha_{ij}^{qq'} S_{s_i^q, s_j^{q'}}(\omega_L)$ as a function of T, where $\alpha_{ij}^{qq'}$ represents the geometric coefficient which depends on the relative positions of magnetic ions i, j and the probed nucleus. In order to reproduce the correct intensity of each experimental curve of Fig. 41, it is necessary to consider only the hydrogens probed by NMR. In fact, when the temperature decreases it is possible to have a loss of NMR intensity followed by an enhancement of the spin-spin $1/T_2$ and the spin-lattice relaxation rate $1/T_1$. When $1/T_2$ overcomes the limit fixed by the experimental setup, a loss of NMR signal may occur [99]. This effect is known as *wipe-out* and was found out in several examples nanomagnets [99]. Nevertheless the wipe-out affects the measured $1/T_1/(\chi T)$ also in Cr_7Ni. As a result, ∼85% of the hydrogens in Cr_7Ni molecule for fields $H_z = 1.68, 2.8, 4.8$ T and only ∼37% for $H_z = 0.47$ T has been considered in calculations. The remaining hydrogens not considered to evaluate

[4] In order to produce an ergodic ME coupling, a slightly site dependent spherically ME has been chosen in such a way to have the mean value of γ=0.8×10^{-7}THz^{-2}.

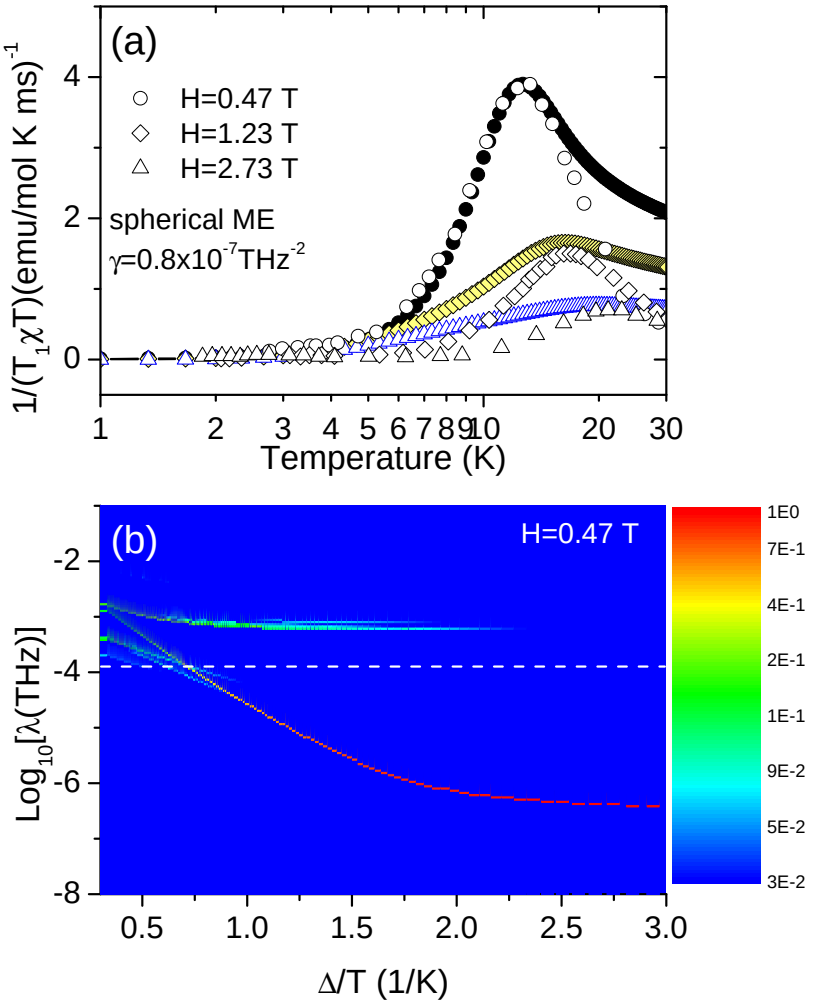

Figure 42: (a) Calculated and measured proton NMR $1/T_1/(\chi T)$ for different applied fields in the case of Cr_8 ring. Experimental points are taken from Ref. [20]. (b) Calculated frequency spectrum of magnetization for $H = 0.47$ T. y axis is $\mathrm{Log}_{10}[\lambda(THz)]$ *1/T*, where the λ_i are the eigenvalues of $-\mathbf{W}$ matrix, i.e. the inverse of the times characterizing the return to equilibrium of cluster magnetization. The color maps $\mathrm{Log}_{10}(A(\lambda_i, T, H)/(\chi T))$, i.e. the the frequency weight of each lorentzian in the magnetization fluctuation spectrum [see Eq. (97)]. Only frequencies with weight greater than 3% are shown in panel (b). The white dashed line represents the angular Larmor frequency ω_L for $H = 0.47$ T.

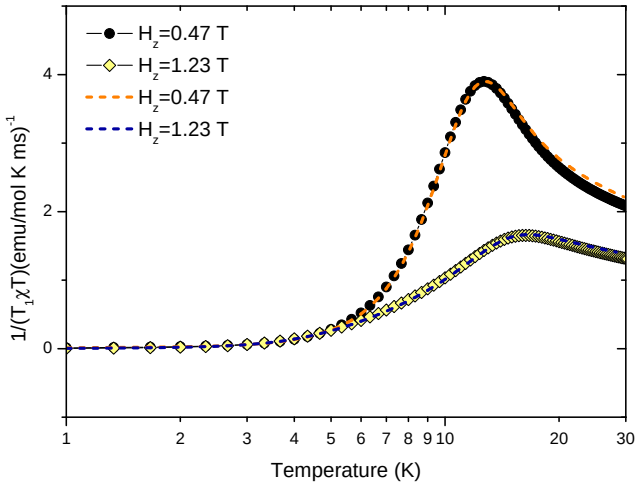

Figure 43: Scatters: calculated $1/T_1/(\chi T)$ with Eq. (107), thus exploiting the fluctuations of magnetization at $H_z = 0.47$ and 1.23 T. Dashed lines: calculated $1/T_1/(\chi T)$ with Eq. (98) and therefore considering the fluctuations of the molecular obervables probed the hydrogens nuclei contained in Cr_8 molecule. It is straightforward to note that the two equations lead to the same result. Thus in homometallic AF ring Cr_8, observing the fluctuations of magnetization is equivalent to probing the fluctuations of any of the molecular observables contained in the sum of Eq. (98).

the proton NMR $1/T_1/(\chi T)$ are the closest to magnetic ions. In fact, these hydrogens experience a faster relaxation of the NMR $1/T_1$ with respect to other hydrogens. Thus, if the corresponding $1/T_2$ overcomes the experimental limit, $1/T_1$ can not be probed in a NMR experience, and therefore these *faster* hydrogens have been neglected in calculations. Besides, there is another striking difference between relaxation dynamics in Cr_7Ni and Cr_8 rings. This difference regards the scaling of $1/T_1/(\chi T)$ curves for the various magnetic field at peak positions. As long as there is a dominant relaxation time of cluster magnetization for Cr_8 compound, the peak of $1/T_1/(\chi T)$ scales as $\frac{1}{\omega_L}$, where $\omega_L = \gamma H$ [5]. If we take, for instance, the curves at $H_z^{(1)} = 0.47$ T and $H_z^{(2)} = 1.23$ T having p_1 and p_2 peak value respectively, it can be found out a rate $\frac{p_1}{p_2} \approx \frac{H_z^{(2)}}{H_z^{(1)}}$ both in calculations and measurements. It is worth to remark that a similar result can be obtained if instead of Eq. (107) Eq. (98) is used to evaluate $1/T_1/(\chi T)$ (see Fig. 43). This result allows to make two main considerations. Since for Cr_8 homometallic cluster it is equivalent to use Eq. (107) and (98) it follows that the molecular observables probed by hydrogen atoms peak at the same temperature. Moreover, it can be

[5] Here γ represents the giromagnetic ratio, and not the spin-phonon coupling strength.

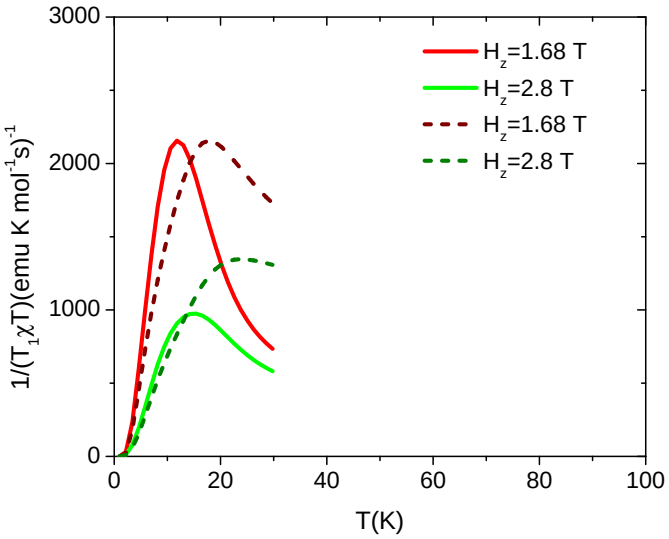

Figure 44: Continuos lines: $1/T_1/(\chi T)$ calculated as a linear combination of local spin-spin fluctuations [see Eq. (98)]. Dashed lines: $1/T_1/(\chi T)$ calculated exploiting Eq. (107), i.e. the fluctuations of cluster magnetization.

argued that observing the fluctuations of magnetization is equivalent to probing the fluctuations of any of the molecular observables contained in Eq. (98). At this point the following question arises: how the calculated $1/T_1/(\chi T)$ would appear in Cr_7Ni if only the fluctuations of molecular magnetization were taken into account. In other words, one may wonder to what extent it is not correct to use Eq. (107) to calculate $1/T_1/(\chi T)$ in Cr_7Ni heterometallic ring. The dashed lines in Fig. 44 represent the calculation of $1/T_1/(\chi T)$ by Eq. (107). It can be noted that the peaks do not occur at the right temperature, differently from the case of Cr_8. Besides, the two curves at $H_z = 1.68$ and 2.8 T scale according to the law $\frac{1}{\omega_L}$, something that does not match with the experimental data. This demonstrates that in Cr_7Ni the proton $1/T_1/(\chi T)$ probes the local spin-spin fluctuations and not the fluctuations of cluster magnetization.

6.6 Conclusions

In this chapter we have investigated the relaxation dynamics in several types of magnetic molecules: the Mn_{12}, Fe_8 nanomagnets, the Fe_{30} icosidodecaedron, the V_{12} antiferromagnetic cluster containing ions with spin 1/2 and the Cr_7Ni heterometallic ring. In nanomagnets a fast relaxation mechanism occurs when the magnetic field applied along the easy axis is high enough so that the two lowest levels belong to one well of

the potential, and the the temperature is low enough so that the lowest level of the other well is not appreciably populated. In other words, the application of a strong enough magnetic field can speed up the relaxation dynamics with decreasing the sample temperature, thus causing the breakdown of the Arrhenius law. In Fe_{30}, V_{12} and Cr_7Ni the relaxation dynamics is investigated by analysis of NMR measurements. In Fe_{30} the relaxation mode characterizing the return of equilibrium of the cluster magnetization falls in the frequency window of NMR, thus allowing to experimentally probe the relaxation time of magnetization. The T-dependence of the relaxation time can be inferred by the peak positions of the measured proton $1/T_1/(\chi T)$ at different applied magnetic fields. This is not the case for V_{12} and Cr_7Ni. In the former case the times characterizing the magnetization dynamics are not detectable in a NMR experiment. Thus the NMR response $1/T_1$ does not show any peak. The latter case is much more complicated. In fact, being a heterometallic ring, in Cr_7Ni the $1/T_1/(\chi T)$ does not simply probe the fluctuations of cluster magnetization, but more generally combinations of molecular observables. Anyhow, peaks in the measured proton $1/T_1/(\chi T)$ occur and calculations reproduce the experimental NMR data very well.

Chapter 7

General conclusions

In this thesis theoretical models within the spin Hamiltonian approach and the corresponding computational techniques have been developed in order to investigate the spin dynamics in several types of magnetic molecules. In particular, the class of the so called nanomagnets can be treated in the strong exchange limit: each molecule well behaves as a single total spin S with an effective potential. This approximation allows to give explanation of many properties of nanomagnets at low temperature thanks to the reduced dimensions of the corresponding spin Hamiltonian in the $(2S + 1)$-fold degenerate spin subspace. Nevertheless, in most magnetic molecules the *single spin* model (known as "Giant spin") can not be applied and the spin Hamiltonian has to be evaluated in the total Hilbert spin space. This difficulty has been overcome by exploiting the irreducible tensor operator technique together with perturbative methods. In fact, the isotropic exchange represents the main interaction in all studied clusters. In order to have a deeper understanding of fundamental features and a major control on technological aspects, it is crucial to know the mechanisms which govern the spin dynamics. Both from a theoretical and an experimental point of view, spin dynamics is characterized by two distinct regimes: coherent and incoherent.

The coherent dynamics has been directly investigated through the analysis of inelastic neutron scattering (INS) measurements and indirectly through the analysis of bulk measurements (such as magnetization and specific heat at high fields). This has allowed to determine the microscopic parameters by comparing the theoretical predictions with experiments. In particular, the parameters of the isotropic exchange, of the crystal fields and of the dipolar interaction of the Cr_8Zn spin segment (or open ring) have been determined by reproducing the experimental INS cross sections. Furthermore, we have investigated the consequences of the breaking of ring symmetry in Cr_8Zn taking

the closed Cr_8 ring as reference. The most relevant effect of the ring opening has been found in the structure of eigenstates of Heisenberg isotropic exchange interaction: the appearance of disjoint quantum fluctuations of the total spin length of the two sublattices causes the usual classification of low-lying states into distinct rotational bands to fail. These fluctuations show up in the measured INS intensity as a function of the scattering wave vector Q, and produce the large decrease of the effective anisotropy with respect to the closed ring. Another consequence is the decrease of the gap between ground- and first-excited multiplets [8]. We have then focused on this last point by analysis of magnetization measurements on Cr_8Cd (open ring) and Cr_8 compounds. In both clusters the magnetization M as a function of applied magnetic field shows a clear staircase structure. By determining the peak positions of dM/dH it is possible to demonstrate that Cr_8Cd shows a more prominent deviation from Landé rule with respect to Cr_8 due to the ring opening [7]. Other two Cr-based rings have been analysed by interpreting magnetization measurements at very high fields: they are the Cr_7Ni and Cr_8Ni heterometallic rings. In both cases a clear step-wise increase of magnetization with increasing field is observed. The very good agreement of high field magnetization measurements up to almost 60 T with calculations shows the spin Hamiltonian approach to be suitable even at very high fields. In particular, in Cr_7Ni these results confirm that the microscopic picture derived from INS experiments [30,68] at zero field perfectly holds even for spin multiplets not accessible to the INS technique. Besides, in Cr_8Ni the magnetization study has proved a spin singlet ground state. Due to the odd number of magnetic sites the AF interactions between neighbouring spins can not be simultaneously satisfied [67], and the system has been regarded as frustrated [66]. Indeed, effects of magnetic frustration can be found in the ground $S = 0$ state [9].
The relaxation dynamics has been investigated in several types of magnetic molecules: the Mn_{12}, Fe_8 nanomagnets, the Fe_{30} icosidodecaedron, the V_{12} antiferromagnetic cluster containing ions with spin 1/2 and the Cr_7Ni heterometallic ring. In nanomagnets we have shown that a fast relaxation mechanism occurs when the magnetic field applied along the easy axis is high enough so that the two lowest levels belong to one well of the potential, and the the temperature is low enough so that the lowest level of the other well is not appreciably populated. In other words, the application of a strong enough magnetic field can speed up the relaxation dynamics with decreasing the sample temperature, thus causing the Arrhenius law to fail. In Fe_{30}, V_{12} and Cr_7Ni the relaxation dynamics is investigated by analysis of NMR measurements. In Fe_{30} the relaxation mode characterizing the return of equilibrium of the cluster magnetization falls in the

frequency window of NMR, thus allowing to experimentally probe the relaxation time of magnetization. The T-dependence of the relaxation time can be inferred by the peak positions of the measured proton $1/T_1/(\chi T)$ at different applied magnetic fields. This is not the case for V_{12} and Cr_7Ni. In the former case the times characterizing the magnetization dynamics are not detectable in a NMR experiment. Thus the NMR response $1/T_1$ does not show any peak. The latter case is much more complicated. In fact, being the Cr_7Ni a heterometallic ring, in this case the $1/T_1/(\chi T)$ does not simply probe the fluctuations of cluster magnetization, but more generally combinations of molecular observables. Anyhow, peaks in the measured proton $1/T_1/(\chi T)$ occur and calculations reproduce the experimental NMR data very well. By summarizing, in all studied clusters the model well captures the main features of the relaxation dynamics. In the future some efforts will be devoted to find out some experimental evidence of the fast relaxation mechanism which governs the relaxation of magnetization in nanomagnets with a double well potential at strong enough applied field and low enough temperature discussed above. Furthermore, analysis of torque measurements on Cr_8Zn and Cr_8Ni compounds would corroborate the here presented microscopic description by means of INS and thermodynamic measurements.

Appendix A

Inelastic and quasi-elastic components of spin dynamics

In Chapter 6 an expression of the quasi-elastic part of the relaxation function $R_{\mathcal{AB}}(t)$ was calculated in first order perturbation theory, the perturbation being a small static magnetic field abruptly switched off at $t = 0$. At $t > 0$ a relaxation of molecular observables will occur, and the characteristic times of this process can be determined by both the quasi-elastic (QE) and inelastic (IN) part of $R_{\mathcal{AB}}(t)$:

$$R^{[QE]}_{\mathcal{A},\mathcal{B}}(t) = \beta \sum_{m,n} p^{(eq)}_m \left(\mathcal{B}_{mm} - \langle \mathcal{B} \rangle_{eq} \right) \nu_{nm}(t) \left(\mathcal{A}_{nn} - \langle \mathcal{A} \rangle_{eq} \right) \tag{111}$$

$$R^{[IN]}_{\mathcal{A},\mathcal{B}}(t) = \sum_{k \neq l} e^{i\Delta_{lk}t} e^{-t/\tau_{lk}} \frac{p^{(eq)}_l - p^{(eq)}_k}{E^{(0)}_k - E^{(0)}_l} \mathcal{B}_{lk} \mathcal{A}_{kl} \tag{112}$$

where $\mathcal{A}$, $\mathcal{B}$ are two generic molecular observables, $E^{(0)}_i$ are the eigenvalues of the unperturbed system, and $p^{(eq)}_i$ are the Boltzmann factors at the equilibrium (for $t > 0$, i.e. after the perturbation has been switched off). $\nu(t) = e^{\mathbf{W}t}$ where $\mathbf{W}$ is the rate matrix, W_{mn} giving the probability per unit time of a transition between the m, n levels of the spin system due to the coupling of the spins with other degrees of freedom (e.g. phonons). Besides the Laplace transform of $R^{[QE]}_{\mathcal{A},\mathcal{B}}(t)$ is:

$$\begin{aligned} \tilde{R}^{[QE]}_{\mathcal{A},\mathcal{B}}[i\omega] &= \beta \sum_{m,n} p^{(eq)}_m \left(\mathcal{B}_{mm} - \langle \mathcal{B} \rangle_{eq} \right) \\ &\quad \times Re \left\{ \left(\frac{1}{i\omega - \mathbf{W}} \right)_{nm} \right\} \left(\mathcal{A}_{nn} - \langle \mathcal{A} \rangle_{eq} \right). \end{aligned} \tag{113}$$

By means of the Equations above it can be found an expression for the generalized susceptibility $\chi^{[QE,IN]}_{\mathcal{A},\mathcal{B}}(\omega) = \chi'^{[QE,IN]}_{\mathcal{A},\mathcal{B}}(\omega) + i\chi''^{[QE,IN]}_{\mathcal{A},\mathcal{B}}(\omega)$ [44]:

$$\chi^{[QE,IN]}_{\mathcal{A},\mathcal{B}} = -R^{[QE,IN]}_{\mathcal{A},\mathcal{B}}(0) + i\omega \tilde{R}^{[QE,IN]}_{\mathcal{A},\mathcal{B}}[i\omega], \tag{114}$$

from which it can be recovered that at $\omega = 0$ there are obviously no dissipative effects since $\chi''^{[QE,IN]}_{\mathcal{A},\mathcal{B}}(\omega = 0)$ is identically zero. Therefore at $\omega \neq 0$ the imaginary parts of QE and IN susceptibility read as follows:

$$\begin{aligned}\chi''^{[QE]}_{\mathcal{A},\mathcal{B}}(\omega) = \omega \tilde{R}'^{[QE]}_{\mathcal{A},\mathcal{B}}[i\omega] &= \omega\beta \sum_{m,n} p_m^{(eq)} \left(\mathcal{B}_{mm} - \langle\mathcal{B}\rangle_{eq}\right) \\ &\quad \times Re\left\{\left(\frac{1}{i\omega - \mathbf{W}}\right)_{nm}\right\}\left(\mathcal{A}_{nn} - \langle\mathcal{A}\rangle_{eq}\right) \qquad (115)\\ \chi''^{[IN]}_{\mathcal{A},\mathcal{B}}(\omega) = \omega \tilde{R}'^{[IN]}_{\mathcal{A},\mathcal{B}}[i\omega] &= \omega \sum_{k\neq l} \frac{\tau_{kl}^{-1}}{(\omega + \Delta_{kl})^2 + \tau_{kl}^{-2}} \frac{p_l^{(eq)} - p_k^{(eq)}}{E_k^{(0)} - E_l^{(0)}} \mathcal{B}_{lk}\mathcal{A}_{kl}. \qquad (116)\end{aligned}$$

Eqs. (116), (115) (out of phase susceptibilities) are crucial to determine the relaxation mechanisms in magnetic molecules, since they directly give information on the spin-spin correlation functions through the fluctuation-dissipation theorem. In addition, it is worth to stress that from Eqs. (111), (112), and from the real part of the $\chi^{[QE,IN]}_{\mathcal{A},\mathcal{B}}(\omega = 0)$ in Eq. (114) the expressions for the Curie and Van Vleck susceptibilities can be obtained:

$$\begin{aligned}\chi^{Curie} = -\chi'^{[QE]}_{\mathcal{A}=\mathcal{B}}(\omega = 0) &= R^{[QE]}_{\mathcal{A}=\mathcal{B}}(t = 0) \\ &= \beta \sum_n \frac{e^{-\beta E_n}}{Z}\left(\mathcal{A}_{nn} - \langle\mathcal{A}\rangle_{eq}\right)^2 \qquad (117)\\ \chi^{VanVleck} = -\chi'^{[IN]}_{\mathcal{A}=\mathcal{B}}(\omega = 0) &= R^{[IN]}_{\mathcal{A}=\mathcal{B}}(t = 0) \\ &= \sum_{k\neq l} \frac{p_l^{(eq)} - p_k^{(eq)}}{E_k^{(0)} - E_l^{(0)}} \left|\langle l\left|\mathcal{A}\right|k\rangle\right|^2 \\ &= 2\sum_{k\neq l} \frac{e^{-\beta E_l^{(0)}}}{Z} \frac{\left|\langle l\left|\mathcal{A}\right|k\rangle\right|^2}{E_k^{(0)} - E_l^{(0)}}, \qquad (118)\end{aligned}$$

where the obervable $\mathcal{A}$ will now represent the total (for homonuclear clusters) or local (for heteronuclear clusters) magnetic moment in the considered molecule. In the latter case the sum of all local susceptibilities has to be performed in order to have the total cluster susceptibility. In Ref. [21] another method to evaluate the generalized susceptibility was proposed. It is based on a perturbative approach in which the magnetic system undergoes relaxation dynamics because of a small oscillating magnetic field (time-dependent perturbation). The basic assumption of this method consists in postulating that the interaction with phonons is rapid enough in order to establish

an equilibium state at the instant value of the magnetic field. By adopting the same symbols used in Ref. [21] this leads to:

$$\chi''^{[QE]}_{\alpha\beta}(\omega) = Im\left\{-i\omega\sum_{nk}\Delta m_{\alpha,nn}(i\omega 1+\mathbf{W})^{-1}_{nk}\times\Delta m_{\beta,kk}\rho_{0k}/kT\right\} \tag{119}$$

where $\mathbf{m}$ is the spin operator of the ion magnetic moment, $\alpha,\beta = x,y,z$, $\mathbf{W}$ is the rate matrix and ρ_0 is the equlibrium density matrix. By observing that

$$Im\left\{-i(i\omega 1+\mathbf{W})^{-1}_{ij}\right\} = Re\left\{\frac{1}{(i\omega-\mathbf{W})_{ij}}\right\} \tag{120}$$

it is straightforward to note that Eqs. (115) and (119) are equivalent. Nonetheless, the two methods presented in Refs. [20, 21] show a tiny discrepancy in the IN part of the generalized suceptibility. In fact, here we report the two expressions of the real part of AC suscetptibility obtained in the two methods mentioned before:

$$\begin{aligned}\chi'^{[IN]}_{\mathcal{A},\mathcal{B}}(\omega) &= -R^{[IN]}_{\mathcal{A},\mathcal{B}}(0)-\omega\tilde{R}''^{[IN]}_{\mathcal{A},\mathcal{B}}[i\omega]\\ &= -\sum_{k\neq l}\frac{p^{(eq)}_l-p^{(eq)}_k}{E^{(0)}_k-E^{(0)}_l}\mathcal{B}_{lk}\mathcal{A}_{kl}\\ &\quad -\omega\sum_{k\neq l}\frac{\Delta_{lk}-\omega}{(\Delta_{lk}-\omega)^2+\tau^{-2}_{lk}}\frac{p^{(eq)}_l-p^{(eq)}_k}{E^{(0)}_k-E^{(0)}_l}\mathcal{B}_{lk}\mathcal{A}_{kl} \qquad (121)\\ \chi'^{[IN]}_{\alpha\beta}(\omega) &= \sum_{n,k\neq n}m_{\alpha,nk}m_{\beta,kn}(\rho_{0k}-\rho_{0n})\frac{\omega_{nk}-\omega}{\hbar[\omega^2_{nk}+\gamma^2_{nk}]} \qquad (122)\end{aligned}$$

where $\Delta_{ij} = \omega_{ij} = (E^{(0)}_i - E^{(0)}_j)/\hbar$ reflects the energy difference expressed as a frequency for the couple of energy levels involved in the relaxation process. Besides, the $\tau^{-1}_{ij} = \gamma_{ij}$ is the average of the lifetimes of levels n and m, and represents the time after which coherence can not be preserved anymore. Differently form the case of the QE part of the out of phase AC susceptibility, the two expressions above do not concide. As regards Eq. (121) we have already demonstrated that *identically* $\chi'^{[IN]}_{\mathcal{A},\mathcal{B}}(\omega=0) = \chi^{VanVleck}$ as pointed out before in Eq. (118) and as can be easily obtained from Eq. (121) by imposing $\mathcal{A}=\mathcal{B}$ and putting $\omega = 0$. Indeed, in order to obtain the Van Vleck susceptibility from Eq. (122) an approximation has to be carried out:

$$\begin{aligned}\chi'^{[IN]}_{\alpha\beta}(\omega=0) &= \sum_{n,k\neq n}m_{\alpha,nk}m_{\beta,kn}(\rho_{0k}-\rho_{0n})\frac{\omega_{nk}}{\hbar[\omega^2_{nk}+\gamma^2_{nk}]}\\ &\cong \sum_{n,k\neq n}m_{\alpha,nk}m_{\beta,kn}\frac{(\rho_{0k}-\rho_{0n})}{\hbar\omega_{nk}} = \chi^{VanVleck}, \qquad (123)\end{aligned}$$

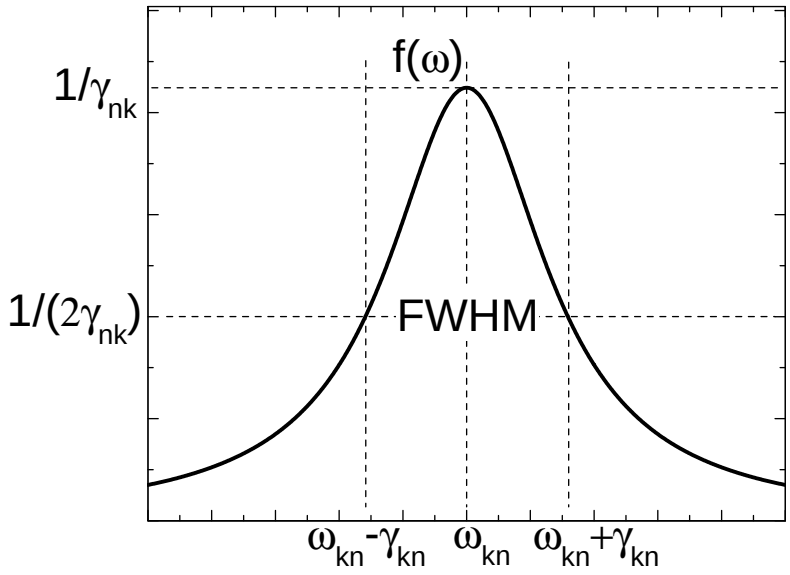

Figure 45: A characteristic Lorentzian centered in ω_{kn} and of FWHM given by $2\gamma_{nk}$.

where the last equivalence is possible only if $|\omega_{nk}| >> \gamma_{nk}$ holds. Therefore, the method proposed in Ref. [20] reveals to be more general than that presented in Ref. [21], since the latter needs a further approximation for the Van Vleck susceptibility to be recovered. Nevertheless, this approximation turns out to be valid and reasonable since it means that the free evolution periods of the system are much smaller than the characteristic times of relaxation processes [20, 101] (level lifetimes $\tau^{(i)}_{life}$ or relaxation times $\tau^{(i)}_{QE}$ as defined in Chapter 3). Moreover, this is the approximation made also by Jensen which allows definitvely to asses that expressions in Eqs. (121) and (122) refer to the same physical quantity [34]. In order to clarify this last point let us consider the IN part of the out of phase susceptibility in Eq. (116) as calculated by the method presented in Ref. [20] and in the following equation as calculated in Ref. [21]:

$$\chi''^{[IN]}_{\alpha\beta}(\omega) \sum_{n,k\neq n} m_{\alpha,nk} m_{\beta,kn} (\rho_{0k} - \rho_{0n}) \frac{\gamma_{nk}}{\hbar[(\omega_{nk} - \omega)^2 + \gamma^2_{nk}]}. \tag{124}$$

It is straightforward to note that in Eq. (124) for n, k fixed the $\chi''^{[IN]}_{\alpha\beta}(\omega)$ has a Lorentzian-type depedence from ω:

$$f(\omega) = \frac{\gamma_{nk}}{\hbar[(\omega_{kn} - \omega)^2 + \gamma^2_{nk}]}. \tag{125}$$

The $f(\omega)$ is a Lorentzian curve centered at $\omega = \omega_{kn}$ and a FWHM $f(\omega = \omega_{kn} \pm \gamma_{nk})$ as can be seen in Fig. 45. Let us define as $g(\omega)$ function the ω-dependence in the corresponding Eq. (116):

$$g(\omega) = \frac{\tau_{lk}^{-1}}{(\omega - \Delta_{lk})^2 + \tau_{lk}^{-2}} \times \frac{\omega}{E_k^{(0)} - E_l^{(0)}}. \tag{126}$$

Differently from $f(\omega)$, the $g(\omega)$ function does not represent a Lorentzian. However, it can be found that $g(\omega)$ presents an absolute maximum at $\omega_{max} = \sqrt{\Delta_{lk}^2 + \tau_{lk}^{-2}}$. Besides, if we take the approximation $\Delta_{lk} >> \tau_{lk}^{-1}$ which is equivalent to postulate $|\omega_{nk}| >> \gamma_{nk}$ we have $\omega \approx \Delta_{lk}$ and as a result:

$$g(\omega = \Delta_{lk}) = \tau_{lk} \tag{127}$$

$$FWHM = 2\tau_{lk}^{-1} \tag{128}$$

which means that the $g(\omega)$ is *effectively* a Lorentzian as far as the approximation $\Delta_{lk} >> \tau_{lk}^{-2}$ holds. By summaryzing, we have demonstrated that the methods presented in Refs. [20,21] are equivalent -though the former from Ref. [20] has revealed to be more general- if the free evolution periods of the system are much more rapid than the typical relaxation times in magnetic molecules.

Bibliography

[1] Gatteschi, D. and Sessoli, R. *Angew. Chem.* **42**(3), 268–297 (2003).

[2] Gatteschi, D., Sessoli, R., and Villain, J. *Molecular Nanomagnets*. Oxford University Press, Oxford, (2006).

[3] Gatteschi, D. and Sessoli, R. *J. Magn. Magn. Mater.* **272-276**, 1030–1036 (2004).

[4] Sakurai, J. J. *Meccanica Quantistica Moderna*. Zanichelli, Bologna, 2nd edition, (1996).

[5] Messiah, A. *Quantum Mechanics*. Dover Publications, Inc., New York, (1999).

[6] Amoretti, G. *Crystal field exchange interaction for magnetic ions in solids, in Magnetic Properties of Matter, Proc. of the National School held in Villa Gualino, Turin, September 8-20, 1986*. World Scientific, Singapore, (1988).

[7] Furukawa, Y., Kiuchi, K., Kumagai, K., Ajiro, Y., Narumi, Y., Iwaki, M., Kindo, K., Bianchi, A., Carretta, S., Timco, G. A., and Winpenny, R. E. P. *Phys. Rev. B* **78**, 092402 September (2008).

[8] Bianchi, A., Carretta, S., Santini, P., Amoretti, G., Guidi, T., Qiu, Y., Copley, J. R. D., Timco, G. A., and Winpenny, R. E. P. *submitted* .

[9] Furukawa, Y., Kiuchi, K., Kumagai, K., Ajiro, Y., Narumi, Y., Kindo, K., Bianchi, A., Carretta, S., Santini, P., Borsa, F., Timco, G. A., and Winpenny, R. E. P. *submitted* .

[10] Lago, J., Micotti, E., Corti, M., Lascialfari, A., Bianchi, A., Carretta, S., Santini, P., Procissi, D., Baek, S. H., Kögerler, P., Baines, C., and Amato, A. *Phys. Rev. B* **76**, 064432 August (2007).

[11] Bianchi, A., Carretta, S., Santini, P., and Amoretti, G. *J. Magn. Magn. Mater.* **310**, 1450 November (2006).

[12] Canepa, F. and Solzi, M. *Chapter 9: AC susceptibility Studies on Magnetic Materials in Condensed Matter: New Research*. Nova Science Publishers, New York, (2006).

[13] Troiani, F., Ghirri, A., Affronte, M., Carretta, S., Santini, P., Amoretti, G., Piligkos, S., Timco, G., and Winpenny, R. E. P. *Phys. Rev. Lett.* **94**, 207208 May (2005).

[14] Affronte, M., Ghirri, A., Carretta, S., Amoretti, G., Piligkos, S., Timco, G. A., and Winpenny, R. E. P. *Appl. Phys. Lett.* **84**(18), 3478–3470 May (2004).

[15] Lis, T. *Acta Crystallogr. Sect. B* **36**, 2042–2046 (1980).

[16] Sessoli, R., Gatteschi, D., Caneschi, A., and Novak, A. *Nature (London)* **365**, 141 (1993).

[17] Luis, F., Bartholomé, J., Fernández, J. F., Tejada, J., Hernández, J. M., Zhang, X. X., and Ziolo, R. *Phys. Rev. B* **55**, 11448 May (1997).

[18] Fort, A., Rettori, A., Villain, J., Gatteschi, D., and Sessoli, R. *Phys. Rev. Lett.* **80**(3), 612–615 January (1998).

[19] Katsnelson, M. I., Dobrovitski, V. V., and Harmon, B. N. *Phys. Rev. B* **59**(10), 6919–6926 March (1999).

[20] Santini, P., Carretta, S., Liviotti, E., Amoretti, G., Carretta, P., Filibian, M., Lascialfari, A., and Micotti, E. *Phys. Rev. Lett.* **94**, 077203 February (2005).

[21] Bertaina, S., Barbara, B., Giraud, R., Malkin, B. Z., Vanuynin, M. V., Pominov, A. I., Stolov, A. L., and Tkachuk, A. M. *Phys. Rev. B* **74**, 184421 November (2006).

[22] Mirebeau, I., Hennion, M., Casalta, H., Andres, H., Güdel, H. U., Irodova, A. V., and Caneschi, A. *Phys. Rev. Lett.* **83**(3), 628 July (1999).

[23] Leuenberger, M. N. and Loss, D. *Nature (London)* **410**, 789 (2001).

[24] Carretta, S., Guidi, T., Santini, P., Amoretti, G., Pieper, O., Lake, B., van Slageren, J., Hallak, F. E., Wernsdorfer, W., Mutka, H., Russina, M., Milios, C. J., and Brechin, E. K. *Phys. Rev. Lett.* **100**, 157203 April (2008).

[25] Ishikawa, N., Sugita, M., Ishikawa, T., Koshihara, S., and Kaizu, Y. *J. Am. Chem. Soc.* **125**, 8694–8695 June (2003).

[26] Zaleski, C. M., adn T. Mallah, J. W. K., Kirk, M. L., and Pecoraro, V. L. *Inorg. Chem.* **46**, 1954–1956 (2007).

[27] Tang, J., Heweitt, I., Madhu, N. T., Chastanet, G., Wernsdorfer, W., Anson, C. E., Benelli, C., Sessoli, R., and Powell, A. K. *Angew. Chem. Int. Ed.* **45**, 1729–1733 (2006).

[28] Osa, S., Kido, T., Matsumoto, N., Re, N., Pochba, A., and Mrozinski, J. *J. Am. Chem. Soc.* **126**, 420–421 (2004).

[29] Aronica, C., Pilet, G., Chastanet, G., Wernsdorfer, W., Jacquot, J.-F., and Luneau, D. *Angew. Chem. Int. Ed.* **45**, 4659–4662 (2006).

[30] Caciuffo, R., Guidi, T., Amoretti, G., Carretta, S., Liviotti, E., Santini, P., Mondelli, C., Timco, G., Muryn, C. A., and Winpenny, R. E. P. *Phys. Rev. B* **71**, 174407 May (2005).

[31] Blundell, S. *Magnetism in Condensed Matter.* Oxford University Press, Oxford, (2006).

[32] Bencini, A. and Gatteschi, D. *EPR of Exchange Coupled Systems.* Springer Verlag, Berlin, (1990).

[33] Abragam, A. and Bleany, B. *Electron Paramagnetic Resonance of Transition Ions.* Clarendon, Oxford, (1970).

[34] Jensen, J. and Mackintosh, A. R. *Rare Earth Magnetism.* Clarendon Press, Oxford, (1991).

[35] Borras-Almenar, J. J., Clemente-Juan, J. M., Coronado, E., and Tsukerblat, B. S. *Inorg. Chem.* **38**, 6081 (1990).

[36] Onofri, E. and Destri, C. *Istituzioni di fisica teorica.* Carocci, Roma, (1998).

[37] Caldirola, P., Cirelli, R., and Prosperi, G. M. *Introduzione alla Fisica Teorica.* Utet, Torino, 2nd edition, (1996).

[38] Liviotti, E., Carretta, S., and Amoretti, G. *J. Phys. Chem.* **117**(7), 3361–3368 August (2002).

[39] Carretta, S., van Slageren, J., Guidi, T., Liviotti, E., Mondelli, C., Rovai, D., Cornia, A., Dearden, A. L., Carsughi, F., Affronte, M., Frost, C. D., Winpenny, R. E. P., Gatteschi, D., Amoretti, G., and Caciuffo, R. *Phys. Rev. B* **67**, 094405 March (2003).

[40] Amoretti, G., Caciuffo, R., Cômbet, J., Murani, A., and Caneschi, A. *Phys. Rev. B* **62**(5), 3022 August (2000).

[41] Caciuffo, R., Amoretti, G., Murani, A., Sessoli, R., Caneschi, A., and Gatteschi, D. *Phys. Rev. Lett.* **81**(21), 4744 November (1998).

[42] Buckmaster, H. A. and Shing, Y. H. *Phys. Status Solidi A* **12**, 325 (1972).

[43] Smith, D. and Thornley, J. H. M. *Proc. Phys. Soc.* **89**, 779 August (1966).

[44] Lovesey, S. W. *Theory of neutron scattering from condensed matter.* Clarendon Press, Oxford, (1984).

[45] Santini, P., Carretta, S., Amoretti, G., Guidi, T., Caciuffo, R., Caneschi, A., Rovai, D., Qiu, Y., and Copley, J. R. D. *Phys. Rev. B* **71**, 184405 May (2005).

[46] Slichter, C. P. *Principles of Magnetic Resonance.* Springer-Verlag, Berlin, (1992).

[47] Moriya, T. *Progr. Theor. Phys.* **16**(23) (1956).

[48] Schnack, J. and Luban, M. *Phys. Rev. B* **63**, 014418 (2000).

[49] Waldmann, O., Guidi, T., Carretta, S., Mondelli, C., and Dearden, A. L. *Phys. Rev. Lett.* **91**, 237202 (2003).

[50] Schanck, J., Luban, M., and Modler, R. *Europhys. Lett.* **56**, 863 (2001).

[51] Garlea, V. O., Nagler, S. E., Zarestky, J. L., Stassis, C., Vaknin, D., Kögerler, P., McMorrow, D. F., Niedermayer, C., Tennat, D. A., Lake, B., Qiu, Y., Exler, M., Schnack, J., and Luban, M. *Phys. Rev. B* **73**, 024414 (2006).

[52] Ghirri, A., Candini, A., Evangelisti, Affronte, M., Carretta, S., Santini, P., Amoretti, G., Davies, R. S. G., Timco, G., and Winpenny, R. E. P. *Phys. Rev. B* **76**, 214405 December (2007).

[53] Ochsenbein, S. T., Waldmann, O., Sieber, A., Carver, G., Bircher, R., Güdel, H. U., Davies, R. S. G., Timco, G. A., Winpenny, R. E. P., Mutka, H., and Fernandez-Alonso, F. *Europhys. Lett.* **79**, 17003 June (2007).

[54] Copley, J. R. D. and Cook, J. C. *Chem. Phys.* **292**, 447 (2003).

[55] Timco, G. A., Batsanov, A. S., Larsen, F. K., Muryn, C. A., Overgaard, J., Teat, S. J., and Winpenny, R. E. P. *Chem. Commun. (Cambridge)* , 3649 (2005).

[56] Furniss, B. S., Hannaford, A. J., Smith, P. W. G., and Tatchell, A. R. *Vogel's Textbook of Practical Organic Chemistry.* Longman Scientific and Technical, New York, 5th ed. edition, (1989).

[57] van Slageren, J., Sessoli, R., Gatteschi, D., Smith, A. A., Helliwell, M., Winpenny, R. E. P., Cornia, A., Barra, A. L., Jansen, A. G. M., Rentschler, E., and Timco, G. A. *Chem.-Eur. J.* **8**, 277 (2002).

[58] Chiorescu, I., Wernsdorfer, W., Müller, A., Bögge, H., and Barbara, B. *Phys. Rev. Lett.* **84**, 3454 (2000).

[59] Rousochatzakis, I., Ajiro, Y., Mitamura, H., Kögerler, P., and Luban, M. *Phys. Rev. Lett.* **94**, 147204 (2005).

[60] Inagaki, Y., Asano, T., Ajiro, Y., Narumi, Y., Kindo, K., Cornia, A., and Gatteschi, D. *J. Phys. Soc. Jpn.* **72**, 1178 (2003).

[61] Nakano, H. and Miyashita, S. *J. Phys. Soc. Jpn.* **71**, 2580 (2002).

[62] Nakano, H. and Miyashita, S. *J. Phys. Soc. Jpn.* **70**, 2151 (2002).

[63] Affronte, M., Guidi, T., Caciuffo, R., Carretta, S., Amoretti, G., Hinderer, J., Sheikin, I., Jansen, A. G. M., Smith, A. A., Winpenny, R. E. P., van Slageren, J., and Gatteschi, D. *Phys. Rev. B* **68**, 104403 September (2003).

[64] Carretta, S., Santini, P., Amoretti, G., Affronte, M., Ghirri, A., Sheikin, I., Piligkos, S., Timco, G., and Winpenny, R. E. P. *Phys. Rev. B* **72**, 060403(R) August (2005).

[65] Micotti, E., Furukawa, Y., Kumagai, K., Carretta, S., Lascialfari, A., Borsa, F., Timco, G. A., and Winpenny, R. E. P. *Phys. Rev. Lett.* **97**, 267204 (2006).

[66] Cador, O., Gatteschi, D., Sessoli, R., Larsen, F. K., Overgaard, J., Barra, A.-L., Teat, S. J., Timco, G. A., and Winpenny, R. E. P. *Angew. Chem. Int. Ed.* **43**, 5196–5200 (2004).

[67] Kahn, O. *Chem. Phys. Lett.* **265**, 109–114 January (1997).

[68] Carretta, S., Santini, P., Amoretti, G., Guidi, T., Copley, J. R. D., Qiu, Y., Caciuffo, R., Timco, G., and Winpenny, R. E. P. *Phys. Rev. Lett.* **98**, 167401 April (2007).

[69] Gatteschi, D., Pardi, L., Barra, A.-L., Müller, A., and Döring, J. *Nature (London)* **354**, 463 December (1991).

[70] Kortz, U., Al-Kassem, N. K., Savelieff, M. G., Kadi, N. A. A., and Sadakane, M. *Inorg. Chem.* **40**, 4742 (2001).

[71] Cador, O., Gatteschi, D., Sessoli, R., Barra, A.-L., Timco, G. A., and Winpenny, R. E. P. *J. Mag. Mag. Mat* **290-291**, 55 April (2005).

[72] MacInnes, E. J. L., Piligkos, S., Timco, G. A., and Winpenny, R. E. P. *Coordination Chemistry Reviews* **249**, 2577 (2005).

[73] Affronte, M., Cornia, A., Lascialfari, A., Borsa, F., Gatteschi, D., Hinderer, J., Horvatic, M., Jansen, A. G. M., and Julien, M.-H. *Phys. Rev. Lett.* **88**, 167201 (2002).

[74] Affronte, M., Lasjaunias, J. C., and Cornia, A. *Eur. Phys. J. B* **15**, 633 (2000).

[75] Carretta, S., Santini, P., Amoretti, G., Affronte, M., Candini, A., Ghirri, A., Tidmarsh, I. S., Laye, R. H., Shaw, R., and McInnes, E. J. L. *Phys. Rev. Lett.* **97**, 207201 November (2006).

[76] Blum, K. *Density Matrix Theory and Applications.* Plenum Press, NY, (1996).

[77] Würger, A. *J. Phys.: Condens. Matter* **10**, 10075–10099 August (1998).

[78] Barra, A.-L., Debrunner, P., Gatteschi, D., Schulz, C. E., and Sessoli, R. *Europhys. Lett.* **35**, 133–138 May (1996).

[79] Santini, P., Carretta, S., Liviotti, E., and Amoretti, G. *Physica B* **374-375**, 109 March (2006).

[80] Leuenberger, M. N. and Loss, D. *Phys. Rev. B* **61**(2), 1286 January (2000).

[81] Müller, A., Krickmeyer, E., Bögge, H., Schmidtmann, M., and Peters, F. *Angew. Chem. Int. Ed.* **37**, 3360 (1998).

[82] Müller, A., Sarkar, S., Shah, S. Q. N., Bögge, H., Schmidtmann, M., Sarkar, S., Kögerler, P., Hauptfleisch, B., Trautwein, A. X., and Schünemann, V. *Angew. Chem. Int. Ed.* **38**, 3238 (1999).

[83] Müller, A., Kögerler, P., and Dress, A. W. M. *Coor. Chem. Rev.* **222**, 193 (2001).

[84] Müller, A., Luban, M., Schröder, C., Modler, R., Kögerler, P., Axenovich, M., Schnack, J., Canfield, P., Bud'ko, S., and Harrison, N. *Chem. Phys. Chem.* **2**, 517 (2001).

[85] Axenovich, M. and Luban, M. *Phys. Rev. B* **63**, 100407 (2001).

[86] Hasegawa, M. and Shiba, H. *J. Phys. Soc. Jpn.* **73**, 2543 (2004).

[87] Lascialfari, A., Gatteschi, D., Borsa, F., and Cornia, A. *Phys. Rev. B* **55**, 14341 (1997).

[88] Julien, M.-H., Zang, Z. H., Lascialfari, A., Borsa, F., Horvatić, M., Caneschi, A., and Gatteschi, D. *Phys. Rev. Lett.* **83**, 227 (1999).

[89] Abbati, G. L., Caneschi, A., Cornia, A., Fabretti, A., and Gatteschi, D. *Inorg. Chim. Acta* **297**, 291 (2000).

[90] Lascialfari, A., Jang, Z. H., Borsa, F., Carretta, P., and Gatteschi, D. *Phys. Rev. Lett.* **81**, 3773 (1998).

[91] Jung, J. K., Procissi, D., Vincent, R., Suh, B. J., Borsa, F., Kögerler, P., Schröder, C., and Luban, M. *J. Appl. Phys.* **91**, 7388 (2002).

[92] Micotti, E., Procissi, D., Lascialfari, A., Carretta, P., Kögerler, P., Borsa, F., Luban, M., and Baines, C. *J. Magn. Magn. Mater.* **272-276**, 1099 (2004).

[93] Borsa, F., Lascialfari, A., and Furukawa, Y. *Novel NMR and EPR Techniques.* Springer, Berlin, (2006).

[94] Baek, S. H., Luban, M., Lascialfari, A., Micotti, E., Furukawa, Y., Borsa, F., van Slageren, J., and Cornia, A. *Phys. Rev. B* **70**, 134434 (2004).

[95] Procissi, D., Suh, B. J., Micotti, E., Lascialfari, A., Furukawa, Y., and Borsa, F. *J. Magn. Magn. Mater.* **272-276**, e741 (2004).

[96] Basler, R., Chaboussant, G., Sieber, A., Andres, H., Murrie, M., Kögerler, P., Bögge, H., Crans, D. C., Krickemeyer, E., Janssen, S., Mutka, H., Müller, A., and Güdel, H. U. *Inorg. Chem.* **41**, 5675–5685 (2002).

[97] Procissi, D., Shastri, A., Rousochatzakis, I., Rafai, M. A., Kögler, P., Luban, M., Suh, B. J., and Borsa, F. *Phys. Rev. B* **69**(094436), 1–7 March (2004).

[98] Carretta, S., Bianchi, A., Liviotti, E., Santini, P., and Amoretti, G. *J. Appl. Phys.* **99**, 08D1011 April (2006).

[99] Belesi, M., Lascialfari, A., Procissi, D., Jang, Z. H., and Borsa, F. *Phys. Rev. B* **72**(014440), 1–9 July (2005).

[100] Bianchi, A., Carretta, S., Santini, P., Amoretti, G., Furukawa, Y., Kiuchi, K., Ajiro, Y., Narumi, Y., Kindo, K., Lago, J., Micotti, E., Arosio, P., Lascialfari, A., and Borsa, F. *submitted* .

[101] Bahr, S., Petukhov, K., Mosser, V., and Wernsdorfer, W. *Phys. Rev. Lett.* **99**, 147205 October (2007).

[102] Borsa, F. and Rigamonti, A. *Magnetic Resonance of Phase Transitions.* Academic Press, New York, (1979).

[103] Torres, F., Hernandez, J., Bohigas, X., and Tejada, J. *Appl. Phys. Lett.* **77**(20), 3248–3250 November (2000).

[104] Leuenberg, M. N. and Loss, D. *Nature* **410**, 789–793 April (2001).

[105] Wernsdorfer, W., Ohm, T., Sangregorio, C., Sessoli, R., Mailly, D., and Paulsen, C. *Phys. Rev. Lett.* **82**, 3903 (1999).

[106] Carretta, S., Liviotti, E., Magnani, N., Santini, P., and Amoretti, G. *Phys. Rev. Lett.* **92**, 207205 May (2004).

[107] Lascialfari, A., Borsa, F., Julien, M. H., Micotti, E., Furukawa, Y., Jang, Z. H., Cornia, A., Gatteschi, D., Horvatic, M., and Slageren, J. V. *J. Magn. Magn. Mater.* , 10042–10047 (2004).

[108] Hernandez, J. M., Zhang, X. X., Luis, F., Tejada, J., Friedman, J. R., Sarachik, M. P., and Ziolo, R. *Phys. Rev. B* **55**(9), 5858–5865 March (1997).

[109] Mirebeau, I., Hennion, M., Casalta, H., Andres, H., Güdel, H. U., Irodova, A. V., and Caneschi, A. *Phys. Rev. Lett.* **83**, 628 (1999).

[110] Hone, D., Scherer, C., and Borsa, F. *Phys. Rev. B* **9**, 965 (1974).

[111] Corti, M., Filibian, M., Carretta, P., Zhao, L., and Thompson, L. K. *Phys. Rev. B* **72**, 064402 (2005).

[112] Procissi, D., Lascialfari, A., Micotti, E., Bertassi, M., Carretta, P., Furukawa, Y., and Kögerler, P. *Phys. Rev. B* **73**, 184417 (2006).

[113] Exler, M. and Schnack, J. *Phys. Rev. B* **67**, 094440 (2003).

[114] de Reotier, P. D. and Yaouanc, A. *J. Phys.: Condens. Matter* **9**, 9113 (1997).

[115] Affronte, M., Guidi, T., Caciuffo, R., Carretta, S., Amoretti, G., Hinderer, J., Sheikin, I., Jansen, A. G. M., Smith, A. A., P.Winpenny, R. E., van Slageren, J., and Gatteschi, D. *Phys. Rev. B.* **68**, 104403 September (2003).

Acknoledgments

There are a lot of people I would like to thank for their persevering assistance during this years of my Ph.D. fellowship in Parma.
First of all, I want to thank my Supervisor, Prof. Paolo Santini for the possibility to study interesting problems in an attractive field of modern research, for his patience and the continuos help and support. I would also like to express gratitude to Prof. Giuseppe Amoretti, for his precise and precious indications. Furthermore, thanks are owing to Dr. Stefano Carretta: without his invaluable discussions and assistance this work would have been more difficult.
I would also like to thank Dr. Tatiana Guidi, for providing experimental data and the relative treatment and for her kind and rich explanations on the neutron scattering technique during an experiment at the ILL in Grenoble.
Besides, there are so many people whose friendship has been fundamental not only during these three years. I want to mention all the people I did not thank in my degree thesis. I begin with my close friends and colleagues of "Area 51" and "Ex sala fax" for discussions (not only in the field of molecular magnetism), rich dinners, help and support in many difficult situations (do you remember when I fainted? Just before going to the ILL...): Chiara, Elisa, Margherita, Fabio, Federico, Matteo, Massimiliano, Massimo ... besides I do not forget the old laboratory colleagues Elisa and Roberto, Gianluca and Matteo... (here and in the following the "..." stand for all the people I am forgetting and I apologize for this reason).
Thanks to my old friends of the glorious 5A at the Marconi High School (Alberto, Luca, Matteo, Michele, Enrico, Filippo, Cristiano, Nicola...): will we be able to make a trip to a capital city around the world? For this purpose I would like to recall the "sublime days in Prague" more than ten years ago...
Thanks to the numerous members of the Fuci company (you are so many to thank all of you!), in particular to Don Nando, Don Marco and Clara for their close friendship. I miss the endless mountain trips during the so many summers spent together in Trentino and the Masses in sunny valleys with apples in the rucksacks and cows around to eat them...
Thanks to my father's cousin Gianfranco, for his precious help, for his wonderful inventions and for having shown me how many things one can do with two hands and a hummer...
Thanks to my cousins and to all my blood relatives, because I think one should not forget his origins, and the number of my relatives clearly indicates that my grandparents were farmers!
Finally, thanks to my family, my mother Mariella and my brother Alessandro, for having encouraged me during these three years. They are all my life.
And very very finally, thanks to Irida, my sun, my moon, my sweet contradiction.
"Oh, it's bliss..."

Alberto Bianchi
Parma, January 2009

Publications

1. *Topological effects on the magnetic properties of closed and open ring-shaped Cr-based antiferromagnetic nanomagnets*
   Y. Furukawa, K. Kiuchi, K. Kumagai, Y. Ajiro, Y. Narumi, M. Iwaki, K. Kindo, A. Bianchi, S. Carretta, G. A. Timco, and R. E. P. Winpenny, Phys. Rev. B **78**, 092402 (2008).

2. *Low-energy spin dynamics in the giant keplerate molecule $\{Mo_{72}Fe_{30}\}$: A muon spin relaxation and ^1H NMR investigation*
   J. Lago, E. Micotti, M. Corti, A. Lascialfari, A. Bianchi, S. Carretta, P. Santini, D. Procissi, S. H. Baek, P. Kögerler, C. Baines, and A. Amato, Phys. Rev. B **76**, 064432 (2007).

3. *Relaxation of the magnetization in a molecule containing $s = 1/2$ ions : V_{12}*
   A. Bianchi, S. Carretta, P. Santini, and G. Amoretti, J. Magn. Magn. Mater. **310**, 1450 (2007).

4. *Relaxation of the magnetization in magnetic molecules*
   S. Carretta, A. Bianchi, E. Liviotti, P. Santini, and G. Amoretti, J. Appl. Phys., **99**, 08D101 (2006).

Submitted for publication

1. *Magnetization and spin dynamics of a Cr-based magnetic cluster: Cr_7Ni*
   A. Bianchi, S. Carretta, P. Santini, G. Amoretti, Y. Furukawa, K. Kiuchi, Y. Ajiro, Y. Narumi, K. Kindo, J. Lago, E. Micotti, P. Arosio, A. Lascialfari, F. Borsa

2. *Rotational bands in open antiferromagnetic rings: a neutron spectroscopy study of Cr_8Zn*
   A. Bianchi, S. Carretta, P. Santini, G. Amoretti, T. Guidi, Y. Qiu, J. R. D. Copley, G. A. Timco and R. E. P. Winpenny

3. *Evidence of spin singlet ground state in the frustrated antiferromagnetic ring Cr_8Ni*
   Y. Furukawa, K. Kiuchi, K. Kumagai, Y. Ajiro, Yasuo Narumi, M. Iwasa, K. Kindo, A. Bianchi, S. Carretta, P. Santini F. Borsa, G. A. Timco, and R. E. P. Winpenny